Proton-neutron symmetry at the limits of collectivity

Inaugural-Dissertation
zur
Erlangung des Doktorgrades
der Mathematisch-Naturwissenschaftlichen Fakultät
der Universität zu Köln

vorgelegt von
Volker Werner
aus Köln

Köln 2004

Berichterstatter:

Prof. Dr. P. von Brentano
Prof. Dr. J. Jolie
Prof. Dr. R.F. Casten

Tag der mündlichen Prüfung: 6. Februar 2004

Für meine Eltern

It is a miracle that curiosity survives formal education.
(Albert Einstein)

Abstract

Two limiting cases of proton-neutron collectivity in nuclear structure are addressed in this work. One of them is the so called limit of weak collectivity, where only a few valence nucleons are present in a nucleus with a well defined core. Such nuclei exhibit single particle degrees of freedom, as well collective ones, which are represented in their level schemes. Low-lying symmetric and mixed-symmetric states probe the proton-neutron structure in medium mass and heavy nuclei. Symmetric means protons and neutrons being in phase, whereas they are not completely in phase in mixed-symmetric states. Such states are also found in another limit of collectivity, the rotational limit, in well-deformed mid-shell nuclei with many valence nucleons. The best known example for a mixed-symmetric state in this case is the scissors mode.

A photon scattering experiment was performed on ^{92}Zr, a nucleus with only two valence protons and two valence neutrons with respect to the inert core ^{88}Sr. Nine states have been observed, five of them for the first time and two of them are candidates for the mixed-symmetric two-phonon 1^+ state and the quadrupole octupole coupled two-phonon 1^- state, respectively. For all the states lifetimes were determined for the first time, and six new spin assignments were made. The primary aim was the determination of the the lifetime of the 2_2^+ state which was shown to be small in the range of 100 fs. From a comparison of the experimental results with the shell model, including data of subsequent experiments, the 2_1^+ and 2_2^+ states are identified as the building blocks of symmetric and mixed-symmetric states, with pronounced neutron and proton character, respectively. Despite the appearance of shell effects and severely broken F-spin, quadrupole collectivity is found to be dominant for both states.

The rare earth isotope ^{164}Dy was investigated with a combination of resonant photon scattering experiments using unpolarized continuous bremsstrahlung, as well as polarized photons with well defined energies produced by a free electron laser. These experiments resulted in the observation of 34 states, ten of them new, and their lifetimes. γ-rays from decays of dipole excited states above 3 MeV to the 2^+ band head of the γ-band were identified. One of the parent states is a main fragment of the scissors mode and the observation of its decay to the 2_γ^+ state is the first time that such a decay is observed in a rotational nucleus. From the discovery of one of the new states, ambiguities in the level scheme were resolved.

Kurzzusammenfassung

Zwei Grenzfälle der Proton-Neutron Kollektivität in der Kernstruktur werden in dieser Arbeit behandelt. Einer ist der sogenannte Grenzfall der schwachen Kollektivität, in dem ein Kern nur wenige Valenznukleonen außerhalb einer abgeschlossenen Hauptschale hat. Solche Kerne weisen sowohl Einteilchen-, als auch kollektive Freiheitsgrade auf, die sich in ihrem Zustandsschema wiederspiegeln. Niedrigliegende symmetrische und gemischtsymmetrische Zustände sind eine Sonde für die Proton-Neutron Struktur in mittelschweren und schweren Kernen. Symmetrisch heißt, daß Protonen und Neutronen in Phase sind, während sie dies in gemischtsymmetrischen Zuständen nicht vollständig sind. Solche Zustände sind auch in einem anderen Grenzfall der Kollektivität bekannt, dem Rotations-Limit, in wohldeformierten Kernen mit vielen Valenznukleonen in der Nähe der Schalenmitte. Das bekannteste Beispiel für einen gemischtsymmetrischen Zustand in diesem Fall ist die Scherenmode.

Ein Photonenstreuexperiment wurde an ^{92}Zr durchgeführt, einem Kern mit nur zwei Valenzprotonen und zwei Valenzneutronen, unter Berücksichtigung eines Schalenabschlusses bei ^{88}Sr. Neun Zustände, davon fünf bisher unbekannte, wurden beobachtet, wovon zwei Kandidaten für den gemischtsymmetrischen Zwei-Phononen 1^+ Zustand, bzw. den Quadrupol-Oktupol gekoppelten Zwei-Phononen 1^- Zustand sind. Für alle beobachteten Zustände wurden erstmalig Lebensdauern bestimmt. In sechs Fällen wurden Zuständen neue Spins zugewiesen. Das Hauptziel des Experiments war die Bestimmung der Lebensdauer des 2_2^+ Zustands im Bereich von 100 fs. Durch einen Vergleich mit dem Schalenmodell, unter Einbeziehung von Daten aus nachfolgenden Experimenten, werden der 2_1^+ und der 2_2^+ Zustand als die Grundbausteine von symmetrischen und gemischtsymmetrischen Zuständen identifiziert, mit ausgeprägtem Neutronen- und Protonencharakter. Trotz des Auftretens von Schaleneffekten und stark gebrochenem F-Spin stellt sich eine dominierende Quadrupolkollektivität für beide Zustände heraus.

Das Seltene-Erden-Isotop ^{164}Dy wurde mittels einer Kombination von Experimenten in resonanter Photonenstreuung untersucht, sowohl unter Verwendung von unpolarisierten Photonen aus kontinuierlicher Bremsstrahlung, als auch polarisierten Photonen wohldefinierter Energie, produziert von einem Freie-Elektronen-Laser. Diese Experimente resultierten in der Beobachtung von 34 Zuständen, zehn davon erstmalig, und ihren Lebensdauern. γ-Übergänge aus den Zerfällen von angeregten Dipolzuständen oberhalb von 3 MeV zum 2^+ Kopf der γ-Bande wurden identifiziert. Einer der zerfallenden Zustände ist ein Hauptfragment der Scherenmode, und die Beobachtung seines Zerfalls zum 2_γ^+ Zustand ist die erstmalige Beobachtung eines solchen Zerfalls in einem Rotationskern. Durch die Entdeckung eines der neuen Zustände wurden Widersprüche im Zustandsschema aufgelöst.

Contents

Abstract v

Kurzzusammenfassung vi

1 Introduction 1

2 Experimental and theoretical techniques 5
- 2.1 Nuclear Resonance Fluorescence . . . 5
  - 2.1.1 Experimental setup at the IfS Stuttgart . . . 5
  - 2.1.2 The NRF technique using unpolarized photons . . . 7
  - 2.1.3 Experimental setup at HIγS . . . 9
  - 2.1.4 Angular correlations with polarized photons . . . 13
- 2.2 The Shell Model . . . 17
  - 2.2.1 The basic concept . . . 17
  - 2.2.2 The Surface Delta Interaction . . . 21
- 2.3 The Interacting Boson Model . . . 24
  - 2.3.1 *sd*-IBM-1 . . . 24
  - 2.3.2 *sd*-IBM-2 . . . 27
- 2.4 The Q-phonon scheme . . . 29
  - 2.4.1 Proton-neutron symmetric Q-phonons . . . 29
  - 2.4.2 Mixed-symmetry in the Q-phonon scheme . . . 31

3 The limit of weakly collective vibrators 35
- 3.1 NRF experiment on ^{92}Zr . . . 35
  - 3.1.1 Experimental details . . . 35
  - 3.1.2 Experimental results for ^{92}Zr . . . 36
- 3.2 Comparison with shell model calculations . . . 41
  - 3.2.1 Shell model description of ^{92}Zr . . . 42
  - 3.2.2 Consequences for low-lying states . . . 45
- 3.3 The N=52 isotones . . . 49
  - 3.3.1 Systematics of symmetric and mixed-symmetric states . . . 50
  - 3.3.2 Breaking F-spin . . . 53
  - 3.3.3 ^{96}Mo at N=54 . . . 56

3.4 Q-phonon purity near closed shells 56
3.4.1 Q-phonons in the shell model 56
3.4.2 Q-phonon purity test for some nuclei 58
3.4.3 Are there low-lying g-bosons? 60

4 The collective rotational limit 63
4.1 The scissors mode 63
4.2 Previous results for ^{164}Dy 64
4.3 NRF experiment on ^{164}Dy at Stuttgart 67
4.3.1 Experimental details 67
4.3.2 Experimental results for ^{164}Dy 67
4.3.3 Decays to the γ-band 72
4.4 NRF experiment on ^{164}Dy at Duke 74
4.4.1 Experimental details 74
4.4.2 Results at 3100 keV 74
4.4.3 Results at 3173 keV 77
4.5 Summary of the results for ^{164}Dy 79

5 Summary and outlook 81

A Parametrizations of the IBM-1 Hamiltonian 85

B Target compositions 89

List of publications 91
Regular publications 91
V. Werner *et al.* – commented 91
Other publications 93
Conference proceedings 97

Bibliography 103

Acknowledgments 111

Erklärung 113

Lebenslauf 115

List of Figures

2.1 Experimental setup at the IfS Stuttgart 6
2.2 Unpolarized angular distributions 7
2.3 FEL at the Duke storage ring 9
2.4 Scheme of a magnetic wiggler in a FEL 10
2.5 Beam profile of HIγS 11
2.6 NRF setup at HIγS 12
2.7 Angular distributions / polarized 16
2.8 Angular distributions / unpolarized 16
2.9 Nuclear potentials 17
2.10 Shell model single particle level scheme 19
2.11 Q-phonon purity of the 2_1^+ state in the IBM-1 30
2.12 Q-phonon scheme for proton-neutron symmetric states 31
2.13 Q-phonon scheme for symmetric and mixed-symmetric states . . . 32

3.1 Photon flux at 4.1 MeV endpoint energy 36
3.2 Photon scattering spectrum of ^{92}Zr 37
3.3 Spin assignment for states in ^{92}Zr 38
3.4 ^{92}Zr energies, experiment vs. shell model 43
3.5 Decay behavior of dipole states in ^{92}Zr 46
3.6 Two-level mixing 47
3.7 Systematics of the N=52 isotones 51
3.8 Mixing-scheme of proton and neutron configurations 52
3.9 F-spin breaking in the IBM-2 54

4.1 Systematics of M1 strengths across the A$\approx$130-200 shell 64
4.2 The ^{164}Dy puzzle 66
4.3 Photon flux at 2.9 MeV endpoint energy 68
4.4 Spin assignment for states in ^{164}Dy 68
4.5 Spectra of ^{164}Dy @ 2.9 MeV and @ 3.6 MeV 73
4.6 Parts of the spectrum @ 3100 keV 75
4.7 Analyzing powers as a function of δ 75
4.8 Beam profile @ 3100 keV 76
4.9 Parity assignments from the spectra 79
4.10 Solution of the ^{164}Dy puzzle 80

List of Tables

3.1 NRF data on ^{92}Zr 39

3.2 Side reactions in NRF on ^{92}Zr 41

3.3 SDI parameters for ^{92}Zr 42

3.4 ^{92}Zr transition strengths, experiment vs. shell model 44

3.5 Amplitudes of main configurations to wave functions of selected states 46

3.6 SDI parameters for ^{94}Mo and $^{92,94}Zr$ 58

3.7 Q-phonon purities around ^{92}Zr 59

4.1 NRF data on ^{164}Dy 69

4.2 Summary of the HIγS results 78

4.3 1^+ states in ^{164}Dy compared to an IBM-2 prediction 80

A.1 Conversions between ECQF parameters 87

B.1 ^{92}Zr target for the IfS experiments 89

B.2 ^{164}Dy target for the low-energy IfS experiment 90

B.3 ^{164}Dy target for the high-energy IfS experiment 90

B.4 ^{164}Dy target for the HIγS experiment 90

Chapter 1

Introduction

In magic or semi-magic nuclei single particle degrees of freedom and shell effects dominate the structure of the lowest states. They correspond to the excitation of particles from within the core and are high in energy. It is a fascinating effect that adding just a few nucleons leads to dramatic changes in the structure of the lowest levels, as it is seen, *e.g.*, from the lowering of the energy of the first 2^+ state in even-even nuclei leaving a closed shell. Collective structures as they are known for vibrational nuclei emerge, forming multiplets of states following the principle of a harmonic oscillator. But there are influences of the underlying shell structure, evident, *e.g.*, from the appearance of intruder states due to two particle, two hole excitations.

Again, there occurs a dramatic change in structure following the addition of only a few valence nucleons causing the appearance of γ-soft or rotational structures. This phenomenon has recently been under discussion, as such fast changes were identified as quantum phase transitions in nuclei, *e.g.*, in [Iac00, Iac01, Cas00, Cas01, Jol01, Wer02b]. The control parameter for such transitions is the number of valence nucleons. The vibrational regime is left abruptly, and rotational structures appear.

Studying influences of slight changes to the number of valence particles in certain mass regions on the resulting nuclear structure is thus an interesting topic in nuclear physics. Several microscopic and collective models are available describing certain aspects of the structure of low-lying states. There is some competition between microscopic models, e.g., the shell model [May49, Hax49] and collective models like the geometrical model [BoM75] or the interacting boson model (IBM) [IaA87]. Microscopic models usually include large configuration spaces which are difficult, if not impossible to handle. On the other hand, collective models make drastic truncations by taking into account only few interactions and neglecting the shell structure. Nevertheless, they proved to be very successful in the description of very constitutional features like rotation or vibration for nuclei with many valence particles. This reflects the fact, that low-lying excitations correspond to collective motions of nuclear matter, where the underlying microscopic structure

does not play the role it plays when only few valence particles are present.

A microscopic model should in principle be able to reproduce collective structures as well. Due to the progress in computing abilities and new approaches like Monte Carlo simulations, it recently became possible to perform microscopic calculations using large model spaces, *e.g.*, [Cau99, Hon95]. In such calculations it was shown that concepts derived in the framework of collective models, like the phonon concept, hold to a high degree in nuclei with only few valence particles [Shi00].

Taking into account separate proton and neutron spaces, one gets whole classes of nuclear states generated by a non-symmetric coupling of protons and neutrons. Such states are already known for a long time. One famous example is the Giant Dipole Resonance, an electric dipole excitation that results from the collective motion of the proton body against the neutron body. But, this mode involves the whole proton and neutron bodies of the nucleus, shifting its excitation energy to some 10 MeV and making a description in modern nuclear structure models hardly possible, even impossible if only valence nucleons above closed nuclear shells are considered. Due to the same reason a description in the nuclear shell model would naturally fail.

Nowadays, a survey of collective effects in nuclei, taking into account separate proton and neutron spaces, is strongly stimulated by the identification of so-called mixed-symmetric structures in a number of nuclei. So far the prime example is given by ^{94}Mo [Pie99b, Pie00, Fra01, Fra03]. Using various experimental methods, states, which are generated by a non-symmetric coupling of protons and neutrons, were identified. These states are regarded as quadrupole phonon excitations from the ground state, where proton-neutron symmetric states are isoscalar excitations, while mixed-symmetric states are formed by the isovector part of the quadrupole operator. A shell model calculation [Lis00] reproduced the dominating collective structures of symmetric and mixed-symmetric states in ^{94}Mo well, while showing also contributions from the underlying shell structure.

The question on the applicability of a collective picture to weakly collective nuclei shall be followed in this work by the investigation of ^{92}Zr. This nucleus has only two valence protons and two valence neutrons, with respect to the doubly magic core ^{88}Sr. Therefore, an experiment was performed at the Institut für Strahlenphysik of the Stuttgart University. Due to the few valence nucleons and its special shell structure ^{92}Zr represents a system where one usually expects that collective pictures break down. From the presented data, data from subsequent experiments, and calculations, states are identified, which are cognate to, or rather building blocks of symmetric and mixed-symmetric structures. It will be shown that a breaking of F-spin, the bosonic analog of isospin, may explain the structure of low-lying levels in ^{92}Zr. Calculations show that collective features dominate those levels to a large extent despite the identified shell effects. Adding only one pair of nucleons results in an almost purely collective behavior, as it is observed in ^{94}Mo.

The second topic of this work deals with another region of nuclear structure, the rotational limit, where many valence nucleons are present and the structures of most low-lying levels have strongly collective character. The most prominent mixed-symmetric excitation in rotational nuclei is the so called scissors mode. This is a M1 excitation that corresponds to a scissors-like oscillation of the deformed proton against the deformed neutron body in a geometrical picture. It was predicted by Lo Iudice and Palumbo [LoP78, LoP79], but at too high excitation energies, because the full proton and neutron bodies were taken into account. A restriction to only the valence nucleons leads to a prediction of the scissors mode at energies of about 3 MeV [Iac81, Iac84], where it was finally discovered in ^{156}Gd [Ric83, BoR84].

A decay of the scissors mode to the γ-band was never observed. Such a decay should be forbidden in the geometrical picture, regarding the scissors mode as a vibrational state (an oscillation of protons against neutrons), that has to be annihilated before exciting a γ-vibration. In contrary, within the IBM such a decay is predicted. Since the 1980's a puzzle was left for ^{164}Dy [Wes88], where corresponding γ-rays were observed but were not placed properly in the decay scheme. In subsequent works [Mar95, Joh95] the question about the existence of such decays arose, but could not be answered. Results of a combination of experiments performed at Stuttgart and at the Free Electron Laser Laboratory at Duke University are presented in this work. The present data finally proves the existence of a decay of a main fragment of the scissors mode to the γ-band, and the puzzle of unplaced transitions in this nucleus is solved, revealing also the existence of an additional state, which had only been assumed so far.

Chapter 2 will give an overview on the experimental and theoretical methods used in this work. In chapter 3 results for ^{92}Zr will be presented and discussed in comparison to theory. Results for ^{164}Dy will be given in chapter 4. Other topics that were treated during my PhD time, which are not discussed in this thesis, are briefly addressed in the commented part of the publication list.

Chapter 2

Experimental and theoretical techniques

In this chapter the experimental techniques and theoretical concepts that were used and applied in this work are discussed briefly. Most of the techniques are explained in detail in other works. Thus this chapter is restricted to an overview on the various topics, giving only the basic ideas, which one may look up when reading through the following chapters.

2.1 Nuclear Resonance Fluorescence

The data, that will be discussed later, was taken using the technique of nuclear resonance fluorescence (NRF) [Met59, Ber85]. The experiments using unpolarized photons were performed at the Institut für Strahlenphysik (IfS) of the Stuttgart University, and polarized photons were available at the Free Electron Laser Laboratory (DFELL) at Duke University. The different experimental setups, the basic concepts of NRF and the data analysis, in particular the use of angular correlations, will be discussed in the following.

2.1.1 Experimental setup at the IfS Stuttgart

Experiments on ^{92}Zr and ^{164}Dy were performed at the Institut für Strahlenphysik (IfS) of Stuttgart University. The Stuttgart 4.3 MV DYNAMITRON accelerator delivers a beam of monoenergetic electrons. The current is typically some hundred μA. The electrons are stopped in a water-cooled thick radiator target consisting of gold. In this stopping-process a continuous bremsstrahlung spectrum is produced, with an endpoint energy equal to the energy of the incident electrons. For a sketch of the Stuttgart NRF setup see Figure 2.1. The sample is placed behind a 98 cm long lead collimator, surrounded by three HPGe detectors that are positioned at 90°, 127° and 150° with respect to the beam axis. The detectors have a photo-

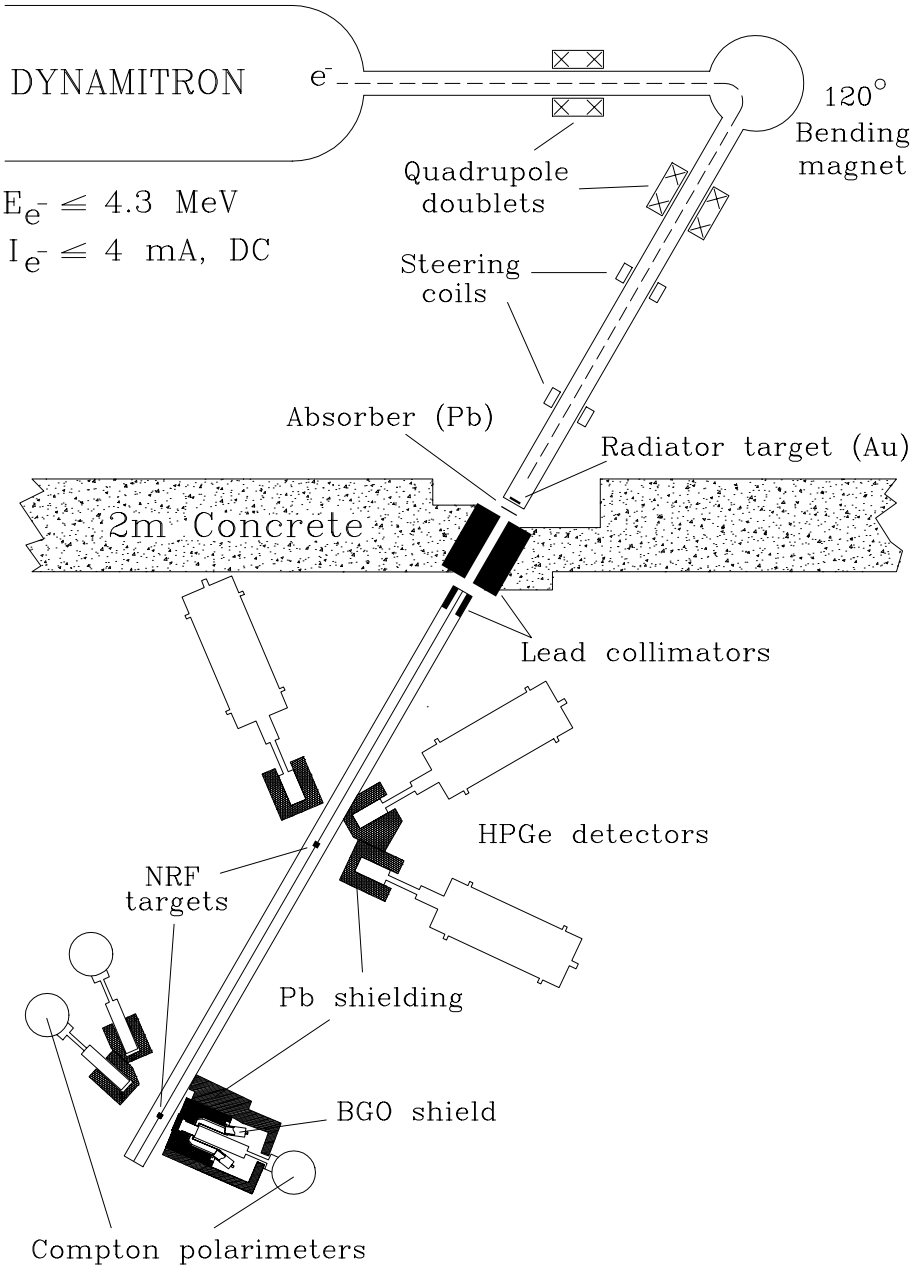

Figure 2.1: *Experimental setup at the IfS Stuttgart (taken from [Mar95]).*

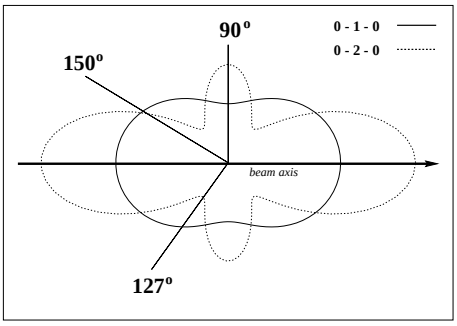

Figure 2.2: *Angular distributions for* $0 \to 1 \to 0$ *and* $0 \to 2 \to 0$ *cascades with unpolarized incident photons.*

peak efficiency of 100% (relative to a $3'' \times 3''$ standard NaI detector at a distance of 25 cm). A second setup may be installed behind the first one, *e.g.* for Compton polarimetry, but it was not used for the experiment presented here. For a more detailed description of the Stuttgart NRF setup see [Kne96].

2.1.2 The NRF technique using unpolarized photons

The Stuttgart experiments were performed using the method of inelastic photon scattering (γ,γ') (NRF), where a beam of high energetic photons is scattered off the target of interest. The target nuclei resonantly absorb photons, so that excited states are populated. As the incoming photons are real photons, they induce selectively dipole and, to a less extent, quadrupole transitions. The excited states of the target nuclei decay back to the ground state or to lower-lying excited states by emitting photons. These decays are observed by the surrounding germanium detectors.

For energy and efficiency calibration a ^{56}Co source is used of which γ-rays following the electron capture decay to ^{56}Fe are observed. For a detailed description of the calibration, see, *e.g.*, [Wer00a].

Direct observables in a photon scattering experiment using bremsstrahlung are the energy E_γ of the photons, the intensity and its angular dependence. For unpolarized incident photons, the angular distribution functions of the emitted photons for $j_i \to j \to j_f = 0 \to 1 \to 0$ and $0 \to 2 \to 0$ cascades are given by

$$W_{0\to1\to0}(\theta) = \frac{3}{4} \cdot \left(1 + \cos^2\theta\right) \text{ and} \tag{2.1}$$

$$W_{0\to2\to0}(\theta) = \frac{5}{7} \cdot \left(1 - 3\cos^2\theta + 4\cos^4\theta\right) , \tag{2.2}$$

which differ the most for $\theta = 90°$ and $\theta = 127°$. This can be seen from Figure 2.2. Thus, in case of a 0^+ ground state, one can easily determine the spin of an excited state by observing the transition back to the ground state, which also yields the excitation energy. Due to the high background at low energies from non-resonant

scattering, the number of observable transitions to lower-lying excited states is usually small. Nevertheless, in many cases at least the transition to the first excited state is observed and yields the branching ratio

$$\frac{\Gamma_f}{\Gamma_0} = \frac{I_{s,f}}{I_{s,0}} \ , \tag{2.3}$$

where Γ_f and $I_{s,f}$ denote the partial decay widths and integrated photon scattering cross sections of the decays to a final state f, where for the ground state $f = 0$. I_s is the energy and solid angle integrated differential cross section as given by the Breit-Wigner resonance formula [BrW36]

$$\frac{d^2\sigma_{abs}(E)}{d\Omega dE} = \pi\lambda\!\!\!^{-2} \cdot \frac{2j+1}{2(2j_0+1)} \cdot \frac{\Gamma_0\Gamma_f}{(E-E_r)^2 + \frac{1}{4}\Gamma^2} \cdot \frac{W(\theta)}{4\pi} \ , \tag{2.4}$$

with the total decay width

$$\Gamma = \sum_{f \geq 0} \Gamma_f \ . \tag{2.5}$$

The I_s are proportional to the efficiency-corrected peak-areas, and are measured by adding ^{27}Al to the target. ^{27}Al shows lines in the spectra for which the integrated cross sections are well known [Pie95]. This allows a calibration of the photon flux N_γ, being inversely proportional to I_s. With a calibration constant $\mathcal{N}_{cal}$, the number of target nuclei of one kind n_x, the relative efficiency of a detector $\epsilon_\theta(E_\gamma)$, the angular distribution factor $W(\theta)$, the peak-area $A(E_\gamma)$, and the photon flux at the excitation energy of the populated state $N_\gamma(E_r)$, the integrated cross section for the γ-decay is given by

$$I_s = \mathcal{N}_{cal} \ \frac{n_{Al}}{n_{target}} \ \frac{A(E_\gamma)}{N_\gamma(E_r) W(\theta) \epsilon_\theta(E_\gamma)} \ . \tag{2.6}$$

With

$$\frac{\Gamma_0^2}{\Gamma} = \frac{2j_0+1}{2j+1} \cdot \left(\frac{E_\gamma}{\pi\hbar c}\right)^2 \cdot I_{s,0} \tag{2.7}$$

and

$$\Gamma = \frac{\Gamma_0^2}{\Gamma} \cdot \left(1 + \sum_{f>0} \frac{\Gamma_f}{\Gamma_0}\right)^2 \tag{2.8}$$

one gets the total decay width of a state and its lifetime by

$$\tau = \frac{\hbar}{\Gamma} \ . \tag{2.9}$$

In the case of an axially symmetric rotor, the Alaga rules [Ala55] can be applied in order to assign a K-quantum number to a given state by calculating the decay branching ratio

$$R_{exp} = \frac{\Gamma_1}{\Gamma_0} \ \left(\frac{E_0}{E_1}\right)^{2\lambda+1} \ , \tag{2.10}$$

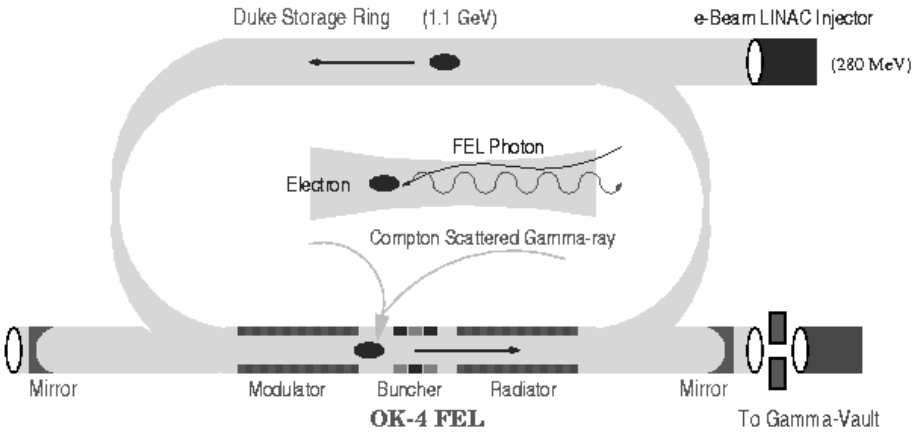

Figure 2.3: *Scheme of the γ-ray production using the free electron laser at the Duke storage ring. Two electron bunches are used for producing synchrotron light in the alternating magnetic fields of the optical klystron OK-4 and γ-rays by Compton backscattering. A buncher in the OK-4 device counters the broadening of the electron pulses (taken from [Higs]).*

where λ is the multipolarity of the radiation, Γ_1 is the decay width to the 2_1^+ state and E_i are the appropriate γ-energies. For dipole states with K-quantum number 0 or 1 and $\lambda = 1$ the Alaga rules give

$$R_{exp} = \begin{cases} 2.0 & \text{for} K = 0 \\ 0.5 & \text{for} K = 1 \end{cases} . \tag{2.11}$$

A detailed review on the NRF method is given in [Kne96].

2.1.3 Experimental setup at HIγS

A NRF measurement on ^{164}Dy using polarized photons was performed at the High Intense Gamma Source (HIγS) of the Triangle Universities Nuclear Laboratory (TUNL) at the Duke Free Electron Laser Laboratory (DFELL) at Duke University. A detailed description of the γ-ray production process at the DFELL can be found in [Car96, Lit97], and the NRF application is demonstrated in [Pie02]. Electrons, accelerated by a 280 MeV LINAC, are injected into the 1.2 GeV storage ring. The production of γ-rays is sketched in Figure 2.3. In the two-bunch mode two bunches of electrons are stored in the ring. The first bunch moves through an optical klystron (OK-4), consisting of two magnetic wigglers and a buncher in between. The scheme of a wiggler is shown in Figure 2.4. On a track of varying magnetic fields the electrons are forced on an oscillating path producing synchrotron light with energies of

$$E_{ph} = \frac{2\gamma^2 hc}{\lambda_w \left(1 + a_w^2\right)} , \tag{2.12}$$

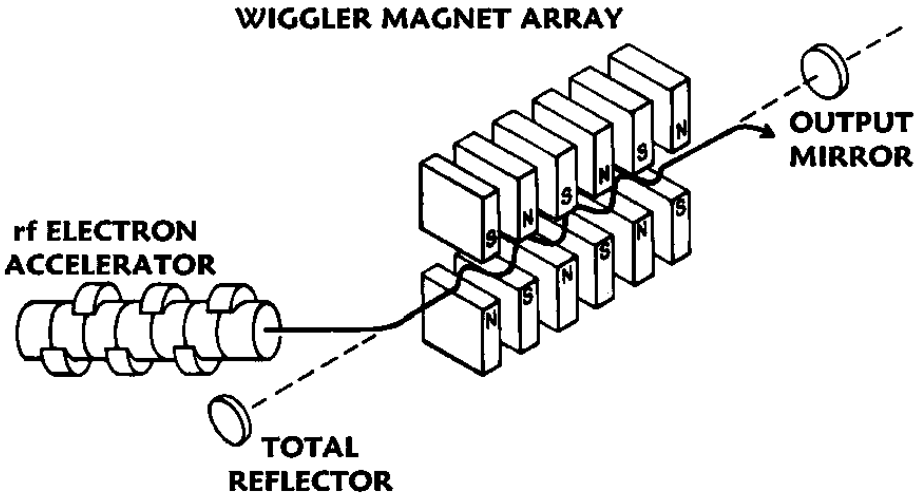

Figure 2.4: *Scheme of a magnetic wiggler in a free electron laser. Electrons are forced on an oscillating path by running through varying magnetic fields producing synchrotron radiation. The light is reflected between two mirrors (taken from [Kelly]).*

which lie in the order of about 1–10 eV. In Eq. (2.12) the amplification factor

$$\gamma = \frac{E_e}{mc^2} \tag{2.13}$$

is tunable by choosing the energy of the electrons in the storage ring, while λ_w is the fixed wiggler period ($\lambda_w = 10$ cm) and a_w is the normalized rms vector potential of the undulator, representing the tunable parameters of the magnetic fields,

$$a_w = \frac{eB_{rms}\lambda_w}{2\pi mc} \ . \tag{2.14}$$

The synchrotron light, which is completely polarized as the electrons are wiggled in a plane, is reflected by mirrors installed on one leg of the storage ring base lines. The length of this optical cavity is one half of the total circumference of the storage ring. Hence, the synchrotron light coincides with the first electron bunch in beam direction inside the OK-4, from which the lasing effect arouses. When reflected by the first (output) mirror the light hits the second electron bunch against the beam direction between the two wigglers. At this point Compton backscattering takes place and the photons gain energy via

$$E_\gamma = \frac{4\gamma^2 E_{ph}}{1 + \frac{4\gamma E_{ph}}{mc^2} + \gamma^2\theta^2} \ . \tag{2.15}$$

Again, the amplification factor γ plays the most important role and is typically $\gamma \approx 1000$, and thus the photons gain about a factor of 10^6 in energy, which makes them usable for nuclear structure experiments. The γ radiation passes through

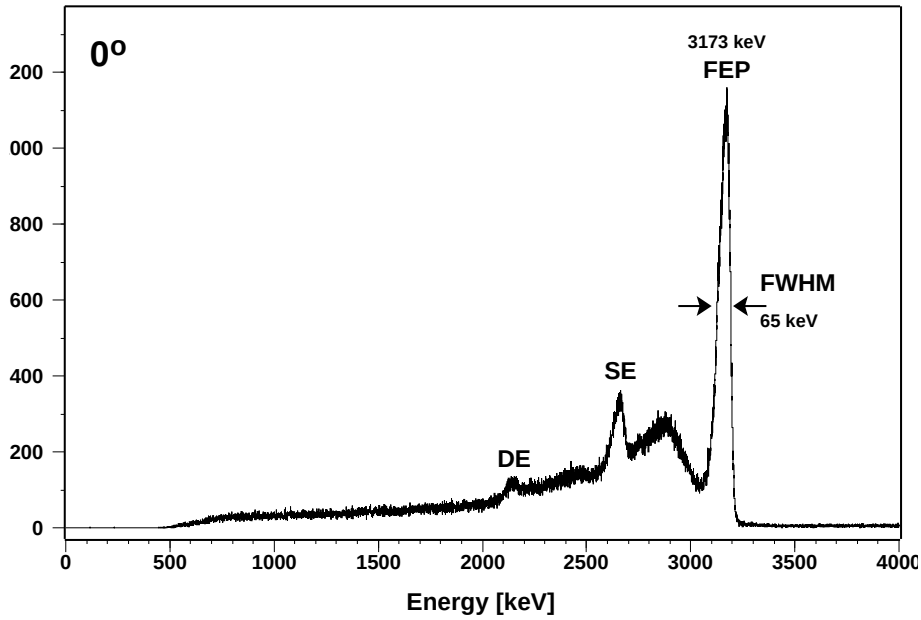

Figure 2.5: *Spectrum of the γ-ray beam, taken with a HPGe detector in beam direction. Marked are the full-energy peak (FEP) and the single- and double-escape lines (SE and DE, respectively). The maximum of the FEP was tuned to 3173 keV, the FHWM is about 65 keV.*

the output mirror, followed by a long lead collimator, and through an evacuated beam pipe to the experimental setup. The outgoing γ-rays are still completely polarized as polarization is conserved in the Compton scattering process. This makes the facility extremely useful for parity measurements. The second advantage of the HIγS facility is that the γ-ray beam is almost monoenergetic. The energy of the γ-rays depend on the angle θ at which the light is scattered, see Eq. (2.15). Therefore, the collimators define the energy spread of the photons, while limiting the photon flux. Because of this, an optimum between photon flux and energy spread must be found for each experiment. Figure 2.5 shows the spectrum of the beam, taken with a 123% HPGe detector at 0° with a reduced beam intensity (and without target). Such measurements allow a check of the position of the intensity maximum of the beam and give an idea on the energy-spread. Nevertheless it cannot be used for a photon flux calibration, as a reduction of the beam also means a reduction of the energy-spread due to room-charge effects of the electron bunches. The NRF setup at HIγS consists of four 60% HPGe detectors, positioned at 90° to the beam axis, two in the horizontal plane and two in the vertical plane, as shown in Figure 2.6. This setup allows a direct measurement of the parities of dipole excitations, much more efficient than using Compton polarimetry for the emitted γ-rays. Compton polarimeters usually have a weak polarization sensitivity, especially for high γ-energies, while at HIγS the incident photons are known to be 100% polarized.

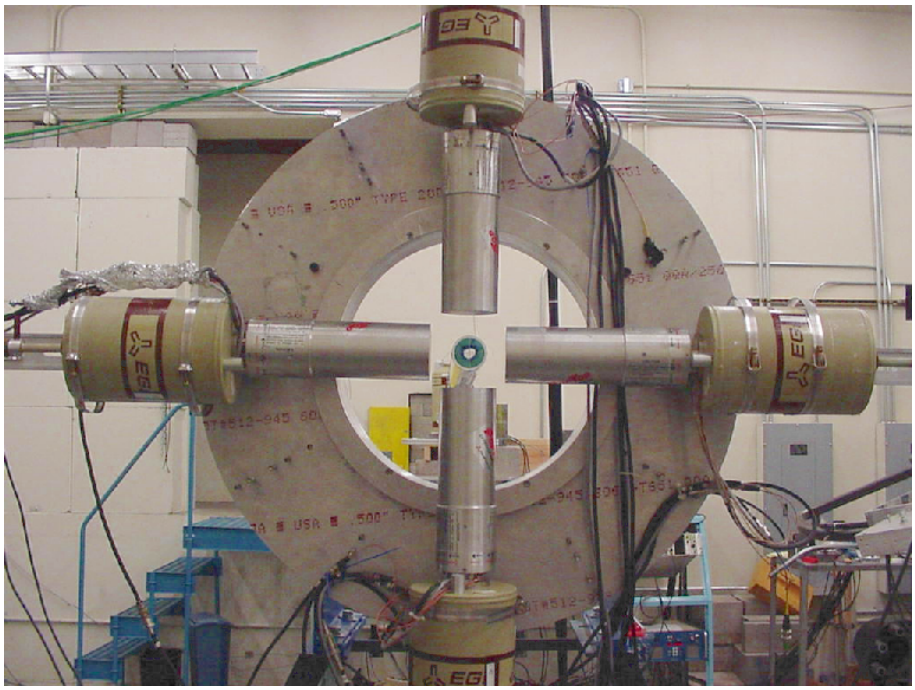

Figure 2.6: *The NRF setup at the HIγS facility consists of four 60 % HPGe detectors perpendicular to the beam axis, two in the horizontal plane and two in the vertical plane. In the middle the cylindrical NRF target can be seen, and in the back the additional* 0° *detector is visible.*

2.1.4 Angular correlations with polarized photons

This section deals with the special situation that the incident photon beam is linearly polarized. The formalism on how polarization affects angular $\gamma\gamma$-correlation functions was given years ago, *e.g.* in [BiR53, Sat55, FaH59, KSW73]. But, various and inconsistent definitions for the multipole mixing parameter δ and different conventions for F-coefficients were used. Thus, the derivation of angular correlation functions for the application on HIγS data will be shown in the following. It is fully consistent with the formulas given in [Pie03], only with slight differences in the notation.

In the following a cascade of two γ-transitions (γ_1,γ_2) from an initial state j_i via an intermediate state j to a final state j_f is considered. In general, electromagnetic transitions have mixed multipolarities, that means that at least two multipolarities ΠL and $\Pi' L'$ occur. The cascade is then written as

$$j_i(\Pi_1 L_1, \Pi_1' L_1') j (\Pi_2 L_2, \Pi_2' L_2') j_f \ . \tag{2.16}$$

A multipole mixing ratio δ can be defined following the phase convention of Krane, Steffen and Wheeler [KSW73] by

$$\delta_n = \frac{\langle j_{n+1} || \vec{j}_N \vec{A}_L^{\Pi} || j_n \rangle}{\langle j_{n+1} || \vec{j}_N \vec{A}_{L'}^{\Pi'} || j_n \rangle} \ , \tag{2.17}$$

where $\vec{j}_N$ is the nuclear current operator and $\vec{A}_L^{\Pi}$ are the multipole fields. The matrix elements in (2.17) are reduced matrix elements as defined by the Wigner-Eckart theorem

$$\langle j_{n+1} m_{n+1} | \vec{j}_N \vec{A}_L^{\Pi} | j_n m_n \rangle = C^{j_{n+1} m_{n+1}}_{j_n m_n \ LM} \ \frac{\langle j_{n+1} || \vec{j}_N \vec{A}_L^{\Pi} || j_n \rangle}{\sqrt{2 j_{n+1} + 1}} \ . \tag{2.18}$$

The $C^{JM}_{j_1 m_1 \ j_2 m_2}$ are Clebsch-Gordan coefficients. The multipole mixing ratios δ defined in Eq. (2.17) differ from those of Biedenharn and Rose, δ_{BR} [BiR53], by

$$\delta_1 = (-1)^{L+L'} \delta_{BR}(\gamma_1) \tag{2.19}$$

$$\delta_2 = \delta_{BR}(\gamma_2) \ . \tag{2.20}$$

Without any knowledge of the polarization the angular directional correlation for two mixed multipole γ-radiations writes

$$W(\theta) = \sum_{\nu} B_\nu(1) A_\nu(2) P_\nu(\cos\theta) \tag{2.21}$$

with the angle θ relative to the quantization axis, the orientation coefficient

$$B_\nu(1) = \frac{1}{1+\delta_1^2} \Big(F_\nu(L_1 L_1 j_i j) + (-1)^{L_1+L_1'} 2\delta_1 F_\nu(L_1 L_1' j_i j) + \delta_1^2 F_\nu(L_1' L_1' j_i j) \Big) \tag{2.22}$$

for the first γ-transition that defines the quantization axis, and the directional distribution coefficient

$$A_\nu(2) = \frac{1}{1+\delta_2^2}\left(F_\nu(L_2L_2j_fj) + 2\cdot\delta_2 F_\nu(L_2L_2'j_fj) + \delta_2^2 F_\nu(L_2'L_2'j_fj)\right) \qquad (2.23)$$

for the second γ-transition. The $F_\nu(LL'j_nj)$ are the well known ordinary F-coefficients, tabulated, *e.g.*, in [FrS65]. They are given by

$$\begin{aligned} F_\nu(LL'j_nj) &= (-1)^{j_n+j-1}\sqrt{(2L+1)(2L'+1)(2j+1)(2\nu+1)} \\ &\quad\cdot \begin{pmatrix} L & L' & \nu \\ 1 & -1 & 0 \end{pmatrix} \begin{Bmatrix} L & L' & \nu \\ j & j & j_n \end{Bmatrix} , \end{aligned} \qquad (2.24)$$

including a Wigner 3j- and a 6j-symbol. If one of the γ-rays is polarized, the appropriate coefficient (2.22) or (2.23) has to be changed. This procedure is given by Fagg and Hanna [FaH59], but one has to be careful as Eqs. (I-4 – I-6) from [FaH59] as explained in their text are somewhat misleading. Here, we switch to the Krane, Steffen and Wheeler phase convention for δ. In our case the first photon which orientates the nucleus is polarized and the $B_\nu(1)$ coefficients have to be modified. Each term of the sum in Eq. (2.21) containing a term of $B_\nu(1)$ is affected. This is done exchanging the term $B_\nu(1)P_\nu(\cos\theta)$ by

$$\begin{aligned} BP_\nu(1) := B_\nu(1)P_\nu(\cos\theta) &+ \frac{1}{1+\delta_1^2}\cos 2\phi P_\nu^{(2)}(\cos\theta) \\ &\cdot[(\pm)_{L_1}\kappa_\nu(L_1L_1)F_\nu(L_1L_1j_ij) \\ &+(-1)^{L_1+L_1'}(\pm)_{L_1'}\kappa_\nu(L_1L_1')2\delta_1 F_\nu(L_1L_1'j_ij) \\ &+(\pm)_{L_1'}\kappa_\nu(L_1'L_1')F_\nu(L_1'L_1'j_ij)] \ , \end{aligned} \qquad (2.25)$$

where the $(\pm)_L$ gives a positive sign if the multipole radiation L is electric, and a negative sign if it is magnetic. ϕ is the rotation angle around the beam axis. The coefficients κ_ν are given by

$$\kappa_\nu(LL') = -\sqrt{\frac{(\nu-2)!}{(\nu+2)!}}\ \frac{C^{\nu 2}_{L1\ L'1}}{C^{\nu 0}_{L1\ L'-1}} \ . \qquad (2.26)$$

The $P_\nu^{(\mu)}(\cos\theta)$ are the unnormalized associated Legendre polynomials. They are given by

$$P_\nu^{(\alpha,\beta)}(x) = (\nu+\alpha)!(\nu+\beta)!\sum_s \frac{\left(\frac{x-1}{2}\right)^{\nu-s}\left(\frac{x+1}{2}\right)^s}{s!(\nu+\alpha+s)!(\beta+s)!(\nu-s)!} \qquad (2.27)$$

$$P_\nu^{(\mu)}(\cos\theta) = \frac{(\nu+\mu)!}{\nu!}\left(\frac{\sin\theta}{2}\right)^\mu P_{\nu-\mu}^{(\mu,\mu)}(\cos\theta) \qquad (2.28)$$

and associated to the usual Legendre polynomials by

$$P_\nu(\cos\theta) = P_\nu^{(0)}(\cos\theta) \ . \qquad (2.29)$$

Finally, the angular correlation function for the case of incident polarized photons is given by

$$W(\theta, \phi) = \sum_{\nu} BP_{\nu}(1) A_{\nu}(2) \ . \tag{2.30}$$

Values of the F-coefficients, the κ_{ν} coefficients, hence the modified orientation coefficients BP_{ν}, the angular distribution coefficients A_{ν}, and finally the angular correlation function (2.30) have been computed using the code MATHEMATICA [MATH]. In Figure 2.7 the angular correlation functions for the spin cascades that are most interesting in NRF experiments are shown, magnetic and electric dipole excitations, and electric quadrupole excitations from a 0^+ ground state and the decay back to the ground state. Arrows above the ΠL multipole radiation denote the polarization of the γ-rays. In the cases of polarized incident photons one obtains distributions for the second (the emitted) γ-rays as shown in Figure 2.7. The photon beam, that is the incoming γ_1, moves in z-direction, which is the quantization axis. The electric vector of the incoming photons is parallel to the x-axis, as it is the case at the HIγS facility. Therefore, even-even nuclei with a 0^+ ground state, excited to a 1^- state by the polarized γ-rays can emit light only perpendicular to the x-axis when decaying to the ground state by a dipole transition. This is an analog to the classical Hertz dipole with no emittance in the direction of the dipole axis, $W(\theta = 90°, \phi) = 0$ for $\phi = 0°, 180°$. For a M1 excitation the situation is the same, but turned by 90° around the z-axis, as the M1 vector is perpendicular to the E1 vector. Therefore, with detectors at $\phi = 0°$ and $\phi = 180°$, one can easily distinguish between an electric and a magnetic dipole excitation. If a 2^+ state is excited and decays to the ground state, the emitted γ-rays show a distribution as shown in bottom part of Figure 2.7.

In the following, the angular distribution in the horizontal plane ($\theta = 90°, \phi = 0°, 180°$) is denoted by W^{hor}, and in the vertical plane ($\theta = 90°, \phi = 90°, 270°$) it is denoted by W^{ver}. As already noted in the previous subsection, these angles are ideal for the determination of the parity of dipole states. This can immediately be seen from Figure 2.7. For a positive parity state one should see the second γ-ray from the decay to the ground state in an even-even nucleus only in the horizontal plane, for a negative parity state in the vertical plane. The analyzing power is defined as

$$P_{ana} = \frac{W^{hor} - W^{ver}}{W^{hor} + W^{ver}} \tag{2.31}$$

and is 100% in these cases. P_{ana} is a function of the multipole mixing parameters $\delta_{1,2}$ alone. If δ_1 is already known from spin and parity of the excited state and the second γ-transition connects the state with a lower-lying excited state, the measurement of the analyzing power allows in principle to determine values for δ_2. However, solutions for δ_2 are not always unique and good statistics are needed. Note that the case of unpolarized light is included in the description above. Unpolarized light is equivalent to adding up horizontal and vertical components

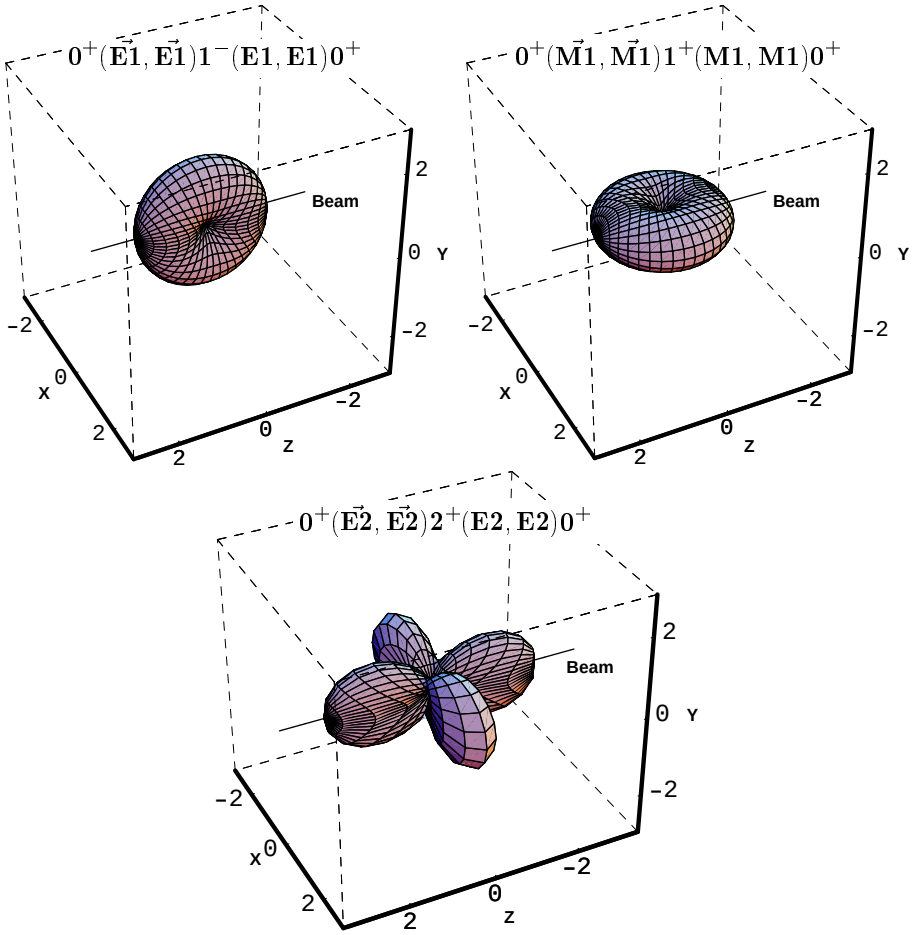

Figure 2.7: *Angular correlation functions $W(\theta,\phi)$, representing the angular distribution of the second γ-ray in the given spin sequences. The distributions for polarized incident γ-radiation are shown. The polarization plane of the electric component of the incoming photons lies in the x-z-plane. The beam direction is parallel to the z-axis, which is the quantization axis.*

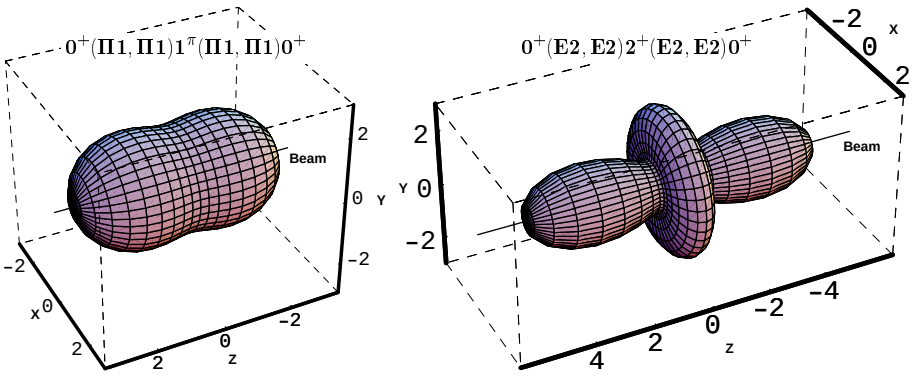

Figure 2.8: *Same as Figure 2.7, but for unpolarized incident γ-radiation. The beam direction is parallel to the z-axis being the quantization axis.*

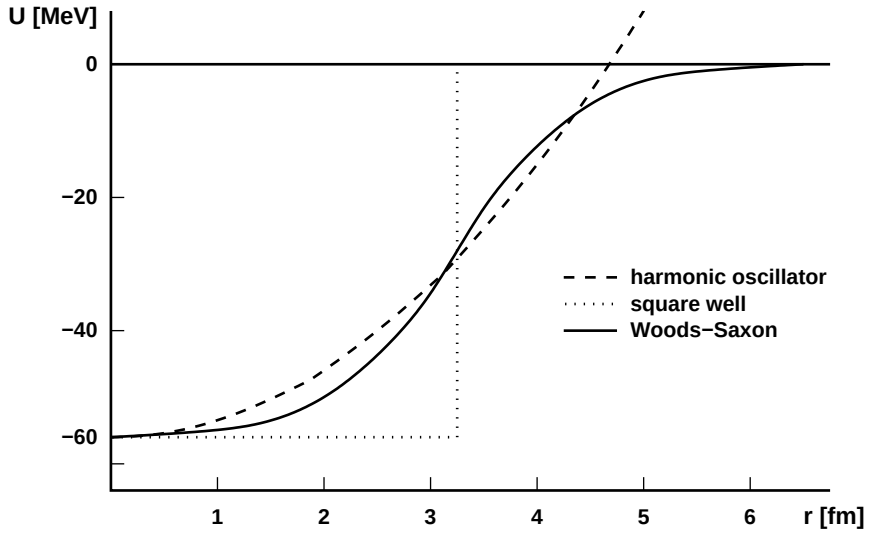

Figure 2.9: *Comparison of harmonic oscillator, square well, and Woods-Saxon potentials. The harmonic oscillator is a good and easily solvable approximation to the more realistic Woods-Saxon potential.*

of the incident photons. This can be achieved by adding

$$W^{unpol}(\theta,\phi) = W^{hor}(\theta,\phi) + W^{ver}(\theta,\phi) \ . \tag{2.32}$$

This leads to the angular distributions shown in Figure 2.8, which are well known in the conventional NRF method using unpolarized γ-rays. They correspond to the angular distributions given by Eqs. (2.1) and (2.2).

2.2 The Shell Model

In this work, calculations for near spherical nuclei were performed within the nuclear shell model. In the following a short introduction to the shell model and the interaction used is given.

2.2.1 The basic concept

In the atomic nucleus, the long range Coulomb interaction competes with the short range attractive nuclear force, binding the constituents of the nucleus, the protons and neutrons. Incorporating one- and two-body terms, the Hamiltonian for the many-body problem of a nucleus with A nucleons is

$$H = \sum_{i=1}^{A} t_i + \sum_{i<j=1}^{A} v_{ij} \ , \tag{2.33}$$

where t_i are the kinetic energies of the nucleons and v_{ij} are the interactions between two particles i and j. The strong nuclear force and its short range allow the assumption that all nucleons inside the nucleus have more or less the same potential energy. In a schematic picture they all are surrounded by the other nucleons, having the same number of neighbors and the same average interaction strength v_{ij}. This would lead to an average potential for all nucleons which is very similar to a square-well. But in the picture of the neighboring nucleons, nucleons close to the edge of the nucleus should be less bound, leading to a softening of the edge of the radial potential. A phenomenological potential describing the shape of the average, or mean-field, nuclear potential is given by the Woods-Saxon potential. In first order the potential can be approximated by a harmonic oscillator as shown schematically in Figure 2.9. An average potential field $U(r)$ can be included in the Hamiltonian (2.33) as

$$H = \sum_i t_i + \sum_i U_i + \sum_{i<j} v_{ij} - \sum_i U_i \tag{2.34}$$

and with

$$H_0 = \sum_i t_i + \sum_i U_i \qquad \text{and} \tag{2.35}$$

$$V_{res} = \sum_{i<j} v_{ij} - \sum_i U_i \tag{2.36}$$

the Hamiltonian writes

$$H = H_0 + V_{res} \ . \tag{2.37}$$

The term H_0 includes the kinetic energy and the mean field and determines the single particle energies of the nucleons, while V_{res} incorporates all two-body interactions between the particles that are not included in the mean-field and is called residual interaction. These residual interactions are the most important part of the Hamiltonian, as they define the structure of a given nucleus.

The discovery, which lead to the nuclear shell model, was the existence of very stable nuclei at the so called *magic* proton and neutron numbers 8, 20, 28, 50, 82 and 126. With a harmonic oscillator potential the energies of the single particle orbitals characterized by the oscillator quantum number n did not show large energy gaps which would be an explanation for the higher magic numbers. Also including a $\boldsymbol{l^2}$ term in H_0 did not lead to the observed single particle energies. This led M. Goeppert-Mayer, J.H.D. Jensen, O. Haxel, and H.E. Suess [May49, Hax49] to the addition of a strong $\boldsymbol{l.s}$ term for spin-orbit splitting. The resulting average nuclear potential is

$$U(r) = \frac{1}{2} m\omega^2 r^2 + C\ \boldsymbol{l}^2 - D\ \boldsymbol{l.s} \tag{2.38}$$

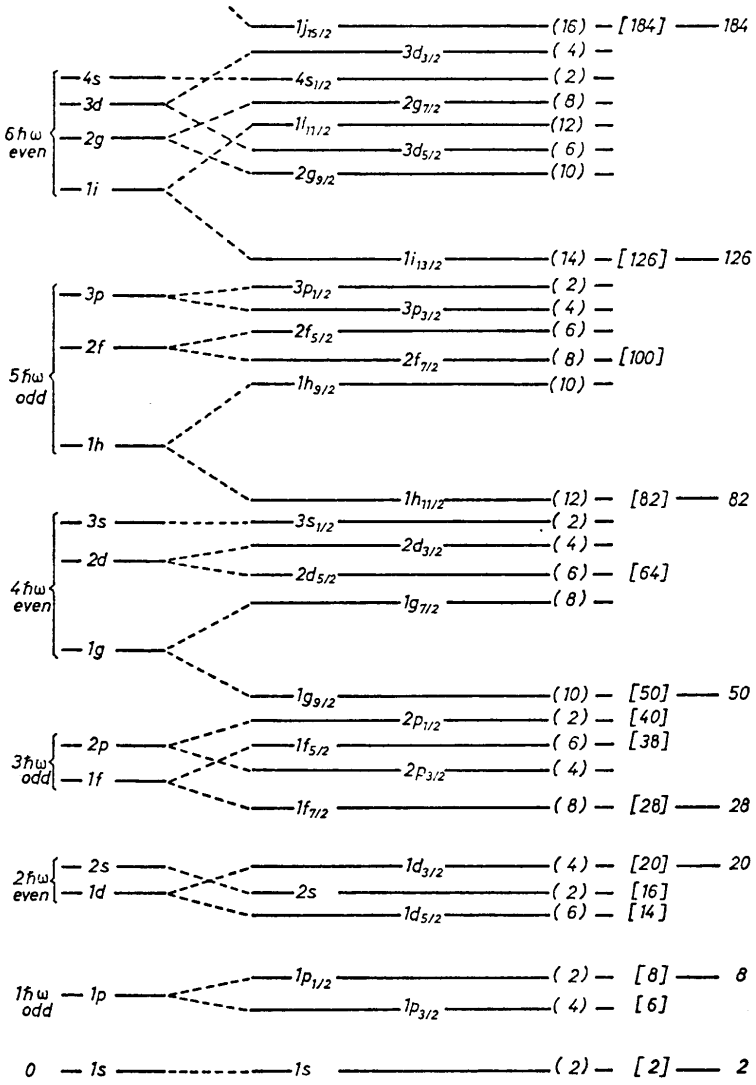

Figure 2.10: *The sequence of single particle levels for a Hamiltonian including a central harmonic oscillator potential, a centrifugal* $\boldsymbol{l}^2$ *term, and a spin-orbit term* $\boldsymbol{l}.\boldsymbol{s}$. *(Taken from [May55].)*

and the $\boldsymbol{l.s}$ term can simply be given as

$$\begin{aligned} -C\ \boldsymbol{l.s} &= -\frac{1}{2}\left(\boldsymbol{j}^2 - \boldsymbol{l}^2 - \boldsymbol{s}^2\right) \\ &= -\frac{1}{2}\left(j(j+1) - l(l+1) - \frac{3}{4}\right) \\ &= \begin{cases} l+1 & \text{for} \quad j = l - \frac{1}{2} \\ -l & \text{for} \quad j = l + \frac{1}{2} \end{cases} . \end{aligned} \tag{2.39}$$

It is known that

$$D \propto \frac{1}{r}\frac{dU(r)}{dr} \tag{2.40}$$

with D from Eq. (2.38). With the shape of the nuclear average potential in mind (Figure 2.9), this makes the spin-orbit force a surface effect. The spin-orbit splitting finally leads to the observed shell structure, and the magic numbers are described correctly, as shown in Figure 2.10. The degeneracy of the harmonic oscillator levels is broken by the $\boldsymbol{l^2}$ term, and the spin-orbit term splits the levels according to the particle spin. n, l, and s are the quantum numbers for the oscillator shell, the angular momentum, and the spin, respectively, and $j = l \pm 1/2$. The resulting orbitals are denoted by nl_j, where l is represented by $s, p, d, f, \ldots$ for $l = 0, 1, 2, 3, \ldots$.

Taking into account the full Hilbert space of the Hamiltonian (2.37) is impossible for practical model calculations, due to the large (infinite) number of particles and orbitals. For the two-body interactions 2^A terms would play a role, producing a matrix that is impossible to diagonalize nowadays. Subsequently, the shell model leads to the idea of a rude truncation of the Hilbert space by the concept of an inert core. In this concept a nucleus with magic proton and neutron numbers is regarded as closed. This means, that no excitations from orbitals below the magic number are allowed. In addition, the number of orbitals above the inert core is limited to only a few orbitals. This limitation is in principle arbitrary - the model space is chosen in order to describe certain physical properties of the atomic nucleus. Thus, the numbers of orbitals and the numbers of valence particles outside the closed shells can be limited. One turns to an effective Hamiltonian and effective operators, so that the Schrödinger equation is modified to

$$H\psi = E\psi \longrightarrow H_{eff}\psi_{eff} = E\psi_{eff} , \tag{2.41}$$

where the derived wave functions ψ_{eff} are generally only a small part of the real and complicated wave functions ψ due to the limitations. Nevertheless, the success of the shell model shows that this small part carries the main physical properties.

In the second quantization the Hamiltonian can be written as

$$H = \sum_{ij}^{A} \langle i|T|j\rangle a_i^\dagger a_j + \sum_{ijkl}^{A} \langle ij|W|kl\rangle a_i^\dagger a_j^\dagger a_l a_k \ , \tag{2.42}$$

with $a_i^\dagger$ and a_i being particle creation and annihilation operators, respectively. Defining a core, the Hamiltonian is written as

$$H = \sum_{i}^{A} \epsilon_i a_i^\dagger a_i + \frac{1}{4} \sum_{ijkl}^{A} \langle ij|V|kl\rangle a_i^\dagger a_j^\dagger a_l a_k \ . \tag{2.43}$$

V is the residual interaction. The ϵ_i are single particle energies which are taken from data and incorporate the average nuclear potential representing the binding energies of a particle in the i-th orbital. Calculations in this work have been carried out using the code RITSSCHIL [Zwa85] which works in the JT-coupled scheme. In this scheme the two-body interaction is written as

$$V = \frac{1}{4} \sum_{j_1 j_2 j_3 j_4} \sum_{m_1 m_2 m_3 m_4} \langle j_1 m_1 j_2 m_2|V|j_3 m_3 j_4 m_4\rangle a^\dagger_{j_1 m_1} a^\dagger_{j_2 m_2} a_{j_4 m_4} a_{j_3 m_3} \ . \tag{2.44}$$

Introducing

$$\tilde{a}_{jm} = (-1)^{j+m} a_{j-m} \tag{2.45}$$

and the tensor coupling

$$\left[a^\dagger_{j1} a^\dagger_{j2}\right]^J_M = \sum_{m1m2} C^{JM}_{j_1 m_1 \ j_2 m_2} a^\dagger_{j_1 m_1} a^\dagger_{j_2 m_2} \tag{2.46}$$

one obtains

$$\begin{aligned} V = \frac{1}{4} \sum_{j_1 j_2 j_3 j_4 JT} \langle j_1 j_2|V|j_3 j_4\rangle^{JT} \sqrt{(2J+1)(2T+1)(1+\delta_{j_1 j_2})(1+\delta_{j_3 j_4})} \\ \times \left[\left[a^\dagger_{j1} a^\dagger_{j2}\right]^{JT} \times [\tilde{a}_{j1} \tilde{a}_{j2}]^{JT}\right]^{00} \ , \end{aligned} \tag{2.47}$$

where J denotes the total spin to which particles 1 and 2 and particles 3 and 4 couple, while T denotes their total isospin.

2.2.2 The Surface Delta Interaction

Finding a good residual interaction for a certain nuclear region is probably the most challenging problem in the nuclear shell model. State of the art methods start from a microscopic description of the nucleon-nucleon interaction, building a so-called G-matrix. Interactions derived in such way are referred to as realistic

interactions. Nevertheless, it is known from M. Dufour and A. Zuker [DuZ96], that the effective interaction and thus the Hamiltonian splits into a monopole and a multipole part. While the multipole part is usually well described by realistic interactions, the monopole part turns out to be unphysical and needs to be corrected. In the framework of this thesis shell model calculations were performed in the A=90 mass region, around ^{88}Sr. In this region, no good realistic interaction is known yet, and one has to turn to schematic interactions, which are approximative effective forces, built in a mathematically simple way while containing the essential physical features. For spherical nuclei, a successful schematic interaction is the surface delta interaction (SDI) [Pla66].

The surface delta interaction incorporates the following assumptions:

- The interaction takes place at the nuclear surface alone.
  This assumption is justified by considering the kinetic energy T of a particle in the nucleus in a given orbital. Due to energy conservation, with the particle inside the potential $U(r)$, the sum $T+U$ has to be constant. Thus, the kinetic energy must be smaller if the particle is on the edge of the potential rather than inside (compare Figure 2.9), and the probability for interactions with other nucleons increases.

- The two-body interaction is a delta force.
  This approximation is justified by the fact that the nucleon-nucleon interaction is of short range. This allows the assumption, that nucleons interact only if they are at the same place.

- The probability of a particle being at the nuclear surface does not depend on its shell model orbit.
  This may be assumed because it is known that the amplitudes of the wave functions for different shell model orbitals do not differ very much at the nuclear surface ($r = R_0$, nuclear radius).

Making these assumptions the interaction between two particles 1 and 2 simply writes

$$V^{SDI}(1,2) = -4\pi A'_T \delta(\boldsymbol{r}(1) - \boldsymbol{r}(2))\delta(\boldsymbol{r}(1) - R_0) \tag{2.48}$$

with the position $\boldsymbol{r}(i)$ for particle i. A'_T is a free parameter, where T labels the isospin to which both particles couple. Though it might seem more elegant to denote this parameter by the total spin S to which the two particles couple, in most cases the notation T is used. The notations are equivalent, as they are related by

$$\left\{ \begin{array}{l} S=0 \\ S=1 \end{array} \right\} \leftrightarrow \left\{ \begin{array}{l} T=1 \\ T=0 \end{array} \right\} . \tag{2.49}$$

If $V^{SDI}(1,2)$ mixes two states with two particles in the orbitals j_1 and j_2 or j_3 and j_4, respectively, the matrix element can be factorized in a radial part and an

angular part,

$$\langle j_1 j_2|V^{SDI}(1,2)|j_3 j_4\rangle = -A'_T\langle M_{rad}\rangle\langle M_{ang}\rangle^{JT} \ . \tag{2.50}$$

The superscript JT denotes the spin and isospin to which the particles are coupled. The value of the radial integral $C(R_0)$ depends only on the nuclear radius and can be combined with the parameter A'_T so that

$$A_T = A'_T \ C(R_0) \ . \tag{2.51}$$

From phenomenological observations one can improve the SDI by a modification, shifting levels with $T = 0$ and $T = 1$ relative to each other and enhancing the description of binding energies. The modified surface delta interaction is

$$V^{MSDI}(1,2) = V^{SDI}(1,2) + B\boldsymbol{\tau}(1).\boldsymbol{\tau}(2) + C \tag{2.52}$$

with the additional parameters B and C, where the isospin term takes the values

$$\langle \boldsymbol{\tau}(1).\boldsymbol{\tau}(2)\rangle^T = 2T(T+1) - 3 \tag{2.53}$$

and thus

$$\langle B\boldsymbol{\tau}(1).\boldsymbol{\tau}(2) + C\rangle^T = \begin{cases} -3B + C & \text{for} \quad T = 0 \\ B + C & \text{for} \quad T = 1 \end{cases} \ . \tag{2.54}$$

In the calculations described later only the SDI was used ($B = C = 0$). In this case matrix elements are given by

$$\begin{aligned} \langle j_1 j_2|V^{SDI}(1,2)|j_3 j_4\rangle^{JT} &= (-1)^{n_1+n_2+n_3+n_4}\frac{A_T}{2(2J+1)} \\ &\times \sqrt{\frac{(2j_1+1)(2j_2+1)(2j_3+1)(2j_4+1)}{(1+\delta_{12})(1+\delta_{34})}}\Big[(-1)^{j_2+j_4+l_2+l_4}C^{J0}_{j_2-\frac{1}{2}\ j_1\frac{1}{2}} \\ &\times C^{J0}_{j_4-\frac{1}{2}\ j_3\frac{1}{2}}\left(1-(-1)^{l_1+l_2+J+T}\right) - C^{J1}_{j_2\frac{1}{2}\ j_1\frac{1}{2}}\ C^{J1}_{j_4\frac{1}{2}\ j_3\frac{1}{2}}\left(1+(-1)^T\right)\Big] \ , \end{aligned} \tag{2.55}$$

which gives for the diagonal matrix elements

$$\begin{aligned} \langle j_1 j_2|V^{SDI}(1,2)|j_1 j_2\rangle^{JT} = -A_T\frac{(2j_1+1)(2j_2+1)}{2(2J+1)(1+\delta_{12})}\Bigg[&\left(C^{J0}_{j_2-\frac{1}{2}\ j_1\frac{1}{2}}\right)^2 \\ &\times\left(1-(-1)^{l_1+l_2+J+T}\right) + \left(C^{J1}_{j_2\frac{1}{2}\ j_1\frac{1}{2}}\right)^2\left(1+(-1)^T\right)\Bigg] \end{aligned} \tag{2.56}$$

for the diagonal matrix elements and one finds the useful relation

$$|\langle j_1 j_2|V^{SDI}(1,2)|j_3 j_4\rangle^{JT}| = R\sqrt{\langle j_1 j_2|V^{SDI}(1,2)|j_1 j_2\rangle^{JT}\langle j_3 j_4|V^{SDI}(1,2)|j_3 j_4\rangle^{JT}} \tag{2.57}$$

between diagonal and off-diagonal matrix elements with

$$R = \begin{cases} 0 & \text{for} \quad (l_1 + l_2 + J = odd) \wedge (T = 0) \\ 1 & \text{else} \end{cases} \quad . \tag{2.58}$$

For the parameters A_T one has to take into account the parameters for the proton-proton ($T = 1$) interaction A_{pp}, for the neutron-neutron ($T = 1$) interaction A_{nn}, and two parameters for the proton-neutron interaction as protons and neutrons may couple to $T = 0$ or $T = 1$, hence $A_{pn}^{T=0}$ and $A_{pn}^{T=1}$, respectively. A more detailed description of the SDI can be found in [BrG77].

2.3 The Interacting Boson Model

Data and shell model calculations will be compared to predictions of the interacting boson model (IBM). For a review refer to [IaA87] and to the references given in the text. This model provides very intuitive access to many aspects of nuclear structure. In the following the basic idea and concept of the IBM shall be discussed, more precisely of the *sd*-IBM in its version 1, not distinguishing between protons and neutrons, and its version 2, introducing the proton and neutron labels.

2.3.1 *sd*-IBM-1

The approximations for the shell model as described in 2.2.1, 2.2.2 form the starting point for the IBM. A doubly magic core is defined and only the valence space of particles in orbitals outside the core or holes inside is considered. Nevertheless, even this extensive truncation of the full shell model leaves the numerical problem of the diagonalization of a huge matrix, if the valence space becomes large. Thus, more truncations have to be made in order to reduce the dimension of the problem. Therefore, for the description of nuclei with even numbers of protons Z and neutrons $A - Z$, only pairs of nucleons occupying the same orbital are considered. Such pairs are allowed to couple to $J = 0$ or $J = 2$ only. This restriction is justified by taking into account that pairing is strong. The pairing force lowers the 0^+ member of the multiplet formed by coupling two nucleons with spin j in the same orbital. Actually, pairing is a phenomenological approach to describe the fact that in a $(j^2)_J$ configuration the 0^+ member is always lowered most relative to the rest of the multiplet, followed by the 2^+ member. This is a characteristic of the short range residual interaction, *e.g.* δ- or δ-like interactions. Due to the Pauli principle, the two particles are favored to be spatially symmetric, that means, occupying the magnetic substates with m and $-m$.

The IBM is founded on a bosonization of the nuclear fermionic system, that means mapping the $(j^2)_{J=0,2}$ configurations to a bosonic space. Therefore, the $J = 0^+$ configuration is represented by an s-boson, while the $J = 2^+$ configuration

is represented by a d-boson. In the IBM-1 no difference is made between proton and neutron bosons. As a counting rule for the boson number N, one starts from the nearest shell closure, regardless of counting particles or holes. One counts every two particles of one kind as one boson. In the second quantization one writes boson creation and annihilation operators as

$$\begin{array}{ll} s^\dagger, d^\dagger_\mu & (\mu = 0, \pm 1, \pm 2) \ , \\ s, d_\mu & (\mu = 0, \pm 1, \pm 2) \ , \end{array} \tag{2.59}$$

where the d-boson has five magnetic substates, the s-boson only has one. Denoting the bosons by $b_{l,m}$ where l denotes the angular momentum and m denotes the magnetic substate, the operators (2.59) fulfill the commutation relations for bosons

$$\begin{array}{ll} [b_{l,m}, b^\dagger_{l',m'}] = \delta_{ll'}\delta_{mm'} & , \\ [b_{l,m}, b_{l',m'}] = [b^\dagger_{l,m}, b^\dagger_{l',m'}] = 0 & . \end{array} \tag{2.60}$$

One constructs spherical tensors introducing

$$\tilde{b}_{l,m} = (-1)^{l+m} b_{l,-m} \ . \tag{2.61}$$

Thus, in the sd-IBM-1 one uses the creation and annihilation operators

$$\begin{array}{ll} s^\dagger, d^\dagger_\mu & (\mu = 0, \pm 1, \pm 2) \ , \\ \tilde{s} = s, \ \tilde{d}_\mu = (-1)^\mu d_{-\mu} & (\mu = 0, \pm 1, \pm 2) \ , \end{array} \tag{2.62}$$

which span a six-dimensional space. The tensor product is used in the same way as given in Eq. (2.46). The complete Hamiltonian of the IBM-1 can be expanded to a sum over all n-body terms using the boson constituents. Usually one restricts the Hamiltonian to include only one- and two-body terms. Also transition operators can be written in terms of boson creation and annihilation operators, where one usually stops at one-body terms. A very useful and more intuitive way is to switch to the multipole expansion of the Hamiltonian and the transition operators. The multipole operators can be written as

$$\boldsymbol{n_d} = (d^\dagger . \tilde{d}) \ , \tag{2.63}$$

$$\boldsymbol{L} = \sqrt{10} \left[d^\dagger \tilde{d} \right]^{(1)} \ , \tag{2.64}$$

$$\boldsymbol{Q}^\chi = \left[d^\dagger \tilde{s} + s^\dagger \tilde{d} \right]^{(2)} + \chi \left[d^\dagger \tilde{d} \right]^{(2)} \ , \tag{2.65}$$

$$\boldsymbol{U} = \left[d^\dagger \tilde{d} \right]^{(3)} \ , \tag{2.66}$$

$$\boldsymbol{V} = \left[d^\dagger \tilde{d} \right]^{(4)} \tag{2.67}$$

and the Hamiltonian takes the form

$$H = E_0 + \varepsilon \ \boldsymbol{n_d} + \lambda \ \boldsymbol{L}.\boldsymbol{L} + \kappa \ \boldsymbol{Q}^\chi.\boldsymbol{Q}^\chi + c_3 \ \boldsymbol{U}.\boldsymbol{U} + c_4 \ \boldsymbol{V}.\boldsymbol{V} \ . \tag{2.68}$$

(There are other representations, *e.g.*, ones using a pairing operator). The transition operators can then be written as

$$\begin{aligned} \boldsymbol{T(E0)} &= \gamma_0 + \beta_0 \, \boldsymbol{n_d} \ , & (2.69)\\ \boldsymbol{T(M1)} &= g \, \boldsymbol{L} \ , & (2.70)\\ \boldsymbol{T(E2)} &= e_B \, \boldsymbol{Q}^{\chi'} \ , & (2.71)\\ \boldsymbol{T(M3)} &= \beta_3 \, \boldsymbol{U} \ , & (2.72)\\ \boldsymbol{T(E4)} &= \beta_4 \, \boldsymbol{V} \ , & (2.73) \end{aligned}$$

including only parity conserving operators as the model describes only positive parity states. For the description of negative parity states, bosons with higher angular momentum, *e.g.*, an f boson (L=3), must be added. In the Consistent Q Formalism (CQF) [WaC82], the same quadrupole operator (2.65) is used for the Hamiltonian and the $E2$ transitions, hence $\chi' = \chi$.

Often a Hamiltonian including only the $\boldsymbol{n_d}$- and the quadrupole terms is used. This is referred to as the Extended Consistent Q Formalism (ECQF) [Lip85]. It describes the key features of atomic nuclei over a broad range of structures. This is due to the importance of the quadrupole interaction, which emerges from the short range residual interaction and also is reflected in the use of δ-forces. The parameter κ is always negative as the quadrupole interaction is attractive. There are different ways of parametrizing the ECQF Hamiltonian, one is [Wer00b]

$$H_{ECQF} = a \, \left[(1-\zeta) \, \boldsymbol{n_d} - \frac{\zeta}{4N} \, \boldsymbol{Q}^{\chi}.\boldsymbol{Q}^{\chi} \right] \ . \qquad (2.74)$$

$N = N_\pi + N_\nu$ is the total number of bosons. Originally, a $\boldsymbol{L}.\boldsymbol{L}$ term was used in the ECQF Hamiltonian (2.74) which is neglected here as it influences only the energies of the eigenstates, but not the wave functions. Other ways of parametrizing the Hamiltonian were used in the past. Switching from one parametrization to another often turned out to be somewhat confusing. Therefore, relations between different parameters used are given in appendix A.

The six-dimensional space spanned by the boson operators shows the algebraic structure of the unitary six-dimensional group U(6). One can construct generators G_i from s- and d-bosons forming a Lie algebra. This procedure is described in detail in [IaA87]. One can show, that the generators of U(6), built by s- and d-boson operators form subalgebras X of U(6) which close under commutation, that means

$$[G_i, G_j] = \sum_k c_{ij}^k G_k \quad \text{, where all } G_{i,j,k} \in \text{X} \ . \qquad (2.75)$$

For example, using only the generators containing d-bosons, no s-bosons, one can construct the subalgebra U(5) - the five-dimensional space spanned by the

d-bosons. Finally, U(6) decomposes into three chains of subalgebras,

$$\mathrm{U}(6) \left\{ \begin{array}{ll} \supset \mathrm{U}(5) \supset \mathrm{O}(5) \supset \mathrm{O}(3) \supset \mathrm{O}(2) & \mathrm{(I)} \\ \supset \mathrm{SU}(3) \supset \mathrm{O}(3) \supset \mathrm{O}(2) & \mathrm{(II)} \\ \supset \mathrm{O}(6) \supset \mathrm{O}(5) \supset \mathrm{O}(3) \supset \mathrm{O}(2) & \mathrm{(III)} \end{array} \right. . \tag{2.76}$$

U(5), SU(3), and O(6) are called the dynamical symmetry limits of the IBM-1 in which a basis can be formulated and the eigenvalue problem can be solved analytically. U(5) corresponds to the anharmonic oscillator (due to its d-boson structure), and thus to vibrational nuclei, SU(3) corresponds to the axially symmetric rotor, and O(6) corresponds to so-called γ-soft rotors which are nuclei with a non-rigid triaxiality. The ECQF Hamiltonian (2.74) covers the dynamical symmetry limits for the parameter combinations

$$\begin{array}{lll} U(5) & \text{for} & (\zeta = 0, \chi \in [\frac{-\sqrt{7}}{2}, \frac{\sqrt{7}}{2}]) \ , \\ SU(3) & \text{for} & \left\{ \begin{array}{ll} (\zeta = 1, \chi = \frac{-\sqrt{7}}{2}) & \text{prolate} \\ (\zeta = 1, \chi = \frac{\sqrt{7}}{2}) & \text{oblate} \end{array} \right\} \ , \\ O(6) & \text{for} & (\zeta = 1, \chi = 0) \ . \end{array} \tag{2.77}$$

There are two parameter sets for the SU(3) limit. Both are connected to the symmetry transformation $d \to -d$. Nevertheless, they represent different types of nuclei. For $\chi = -\sqrt{7}/2$ one obtains a prolate deformed rotor, and the limit which was usually denoted with SU(3), and for $\chi = \sqrt{7}/2$ one obtains an oblate deformed rotor which may be denoted as $\overline{\mathrm{SU(3)}}$.

2.3.2 *sd*-IBM-2

The proton neutron extension of the *sd*-IBM-1 is the *sd*-IBM-2 [Ari77, Ots78, Ots78b, IaA87], introducing two kinds of s- and d-bosons. Thus, the model space is constructed upon the boson operators

$$\begin{array}{ll} s^\dagger_\rho, d^\dagger_{\rho,\mu} & (\mu = 0, \pm 1, \pm 2) \\ \tilde{s}_\rho, \ \tilde{d}_{\rho,\mu} & (\mu = 0, \pm 1, \pm 2) \end{array} \quad , \ \rho = \pi, \nu \tag{2.78}$$

for protons and neutrons, where the tilde above the annihilation operators denotes the transformation to spherical tensors as in Eq. (2.62). The underlying algebra of the IBM-2 is $\mathrm{U}_\pi(6) \times \mathrm{U}_\nu(6)$, with the subgroup $\mathrm{U}_{\pi+\nu}(6)$ derived by just adding the generators of $\mathrm{U}_\pi(6)$ and $\mathrm{U}_\nu(6)$. In analogy to the reduction chains of the IBM-1 one finds such chains for the IBM-2, leading to dynamical symmetry limits, *e.g.*, $\mathrm{U}_{\pi+\nu}(5)$, $\mathrm{SU}_{\pi+\nu}(3)$, or $\mathrm{O}_{\pi+\nu}(6)$. The distinction between protons and neutrons enriches the structure of the IBM-1. On the one hand, additional dynamical symmetry limits appear which shall not be discussed here, and on the other hand one finds eigenstates where protons and neutrons are not in phase. Therefore, the F-spin formalism was introduced [Ots78]. F-spin is a bosonic analogon to the

isospin formalism. Proton and neutron bosons have $F = 1/2$ and the z-projection is $F_z = +1/2$ for protons and $F_z = -1/2$ for neutrons. For a system of N_π proton bosons and N_ν neutron bosons the maximum F-spin is

$$F_{max} = \frac{N_\pi + N_\nu}{2} \geq F \geq \frac{|N_\pi + N_\nu|}{2} \ , \tag{2.79}$$

and the creation and annihilation operators are

$$F_+ = s_\pi^\dagger s_\nu + \sum_\mu d_{\pi,\mu}^\dagger \tilde{d}_{\nu,\mu} \ , \tag{2.80}$$

$$F_- = s_\nu^\dagger s_\pi + \sum_\mu d_{\nu,\mu}^\dagger \tilde{d}_{\pi,\mu} \ . \tag{2.81}$$

The projection operator is given by

$$F_z = \frac{1}{2}\left(\left(s_\pi^\dagger s_\pi + \sum_\mu d_{\pi,\mu}^\dagger \tilde{d}_{\pi,\mu}\right) - \left(s_\nu^\dagger s_\nu + \sum_\mu d_{\nu,\mu}^\dagger \tilde{d}_{\nu,\mu}\right)\right) \ . \tag{2.82}$$

The Hamiltonian of the IBM-2 can be written as

$$H = H_\pi + H_\nu + V_{\pi\nu} \tag{2.83}$$

where H_π and H_ν can be written in a multipole expansion completely analog to that of the IBM-1, given in Eq. (2.68). The term of the proton-neutron interaction $V_{\pi\nu}$ contains cross terms of the proton and neutron multipole operators of the kind, *e.g.*, $\boldsymbol{Q}_\pi^{\chi_\pi}.\boldsymbol{Q}_\nu^{\chi_\nu}$. The transition operators are sums over the proton and neutron transition operators which are analog to those given in (2.69)–(2.73), *e.g.*, the M1 and E2 transition operators are given by

$$\boldsymbol{T(M1)} = \sqrt{\frac{3}{4\pi}}\left(g_\pi \boldsymbol{L}_\pi + g_\nu \boldsymbol{L}_\nu\right) \ , \tag{2.84}$$

$$\boldsymbol{T(E2)} = e_\pi \boldsymbol{Q}_\pi^{\chi_\pi} + e_\nu \boldsymbol{Q}_\nu^{\chi_\nu} \ . \tag{2.85}$$

Both operators can be divided into F-scalar (denoted by s) and F-vector (denoted by v) parts [Har87]:

$$\boldsymbol{T(M1)}_s = \frac{g_\pi + g_\nu}{2}\left(\boldsymbol{L}_\pi + \boldsymbol{L}_\nu\right) \ , \tag{2.86}$$

$$\boldsymbol{T(M1)}_v = \frac{g_\pi - g_\nu}{2}\left(\boldsymbol{L}_\pi - \boldsymbol{L}_\nu\right) \ , \tag{2.87}$$

$$\boldsymbol{T(E2)}_s = \frac{e_\pi + e_\nu}{2}\left(\boldsymbol{Q}_\pi^{\chi_s} + \boldsymbol{Q}_\nu^{\chi_s}\right) \ , \tag{2.88}$$

$$\boldsymbol{T(E2)}_v = \frac{e_\pi - e_\nu}{2}\left(\boldsymbol{Q}_\pi^{\chi_v} - \boldsymbol{Q}_\nu^{\chi_v}\right) \tag{2.89}$$

with

$$\chi_s = \frac{e_\pi \chi_\pi + e_\nu \chi_\nu}{e_\pi + e_\nu} , \tag{2.90}$$

$$\chi_v = \frac{e_\pi \chi_\pi - e_\nu \chi_\nu}{e_\pi - e_\nu} . \tag{2.91}$$

The g_ρ are the orbital g-factors and usually set to $g_\pi = 1$ and $g_\nu = 0$, while e_ρ are effective charges. For the neutron it is common to use small values $e_\nu \approx 0$. One often uses a shortened version of the Hamiltonian (2.83), only including the boson number operators $\boldsymbol{n}_{d\rho}$ and the quadrupole interaction, which is again related to the dominance of the pairing interaction. In addition, the Majorana operator

$$\begin{aligned} \boldsymbol{M}_{\pi\nu} = & \left[s_\nu^\dagger \times \tilde{d}_\pi^\dagger - s_\pi^\dagger \times \tilde{d}_\nu^\dagger\right]^{(2)} . \left[\tilde{s}_\nu \times \tilde{d}_\pi - \tilde{s}_\pi \times \tilde{d}_\nu\right]^{(2)} \\ & - 2 \sum_{k=1}^{3} \left[d_\nu^\dagger \times \tilde{d}_\pi^\dagger\right]^{(k)} . \left[\tilde{d}_\nu \times \tilde{d}_\pi\right]^{(k)} \end{aligned} \tag{2.92}$$

is introduced, which represents a symmetry energy favoring states with protons and neutrons in phase. This operator causes an overall energy shift for states with $F < F_{max}$, which are called mixed-symmetry states. The states with $F = F_{max}$ are those that are described by the IBM-1. Finally the Hamiltonian is

$$H = E_0 + \varepsilon_\pi \, \boldsymbol{n}_{d\pi} + \varepsilon_\nu \, \boldsymbol{n}_{d\nu} + \kappa \, (\boldsymbol{Q}_\pi^{\chi_\pi} + \boldsymbol{Q}_\nu^{\chi_\nu}) . (\boldsymbol{Q}_\pi^{\chi_\pi} + \boldsymbol{Q}_\nu^{\chi_\nu}) + \lambda' \, \boldsymbol{M}_{\pi\nu} . \tag{2.93}$$

This form of the Hamiltonian conserves F-spin if $\varepsilon_\pi = \varepsilon_\nu$ and $\chi_\pi = \chi_\nu$. Nevertheless, as the quadrupole interaction between non-identical nucleons is known to be large, one often omits the proton-proton and the neutron-neutron parts, so that the Hamiltonian is reduced to

$$H = E_0 + \varepsilon_\pi \, \boldsymbol{n}_{d\pi} + \varepsilon_\nu \, \boldsymbol{n}_{d\nu} + \kappa' \, \boldsymbol{Q}_\pi^{\chi_\pi} . \boldsymbol{Q}_\nu^{\chi_\nu} + \lambda' \, \boldsymbol{M}_{\pi\nu} . \tag{2.94}$$

Note that the M1 operator in the IBM-2 is non-diagonal contrary to the IBM-1. In fact eigenstates of the IBM-2 Hamiltonian that differ by $\Delta F = 1$ are connected by the M1 operator. A very intuitive understanding of mixed-symmetry states, especially those with $F = F_{max} - 1$ which will be discussed in this work, is given by the Q-phonon scheme that will be described in the next section.

2.4 The Q-phonon scheme

2.4.1 Proton-neutron symmetric Q-phonons

From data and nuclear models like, *e.g.*, the IBM, one learns about quadrupole collectivity in the low-lying excitations of even-even nuclei. Thus, in nearly all

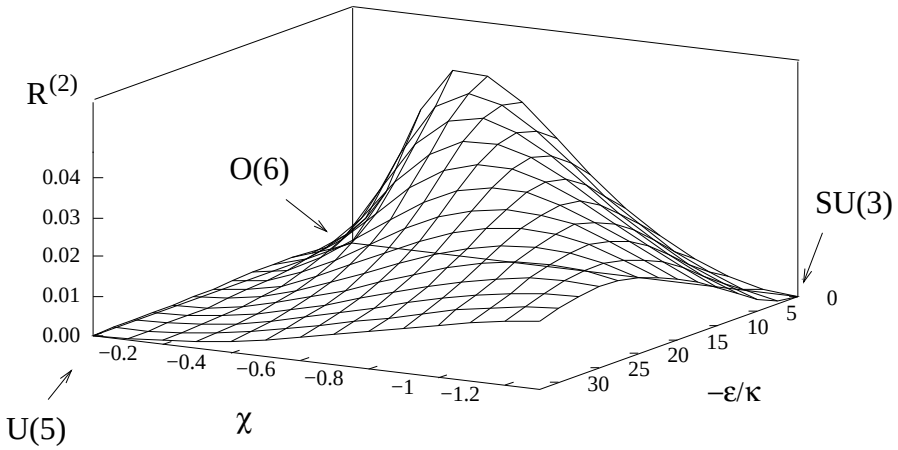

Figure 2.11: *The residual wave function $R^{(2)}$ of the 2_1^+ state from IBM-1 calculations over the whole parameter space of the ECQF for $N = 10$ bosons (taken from [Pie94]).*

even-even nuclei the first excited state is a 2^+ state, followed by a 4^+ state and so on. Taking into account the importance of the quadrupole interaction one can build a simple and intuitive scheme describing the low-lying levels of even-even nuclei as excitations by the E2, respectively quadrupole operator $\boldsymbol{Q}$. This scheme, hence called Q-phonon scheme, was invented by Siems and Otsuka [Sie94, Ots94]. The assumptions made are the following. The first 2^+ state is created by acting the quadrupole operator on the ground state,

$$|2_1^+\rangle_Q = \mathcal{N}_Q \; \boldsymbol{Q} \; |0_1^+\rangle \tag{2.95}$$

with a proper normalization constant $\mathcal{N}_Q$. In the framework of the IBM-1 it was shown by Pietralla *et al.* [Pie94] by calculations over the whole parameter space of the ECQF Hamiltonian that this assumption holds for all nuclei within an accuracy of only a few percent. The small deviations ($< 7\%$) from (2.95) stem from admixtures of higher Q-configurations to the first 2^+ state, while (2.95) is exact in the dynamical symmetry limits of the IBM. This is depicted in Figure 2.11 showing the portion of higher Q-configurations $R^{(2)}$ admixed to the 2_1^+ state. Following the Q-phonon scheme, higher-lying levels are multi-phonon configurations by coupling Q-phonons to a spin J. Thus, *e.g.*, a two-phonon multiplet is constructed by

$$|J^+\rangle_{QQ} = \mathcal{N}_{QQ}^{(J)} \; (\boldsymbol{QQ})^{(J)} \; |0_1^+\rangle = \frac{\mathcal{N}_{QQ}^{(J)}}{\mathcal{N}_Q} \; \boldsymbol{Q} \; |2_1^+\rangle_Q \quad \text{with} \quad J = 0, 2, 4 \tag{2.96}$$

and so on. Note that a two-phonon 0^+ state is not always apparent, *i.e.* within the ECQF in the O(6) dynamical symmetry limit modeling γ-soft nuclei it is identical to the ground state and thus the first excited 0^+ state in such nuclei

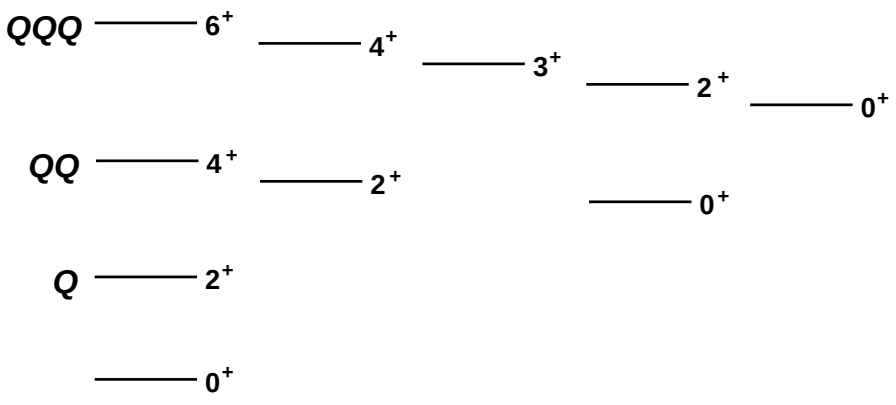

Figure 2.12: *Level scheme for vibrational nuclei built by Q-phonons. E2 transitions are allowed only between states that differ by* $\Delta Q = 1$.

is usually a three-phonon state. It was shown for higher-lying states that the Q-phonon scheme holds to a large extent over a broad range of structures, while one has to orthogonalize the multi-Q-configurations for a given spin J [Pie98].

In the Q-phonon scheme E2 transitions are only allowed between states that differ by one Q-phonon because $\boldsymbol{Q}$ is the E2 transition operator. Hence the selection rule is $\Delta Q = 1$. A typical Q-phonon scheme is illustrated in Figure 2.12. Despite the missing 0^+ state the level scheme of γ-soft nuclei looks very similar to that of vibrational nuclei. In the IBM this is understood due to the underlying O(5) algebra.

The level scheme looks very different in rotational nuclei, characterized by their K-quantum number. In such rotational nuclei, the quadrupole operator should rather be seen as an angular momentum driving operator. Nevertheless, the Q-phonon scheme also holds in the rotational limit.

2.4.2 Mixed-symmetry in the Q-phonon scheme

In general there are proton and neutron quadrupole operators, so that the Q-phonon scheme can be expanded for the description of mixed-symmetry states. For a symmetric coupling of the proton and neutron quadrupole operators one obtains a proton-neutron symmetric Q-phonon by

$$\boldsymbol{Q}_s = \boldsymbol{Q}_\pi + \boldsymbol{Q}_\nu \ , \tag{2.97}$$

which is identical to the Q-phonon given in the previous section. Hence

$$|2^+_{1s}\rangle = |2^+_1\rangle_Q = \mathcal{N}_s \ \boldsymbol{Q}_s \ |0^+_1\rangle \tag{2.98}$$

gives the proton-neutron symmetric one phonon 2^+ state. A second combination of the proton and neutron quadrupole operators is

$$\boldsymbol{Q}_m = \boldsymbol{Q}_\pi - a \ \boldsymbol{Q}_\nu \ , \tag{2.99}$$

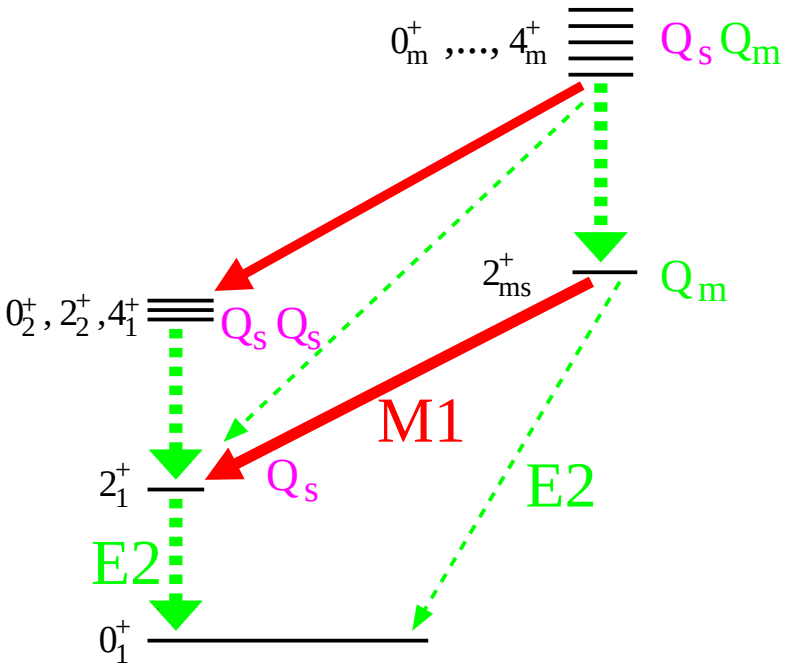

Figure 2.13: *Schematic picture of low-lying one- and two-phonon states. Dashed arrows denote E2, solid arrows M1 transitions. Strongly collective E2 transitions are expected from the creation or annihilation of a symmetric Q-phonon. Weakly collective E2 transitions are expected for a mixed-symmetric Q-phonon. M1 transition occur from the exchange of one Q_s- with one Q_m-phonon.*

where a is inserted in order to grant orthogonality to the symmetric Q-phonon. Acting this operator on the ground state gives a second, the mixed-symmetric one-phonon 2^+ state

$$|2^+_m\rangle = \mathcal{N}_m \; \boldsymbol{Q}_m \; |0^+_1\rangle \; . \tag{2.100}$$

In the IBM-2, using Hamiltonian (2.93) within the limit of good F-spin ($\varepsilon_\pi = \varepsilon_\nu$ and $\chi_\pi = \chi_\nu$), the mixed-symmetric Q-phonon writes [Kim98]

$$\boldsymbol{Q}_m = \frac{N}{2N_\pi}\boldsymbol{Q}_\pi - \frac{N}{2N_\nu}\boldsymbol{Q}_\nu \; . \tag{2.101}$$

However, if F-spin is broken, orthogonalizing the symmetric and mixed-symmetric Q-phonons becomes more complicated. Assuming good F-spin, the Q-phonon scheme gives a good understanding of mixed-symmetry states and the expected experimental signatures. Figure 2.13 shows a scheme of the lowest symmetric and mixed-symmetric one- and two-phonon levels in even-even nuclei. It shows that a strongly collective E2 transition from the symmetric one-phonon state to the ground state is expected, while the 2^+_m state is of comparably weak collectivity. This may qualitatively be understood by the relative sign in between the proton

and neutron operators. Actually, the relative sign in both operators may change as there is a phase ambiguity, but the lower one-phonon 2^+ state with the large E2 strength to the ground state is always the symmetric one, while the other one has mixed-symmetric character. This is shown in [HeS86] for the simplification of a two-level system.

In the phonon picture one expects a coupling of phonons. Thus, two symmetric phonons form a triplet of states as described in 2.4.1. But a mixed-symmetry Q_m-phonon may couple to the symmetric Q_s as well. As then we deal with non-identical phonons, a quintuplet of states is formed with spins 0^+, 1^+, 2^+, 3^+, and 4^+,

$$|J_m^+\rangle = \mathcal{N}_m^{(2,J)} \; (\boldsymbol{Q}_m \boldsymbol{Q}_s)^{(J)} \; |0_1^+\rangle \; . \tag{2.102}$$

In terms of the IBM-2 these states have an F-spin of $F = F_{max} - 1$, belonging to the same representation of U(6) as the one-phonon mixed-symmetry state. The 1^+ member of this multiplet evolves into the well-known scissors mode for rotational nuclei. The scissors mode itself will be discussed in more detail in chapter 4. In the geometrical picture the scissors mode is formed by a scissors-like rotation of the deformed proton body versus the deformed neutron body. This is the most prominent M1 excitation at low energies around 3 MeV. Figure 2.13 shows the general feature, that the annihilation or creation of a Q_s-phonon should lead to a strongly collective E2 transition, while for the Q_m-phonon only a weakly collective transition is expected. Evaluating the M1 and the quadrupole operators in the IBM-2 one gets the result, that the exchange of a Q_m- and a Q_s-phonon should result in a large M1 transition with a matrix element in the order of one nuclear magneton. Thus (outside the U(5) limit where two-phonon transitions are strictly forbidden), also the creation operator for the 1_m^+ state $(Q_s Q_m)^{(1)}$ leads to a M1 transition from the ground state.

Again, for the rotational limit this simple phonon picture is not as obvious as it is for vibrational nuclei. Herein, the scissors mode forms the band head of a mixed-symmetric $K = 1$ rotational band, and a relatively low-lying mixed-symmetric 2^+ state is missing. Nevertheless, such a one-phonon state still exists becoming a member of the $K = 1$ band. Actually, in the IBM-2 one finds three 2^+ states with $F_{max} - 1$, one belonging to the $K = 1$ band, one being the band head of a $K = 2$ band, and one being member of a $K = 0$ band. Nevertheless, due to the selection rules in the SU(3) limit only the member of the $K = 1$ band can be excited from the ground state and therefore be identified with the one-phonon 2_m^+ state. A detailed description including transition strengths and a proper algebraical classification of F_{max} and $F_{max} - 1$ states in the F-spin symmetric limits of the IBM-2 can be found in the work of Van Isacker *et al.* [Isa86].

Chapter 3

The limit of weakly collective vibrators

The findings of mixed-symmetric states in ^{94}Mo and ^{96}Ru were the motivation for the study on the N=52 isotone ^{92}Zr. N=50 is a magic neutron shell closure, and a proton sub-shell closure at Z=38 makes this region of the nuclear chart especially interesting. The question, whether shell effects have influence on the collective phonon picture for symmetric and mixed-symmetric states arises. Therefore, ^{92}Zr is an ideal candidate for extending the studies on the proton-neutron structure of states in this region, as it has only two valence protons and two valence neutrons, with the doubly magic core ^{88}Sr (Z=38, N=50). Such a system, where collective effects are expected to compete with single particle degrees of freedom, is what may be called a system at the "limit of weak collectivity". It gives an opportunity to have a look at the "birth" of collectivity as it emerges from the underlying shell structure when deformation driving particles are added. In this chapter the results of a NRF experiment using continuous bremsstrahlung are presented. Data on ^{92}Zr is discussed in comparison with a shell model calculation. Conclusions on the Q-phonon purity of states in this nucleus and its nearest even-even neighbors are drawn from the analysis of shell model calculations.

3.1 NRF experiment on ^{92}Zr

3.1.1 Experimental details

The experiment was performed at the NRF facility of the IfS Stuttgart (see section 2.1.1) using the front NRF setup with three 100% HPGe detectors. The target consisted of 1.351 g ZrO_2, enriched in ^{92}Zr to 91.4%. For an online calibration of the photon flux, 0.761 g of ^{27}Al were added to the target. The composition of the target is included in appendix B. Two endpoint energies of the photon flux were chosen in order to be sensitive in different energy regions. First, the target was

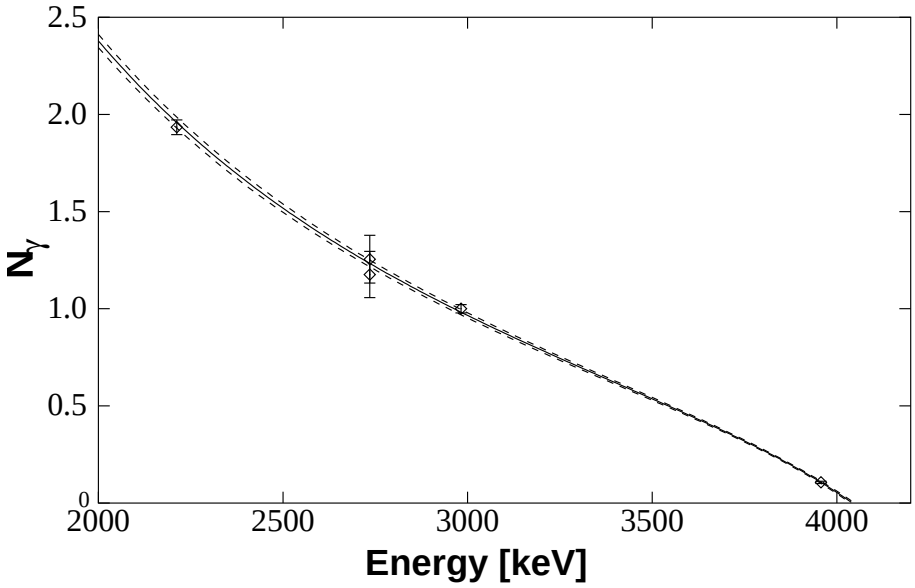

Figure 3.1: *Photon flux calibration for the experiment on ^{92}Zr at 4.1 MeV endpoint energy. The data points are from the calibration standard ^{27}Al, to which the Schiff formula [Sch51] is fitted. The dashed lines give the error of the function.*

irradiated at a photon endpoint energy of 3.1 MeV for 7 days. In that time we had about 85 hours beam on target with an average electron current of 250 μA on the radiator target. Another 5 days the target was irradiated at an endpoint energy of 4.1 MeV, resulting in about 100 hours beam on target with about 210 μA current on the radiator target. Choosing an endpoint energy well below the excitation energies of the strong dipole excitations avoids the feeding of lower-lying states from these states, which would falsify the results. The low-energy measurement was sensitive in the region around 2 MeV where the mixed-symmetry 2^+_m state was expected. The high-energy measurement covered the energy region at 3 MeV where two-phonon dipole excited states are expected. Figure 3.1 shows the interesting part of the photon flux calibration of the high-energy measurement.

3.1.2 Experimental results for ^{92}Zr

In the NRF experiments on ^{92}Zr nine levels have been observed, five of them for the first time, for all states spins have been assigned. The spin assignment for the states at 3263 keV and 3472 keV have been consolidated to be $J^\pi = 2^+$ and $J^\pi = 1^+$, respectively. For all states lifetimes have been determined for the first time. Most results have already been published in [Wer02]. The high-energy part of the spectrum is shown in Figure 3.2. The spectrum is dominated by the ground state decays of two strong dipole excitations at 3472 keV and 3638 keV. The spins of the excited states have been determined from the intensity ratio in

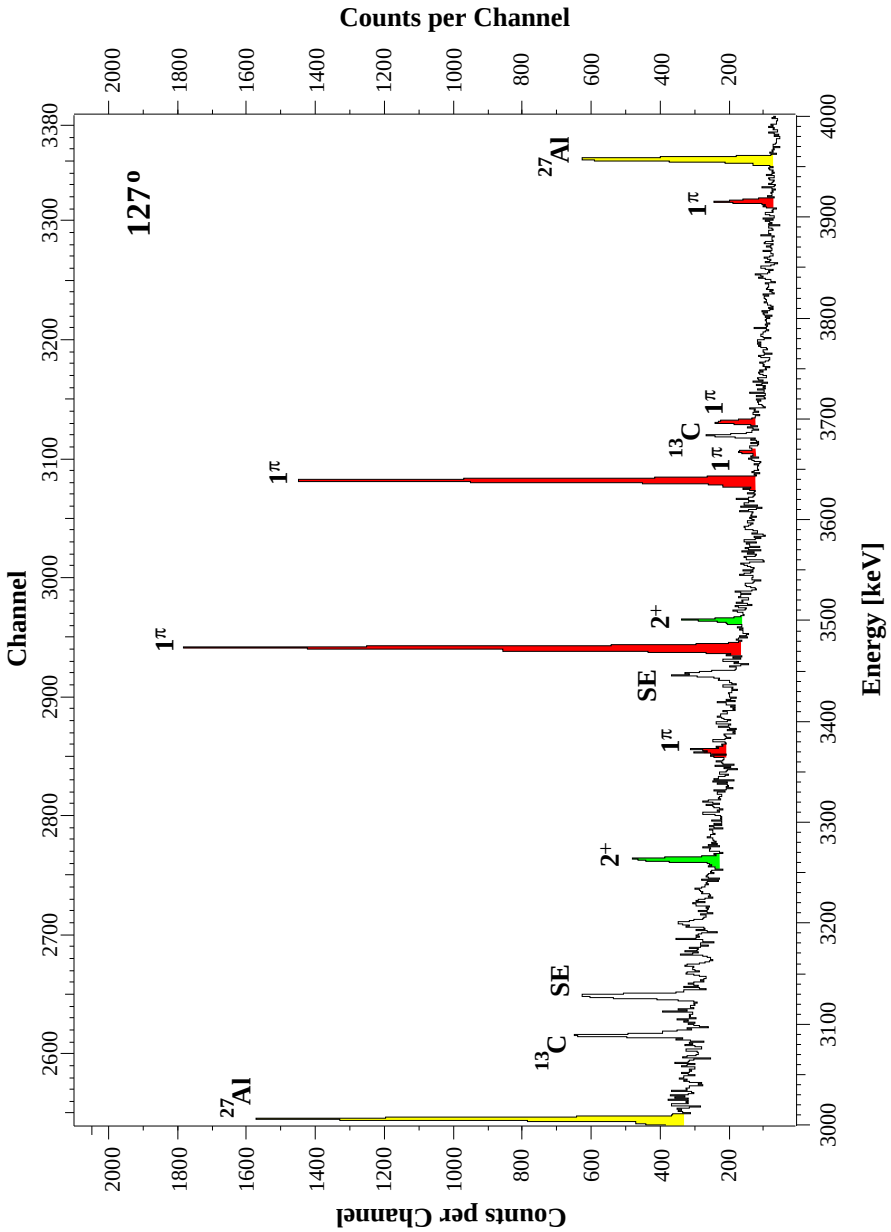

Figure 3.2: *The high-energy part of the spectrum of the Compton suppressed detector at 127°, taken during the photon scattering experiment for ^{92}Zr. Marked lines stem from dipole or quadrupole excitations in ^{92}Zr, from the calibration standard ^{27}Al, and from the background.*

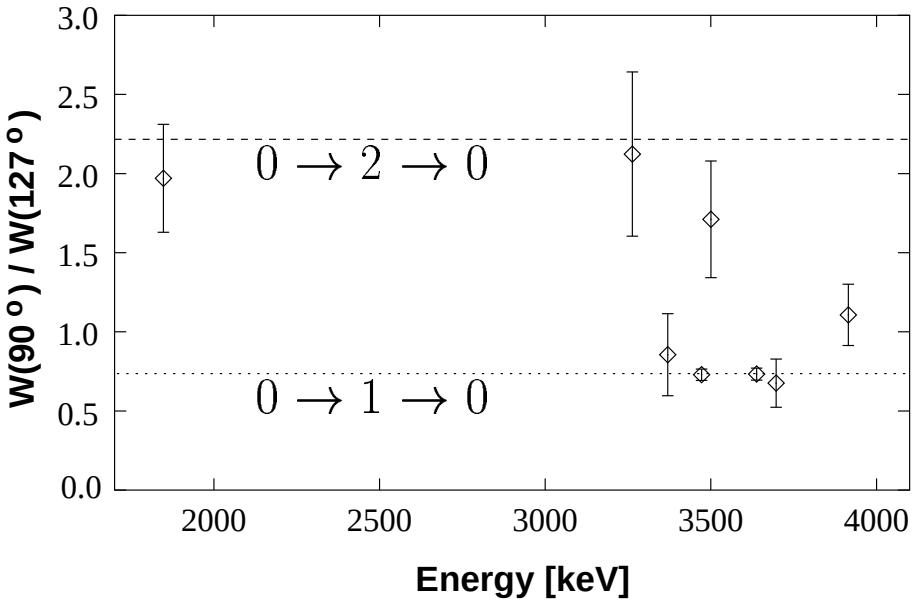

Figure 3.3: *Angular distribution ratio $W(90°)/W(127°)$ for the ground state transitions of states in ^{92}Zr. Dashed lines give the expectation values for dipole and quadrupole states. The data point at 1847 keV stems from the low-energy measurement, the others from the high-energy measurement.*

the detectors at 90° and 127° with respect to the beam axis. Figure 3.3 shows the data points for these spin assignments, together with two dashed lines showing the expected values for dipole or quadrupole excitations from the ground state. The combined information deduced from the NRF data of both measurements is summarized in Table 3.1.

2^+ states

Three 2^+ states have been observed. The most important result of this experiment was the lifetime of the second excited 2^+ state. The relative errors for the 2_2^+ state are somewhat large because both lines from its decay were contaminated by peaks stemming from the background. Using a long background measurement subsequent to the low-energy measurement the contaminants have been subtracted. The 2_2^+ state shows a short lifetime of only 118^{+33}_{-21} fs and a preferential decay to the 2_1^+ state. Together with the known multipolarity of the $2_2^+ \rightarrow 2_1^+$ transition this gives an M1 strength of 0.46(15) μ_N^2. This is the main signature for a mixed-symmetric one-phonon 2^+ state, so that for the first time the 2_2^+ state of a nucleus can be identified as the 2_m^+ state. It will be discussed later how good this assignment applies in the case of ^{92}Zr.

Spin and parity of the state at 3263 keV have been unambiguously determined to be 2^+ with this experiment as can be seen from Figure 3.3. This state shows an

Table 3.1: *Data obtained from the NRF experiments on ^{92}Zr. For each state the level energy E_x, spin and parity J_x^π of initial and final states for the transitions, the integrated photon scattering cross section of the state $I_{s,0}$, the ground state decay width Γ_0, branching ratios Γ_f/Γ_0, multipole mixing ratios δ, reduced transition strengths to lower-lying states $B(\Pi\lambda)\downarrow$, and the lifetime τ is given. Transition strengths are given in W.u. for E2 transitions, in μ_N^2 for M1 transitions, and in $10^{-3}e^2fm^2$ for E1 transitions. In case of unknown multipolarity, Γ_f/Γ_0 is affected by a factor resulting from the angular distribution, and is given under the assumption of a pure dipole transition, as well as the transition strength. As errors always the last digits are given.*

E_x [keV]	J_i^π	J_f^π	$I_{s,0}$ [eV·b]	Γ_0 [meV]	Γ_f/Γ_0	δ	$B(\Pi\lambda)\downarrow$	τ [fs]
				^{92}Zr				
1847.6(5)	2_2^+	0_1^+	2.4(3)	1.6(4)	1.0	E2	E2 3.7(8)	118^{+33}_{-21}
		2_1^+			2.6(6)	$+0.032^{+22}_{-21}$*	M1 0.46(15)	
							E2 0.3(1)	
3263.2(5)	2^+	0_1^+	3.1(2)	7.4(7)	1.0	E2	E2 1.0(1)	20.6^{+22}_{-18}
		2_1^+			3.3(3)	-0.27^{+9}_{-5}*	M1 0.16(2)	
							E2 1.2(2)	
3370(1)	$1^{(-)}$*	0_1^+	1.5(2)	1.45(17)	1.0	(E1)	E1 0.037(4)	455^{+61}_{-48}
							(M1 0.0033(4))	
3472.3(5)	1^+◇	0_1^+	27.6(10)	45.2(18)	1.0	M1	M1 0.094(4)	9.3^{+4}_{-4}
		2_1^+			0.37(2)	M1,E2	(M1 0.09(1))	
		0_2^+			0.19(2)	M1	M1 0.08(1)	
3500.4(5)	2^+	0_1^+	2.7(2)	1.75(15)	1.0	E2	E2 0.17(1)	376^{+35}_{-29}
3638.4(5)	1^-◇	0_1^+	37.0(13)	51.5(22)	1.0	E1	E1 1.03(4)	10.5^{+5}_{-4}
		0_2^+			0.21(3)	E1	E1 0.9(1)	
3667(1)	1	0_1^+	1.8(3)	2.1(3)	1.0	dipole	M1 0.0037(6)	314^{+58}_{-43}
							E1 0.040(7)	
3697.3(5)	1	0_1^+	4.2(4)	9.6(11)	1.0	dipole	M1 0.016(2)	35.7^{+48}_{-38}
							E1 0.18(2)	
		2_1^+			0.93(14)		(M1 0.04(1))	
							(E1 0.4(1))	
3915.4(5)	1	0_1^+	11.8(14)	15.6(19)	1.0	dipole	M1 0.022(3)	42.1^{+59}_{-46}
							E1 0.25(3)	

* Parity assignments, branching ratios, or multipole mixing ratios taken from NDS [Bag00].
◇ Parity assignment from [FraPC].

enhanced M1 strength of 0.16(2) μ_N^2 to the 2_1^+ state. This strong M1 transition should correspond to a spin-flip transition between the $d_{3/2}$ and $d_{5/2}$ neutron orbitals, which will be discussed below. The angular distribution ratio for the known 2^+ state at 3500 keV is a bit low, but clearly in favor of the 2^+ assignment (see Figure 3.3). Only spin and parity for this state were already known [Bag00], while lifetime information is from the present data.

$J = 1$ states

The two strongest dipole excited states at 3472 keV and 3638 keV, respectively, are candidates for being members of two-phonon multiplets. The one with positive parity at 3472 keV should correspond to the mixed-symmetric two-phonon 1^+ state. The other is a candidate for another two-phonon state, built by a quadrupole and an octupole phonon, $(2_1^+ \otimes 3_1^-)^{(1^-)}$. Such states are expected close to the sum-energy of both constituents [Met76, Bre94, Rob94], which is 934 keV + 2340 keV = 3274 keV. Such excitations were extensively investigated in the A≈130-190 mass region [Zil90, Her95, Kne96, Fra98, Pie99], as well as in the even Tin [Bry99] and Cadmium [Koh01] isotopes. Thus, assuming that the state at 3638 keV has negative parity, which has actually been proven in a recent experiment at the DFELL at Duke University [FraPC], would signify an extraordinary strong anharmonicity in the coupling of the 2^+ and the 3^- phonon. Also the $1^{(-)}$ state at 3370 keV is a candidate for a negative parity two-phonon dipole excitation. The ground state transition strength of this state is small compared to that of the 3638 keV state. Nevertheless, this would fit to the finding, that the E1 excitation strength drops from usually large E1 strengths in semi-magic nuclei, before rising towards mid-shell nuclei [And01].

The $1^{(+)}$ state at 3124 keV (spin assignment from [Fra03b]) was not observed in this experiment as it is covered by a wide single-escape peak of the 3638 keV γ-line.

Side reactions

The ZrO_2 target had impurities of other Zirconium isotopes, the largest impurity was ^{90}Zr with 4.65 % in the target. From this nucleus the 2_1^+ state at 2186 keV and the 2^+ state at 3842 keV were observed, although as tiny peaks in the spectrum. Nevertheless lifetimes were deduced. These lifetimes are given in Table 3.2 and compared to values from [EkL92]. Both results are in fair agreement with the listed values.

Another impurity in the target was 2.03 % of ^{94}Zr. Despite this small amount of material the 1^- state at 2846 keV was observed, which is the candidate for the $(2_1^+ \otimes 3_1^-)^{(1^-)}$ state in ^{94}Zr. The lifetime of this state was not known and amounts to 6.7^{+26}_{-14} fs, leading to a large E1 excitation strength for this state compared, *e.g.*, to the dipole excitations in ^{92}Zr. The data on this state is also given in Table

Table 3.2: *Results for $^{90,94}Zr$. The same quantities as in Table 3.1 are given. In addition, in the last column, lifetimes known from literature are listed.*

E_x [keV]	J_i^π	J_f^π	$I_{s,0}$ [eV·b]	Γ_0 [meV]	Γ_f/Γ_0	δ	$B(\Pi\lambda)\downarrow$	τ [fs]	τ_{Lit} [fs]
					^{90}Zr				
2186.9(5)	2^{+*}	0_1^+	25.5(40)	6.5(8)	1.0	E2	E2 6.8(8)	101^{+13}_{-10}	127.5(36)*
		0_2^+			0.027(5)*	E2	E2 6.6(14)		
3842(1)	2^{+*}	0_1^+	41(10)	31(7)	1.0	E2	E2 1.9(5)	21^{+7}_{-4}	22.4(23)*
					^{94}Zr				
2846.4(5)	1^{-*}	0_1^+	113(7)	88(25)	1.0	E1	E1 3.7(11)	6.7^{+26}_{-14}	
		2_1^+			0.11(3)*	E1	E1 1.3(5)		

* Parity assignments, branching ratios, or multipole mixing ratios taken from NDS [EkL92, Tul92].

3.2. Hints at eventual γ-lines were seen at 1872 keV, 2164 keV, 2223 keV and 3593 keV, but each only very small and only in one detector. Therefore, these lines were not taken into account in the data analysis.

3.2 Comparison with shell model calculations

The presented NRF experiment on ^{92}Zr and shell model calculations [Wer02] initiated two subsequent experiments performed by C. Fransen *et al.* One was done using the $(n, n'\gamma)$ technique at the University of Kentucky [Fra03b]. From this experiment more information about excited states, their decays and their lifetimes became accessible. In addition, a NRF experiment with polarized photons at the DFELL was performed [FraPC], leading to parity assignments for the two strongest dipole excitations below 4 MeV. All the new information was the input for a shell model calculation on ^{92}Zr which differs from the calculation given in [Wer02], while improving especially the description of transition rates. The new calculation does not base on parameters that were derived for ^{94}Mo [Lis00] any more but introduces a scheme for fitting shell model parameters, being the starting point for further calculations for neighboring nuclei. The shell model should answer some questions on the competition between collective and single particle degrees of freedom. The previous calculations on ^{94}Mo in the shell model [Lis00, Bre02] showed that a considerable amount of M1 strength between mixed-symmetric and symmetric states has orbital character, and showed collectivity in the lowest 2^+ state. These conclusions were backed by a QPM analysis of ^{94}Mo [LoS00, LoS02], but cannot simply be adopted to ^{92}Zr where shell structure confronts us with a completely different situation.

Table 3.3: *SDI parameters for ^{92}Zr. ϵ_x^ρ are the single particle energies for protons or neutrons in orbital x and $A^T_{\rho\rho'}$ are the interaction parameters. e_ρ are the effective E2 charges and g_ρ^σ the orbital and spin g-factors.*

$\epsilon^p_{g_{9/2}}$	$\epsilon^p_{p_{1/2}}$	$\epsilon^n_{d_{5/2}}$	$\epsilon^n_{s_{1/2}}$	$\epsilon^n_{g_{7/2}}$	$\epsilon^n_{d_{3/2}}$	$\epsilon^n_{h_{11/2}}$	$A^{T=1}_{pp}$	$A^{T=1}_{nn}$	$A^{T=1}_{pn}$	$A^{T=0}_{pn}$
[MeV]										
0.0	-0.7	0.0	1.5	1.9	2.0	3.5	0.31	0.24	0.27	0.20

e_p	e_n	g^l_p	g^l_n	g^s_p	g^s_n
2.1	1.1	1	0	3.7983	-2.6019

3.2.1 Shell model description of ^{92}Zr

Shell model calculations were performed using the code RITSSCHIL [Zwa85] and the surface delta interaction (SDI). ^{88}Sr was used as a core due to the proton sub-shell closure at Z=38 and the neutron shell closure at N=50. All orbitals up to the next shell closures were taken into account, thus the valence space is spanned by particles in the orbitals $\pi(2p_{1/2})$, $\pi(1g_{9/2})$, $\nu(2d_{3/2})$, $\nu(3s_{1/2})$, $\nu(1g_{7/2})$, $\nu(2d_{3/2})$, and $\nu(1d_{11/2})$. Parameters that have to be determined are thus single particle energies for each orbital, whereas the use of relative energies is satisfactory as we are not interested in binding energies. The interaction has another four parameters to fix, namely the parameters for the proton-proton interaction A_{pp}, the neutron-neutron interaction A_{nn} and the parameters for the proton-neutron $T = 0$ and $T = 1$ interaction, $A^{T=0}_{pn}$ and $A^{T=1}_{pn}$, as described in section 2.2.2. For E2 transitions the effective charges for protons and neutrons, e_p and e_n, have to be fixed, and for M1 transitions the g-factors. The orbital g-factors were set to the bare values $g^l_p = 1$ for protons and $g^l_n = 0$ for neutrons, and the spin g-factors to the free proton and neutron values with a quenching factor of 0.7, hence $g^s_p = 3.7983$ and $g^s_n = -2.6019$.

Start values for single particle energies were obtained from the nearest neighbors of the core, *i.e.*, for neutron energies ^{89}Y and for proton energies ^{89}Sr. In these nuclei only one valence nucleon should create the lowest states by being excited from the ground state, where it is in the lowest orbital, to higher-lying orbitals. Energies of the lowest states with spins according to the orbitals of interest are taken to be the single particle energies. Furthermore, ^{90}Zr and ^{90}Sr with two valence neutrons or two valence protons, respectively, were taken into account. The neutron-neutron (n-n) and proton-proton (p-p) interaction parameters were fitted in order to reproduce the spectra of these nuclei. Finally, the proton-neutron (p-n) interactions were fitted to the spectrum of ^{90}Y with one valence neutron and one valence proton. This gave a first set of parameters for the description of ^{92}Zr, but it turned out that the spectrum and key properties of the eigenstates were not well described, yet. Therefore, the p-n parameters

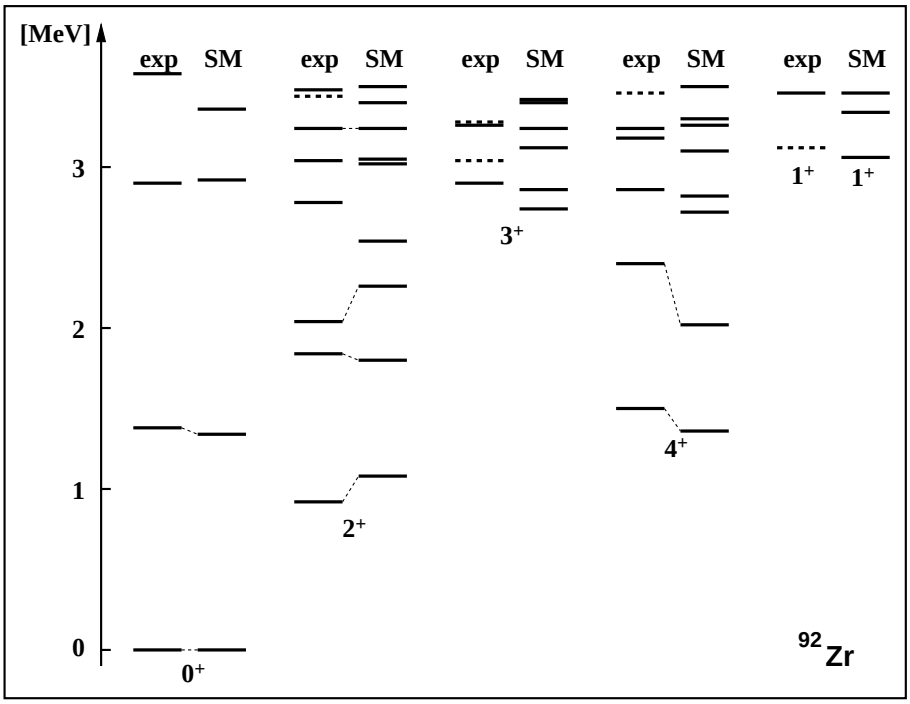

Figure 3.4: *Calculated and measured excitation energies of positive parity states with spin $J = 0, \ldots, 4$. States that are drawn with dashed lines are of unknown parity. States that were identified in the calculation are connected to their shell model counterparts.*

had to be adjusted. An observable that is sensitive especially to the $T = 0$ (or $S = 1$, see section 2.2.2) p-n interaction is the g-factor of the 2_1^+ state. This was measured to have a negative value of $g(2_1^+) = -0.18(1)$ [Jak99], which hints at a large neutron contribution to this state. The reproduction of this g-factor causes a strong change in the strength of the $T = 0$ p-n interaction. Afterwards, small adjustments to the single particle energies were made. This point is a bit delicate as usually single particle energies are not changed, but in this case it is necessary for compensating effects that are not incorporated in the simple effective Hamiltonian. Nevertheless, making changes to the single particle energies is similar to the monopole corrections [DuZ96] mentioned in section 2.2.2. For ^{92}Zr the parameter set given in Table 3.3 was obtained. The calculated and experimental spectra are compared in Figure 3.4 for all states with spin $J = 0, \ldots, 4$ up to 3.5 MeV, where some additional experimental information was taken from the $(n, n'\gamma)$ data. The discussion is restricted to positive parity states as E1 transitions are not allowed in the valence space used, and a proper description of negative parity states is probably not possible without breaking the ^{88}Sr core.

The agreement between data and calculated energies is fair. Deviations in energy are moderate in view of the simplicity of the interaction. States that are plotted with dashed lines have unknown parities and may be wrong in that

Table 3.4: *Comparison of electromagnetic transition strengths from data and shell model between states for which corresponding counterparts were identified. In cases of known g-factors their comparison is given, too.*

			experiment		**shell model**	
E_i	J_i	J_f	$B(M1)$	$B(E2)$	$B(M1)$	$B(E2)$
[keV]			$[\mu_N^2]$	[W.u.]	$[\mu_N^2]$	[W.u.]
935	2_1^+	0_1^+		6.4(5)		6.2
			$g(2_1^+) = -0.18(1)$		$g(2_1^+) = -0.18$	
1383	0_2^+	2_1^+		14.4(5)		3.5
1496	4_1^+	2_1^+		4.05(11)		4.2
			$g(4_1^+) = -0.50(11)$		$g(4_1^+) = -0.38$	
1847	2_2^+	0_1^+		3.4(4)		3.0
		2_1^+	0.37(4)	0.4(5)	0.29	0.3
				–	$g(2_2^+) = +1.07$	
2067	2_3^+	0_1^+		<0.005		0.2
		2_1^+	<0.024	<16	0.03	12.0
		2_2^+	<0.04	<430	0.18	0.9
2398	4_2^+	2_1^+		6.1(8)		2.4
		4_1^+	0.26(3)	2.3(11)	0.47	0.1
				–	$g(4_2^+) = +1.15$	
2909	3_1^+	2_1^+	<0.01	<1.8	0.01	0.02
		4_1^+	0.007(2)	4.5(8)	0	7.6
			0.018(3)	1.3(4)		
		2_2^+	–	–	0.002	0.2
		2_3^+	0.06(1)	3.0(3)	0.09	3.6
3263	2_6^+	0_1^+		1.1(1)		0.2
		2_1^+	0.19(2)	0.07(1)	0.24	0.15
3472	1^+	0_1^+	0.094(4)		0.13	
		2_1^+	<0.09	<8	0.05	1.8
		0_2^+	0.08(1)		0.13	

picture. Levels from data and calculation that are connected will be discussed in the following. Table 3.4 gives transition strengths between states, as well as some g-factors, from which structural information can be obtained in comparison with the shell model results. Effective charges for the E2 operator were adjusted in order to reproduce the ground state transition strengths of the $2^+_{1,2}$ states. These two states are candidates for the symmetric 2^+_s and the mixed-symmetric 2^+_m states and should be most sensitive to changes in the effective charges. The values $e_p = 2.1$ and $e_n = 1.1$ were chosen. In Table 3.4 data is compared to appropriate states from the calculation. A large part of the data stems from $(n, n'\gamma)$. From the model one can obtain information about configurations that play a role in the wave functions of some selected states.

3.2.2 Consequences for low-lying states

$0^+_{1,2}$ states

The ground state and the first excited 0^+ state in ^{92}Zr are found to be strongly mixed. As it is very low in energy (1383 keV), a first assumption for the structure of the 0^+_2 state could be that it is a two-proton excitation, that means, the two protons are excited from the $p_{1/2}$ orbital to the $g_{9/2}$ orbital coupling to spin $j = 0$. This is indeed reflected in the calculated wave functions. The main configurations are given in Table 3.5 and show that such a two-particle excitation takes place, and that both configurations with two protons in the $p_{1/2}$ orbital, or two protons in the $g_{9/2}$ orbital, respectively, are almost completely mixed. Note, that this holds for all seniority[1] $\nu = 0$ configurations in the 0^+ wave functions (only one is given in Table 3.5). The absolute values of the amplitudes with the two protons in one of both orbitals are almost equal, but the relative sign is different just as for the two $\nu = 0$ configurations given. From the configurations listed in Table 3.5 one finds that higher configurations ($\nu = 2, 4$) play a larger role for the 0^+_2 state than for the 0^+_1 state, but are still small. Again, this property of the main configurations of the two states is very similar similar for the others. A strong mixing of the two 0^+ states had already been discussed in [Hey88] and is fully confirmed by the calculation presented here. The NRF data also gives some confirmation for the findings within the model. The two strong dipole excitations at 3472 keV and 3638 keV show equally large transition strengths to the $0^+_{1,2}$ states within the error, as shown in Figure 3.5. The strong mixing of the 0^+ states in ^{92}Zr also appears in ^{90}Zr, where it can easily be understood in terms of a two-level mixing. Taking into account the two $T = 1$ proton configurations $(p^2_{1/2})_0$ and $(g^2_{9/2})_0$, the p-p interactions ($A^{T=1}_{pp}$) mixes both configurations. Figure 3.6 illustrates this for different interaction strengths, calculated with the surface delta interaction. At exactly one point the wave-functions are completely mixed.

[1] The seniority ν of a configuration is the number of particles in one orbital that do not couple pairwise to $j = 0$.

Table 3.5: *Amplitudes of the main configurations contributing to the wave functions of the lowest 0^+, 2^+ and 4^+ states, and to the 2^+_7 state. Neglected components contribute to less than 10% each to the total wave functions. Contributions in the top part are the most important one-phonon amplitudes, in the middle-part one finds the main two-phonon amplitudes, while the bottom part corresponds to spin-flip excitations.*

	0^+_1	0^+_2	1^+_1	2^+_1	2^+_2	2^+_7	4^+_1	4^+_2
$[\pi(p^2_{1/2})_0\ \nu(d^2_{5/2})_J]_J$	-0.61	-0.65	–	-0.60	-0.38	0.09	0.68	-0.23
$[\pi(g^2_{9/2})_0\ \nu(d^2_{5/2})_J]_J$	0.63	-0.55	–	0.63	0.06	0.02	-0.67	-0.05
$[\pi(g^2_{9/2})_J\ \nu(d^2_{5/2})_0]_J$	–	–	–	0.22	-0.74	0.07	-0.13	-0.78
$[\pi(g^2_{9/2})_2\ \nu(d^2_{5/2})_2]_J$	-0.11	-0.21	0.74	-0.01	0.11	-0.17	-0.09	-0.22
$[\pi(g^2_{9/2})_4\ \nu(d^2_{5/2})_4]_J$	-0.07	-0.11	0.49	-0.03	0.05	0.20	0.04	-0.01
$[\pi(p^2_{1/2})_0\ \nu(d_{5/2}d_{3/2})_J]_J$	–	–	0.19	-0.06	-0.02	-0.46	0.07	0.03
$[\pi(g^2_{9/2})_0\ \nu(d_{5/2}d_{3/2})_J]_J$	–	–	-0.31	0.08	-0.03	0.51	-0.09	-0.10

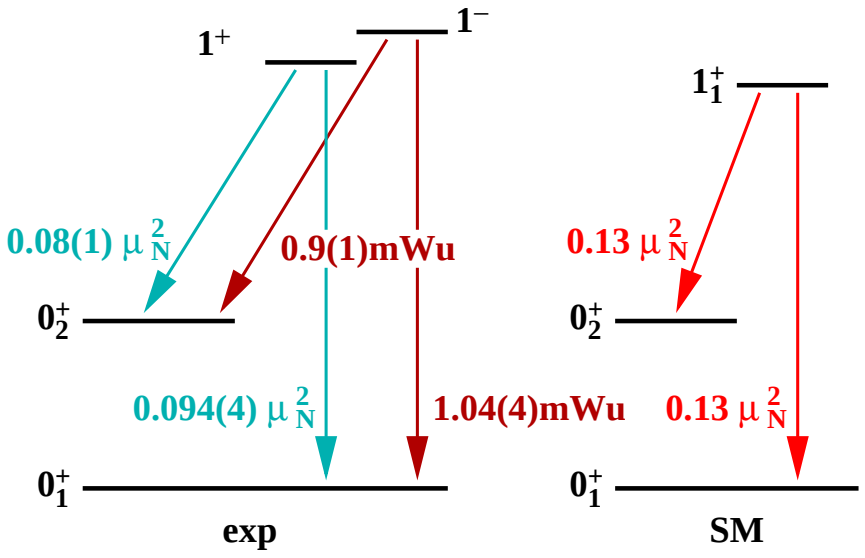

Figure 3.5: *The decays of the strongest dipole excitations in ^{92}Zr show equally large transition strengths to the ground state and the lowest excited 0^+ state. This behavior is also expected within the shell model as shown to the right. It is connected to the strong mixing between both 0^+ states.*

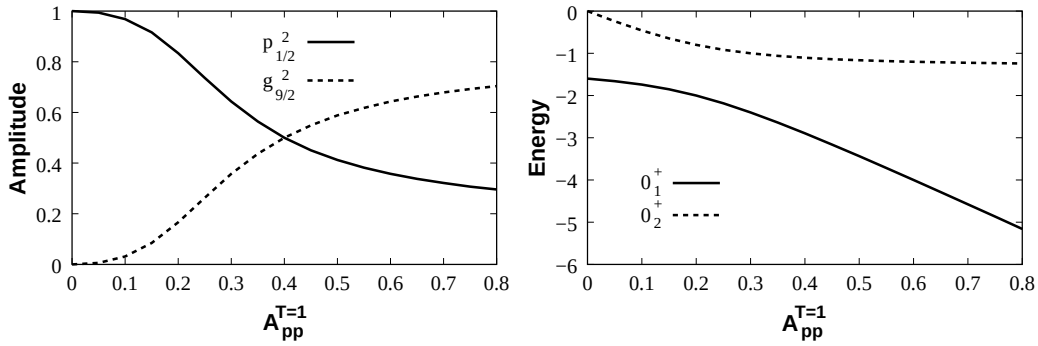

Figure 3.6: *Two-level mixing in the example of ^{90}Zr. On the left hand side the amplitudes of the two configurations are shown as a function of the interaction parameter $A_{pp}^{T=1}$, on the right hand side the energies of the resulting 0^+ states are displayed.*

Note, that this is in general not the point of the closest distance of both levels, because SDI has not only off-diagonal matrix elements. This is also illustrated on the right hand side of Figure 3.6. Of course, for ^{92}Zr the situation is more complicated due to the neutron space and the p-n interaction. But for the lowest 0^+ states the situation is very similar to a two-level mixing.

$2^+_{1,2}$ states

The 2^+_1 state is usually expected to be a p-n symmetric state. In ^{92}Zr this does not seem to be the case. Already from the negative g-factor of this state an enhanced neutron content is evident. Another hint is the E2 transition strength to the ground state of only 6.4 W.u. which is smaller than in the N=52 isotones ^{94}Mo and ^{96}Ru. This behavior is nicely reproduced by the shell model calculation. Taking into account contributions with seniority $\nu = 2$ alone to the wave function, that means only the two protons or the two neutrons contribute to the final level spin, one gets a neutron extent of 77.5 %. Therein, the main part is due to configurations as they are included in Table 3.5. The proton extent of the 2^+_1 state amounts to only 6.0 %, while the residual wave function contains configurations with seniority $\nu = 4$. Thus, the 2^+_1 state in ^{92}Zr is of dominant neutron character. An easy explanation is given by looking at the proton valence space. The lowest orbital is a $p_{1/2}$ orbital in which the two protons cannot couple to $j = 2$. For a proton $j = 2$ configuration, both particles have to be excited to the $g_{9/2}$ orbital first, while the neutrons can couple to $j = 2$ in their lowest orbital, $d_{5/2}$. Therefore, a proton $j = 2$ configuration is blocked.

From data the 2^+_2 state seems to be the mixed-symmetric one-phonon state in ^{92}Zr due to its large M1 strength to the 2^+_1 state, which is well reproduced by the calculation. By setting the difference between the effective proton and neutron charges to $e_p - e_n = 1$, also the E2 strength to the ground state is fixed. This E2

strength is remarkably large for a mixed-symmetric state. In other nuclei in the mass region it was found to be about 1/10 of the E2 strength of the symmetric 2_1^+ state, *i.e.*, 1 W.u.. Looking at the wave functions, it becomes clear that the 2_2^+ state is not purely mixed-symmetric, but has a large proton content. The main configurations are again included in Table 3.5. The seniority $\nu = 2$ neutron content amounts only to 15.4 % while the proton extent is enhanced with 69.1 %. Finally the model predicts a larger g-factor of $g(2_2^+) = 1.07$ for this state.

From Table 3.5 one can recognize a reflection of phonon structures of both 2^+ states. It is striking that the largest contributions to their wave functions are of $\nu = 2$ kind, which means that two neutrons or two protons couple to spin $j = 2$, while the other two couple to $j = 0$. This is very similar to a foundation of the sd-IBM, allowing two particles in one orbital to couple only to $j = 0, 2$. In a spherical nucleus like ^{92}Zr this may be compared with the U(5) limit of the IBM, and a phonon excitation were equivalent to creating one d-boson by coupling two particles to $j = 2$. At this point this may be taken as a hint that the phonon picture may still be important for the two lowest 2^+ states, although they are neither p-n symmetric nor mixed-symmetric states. Note that this is only a very simplified, but intuitive way of looking into the shell model wave functions of the states. There is still a huge amount of other configurations that are not included in the simplifying scheme of the IBM. Those may be small one by one, but their sum might lead to effects that cannot be neglected.

The 1_1^+ state

The calculated 1_1^+ state shows the largest M1 transition strength of 0.13 μ_N^2 to the ground state. This is in the same order as the experimental M1 ground state transition strength of the 1^+ state at 3472 keV. Also the decay properties to lower-lying states are very well described (see Table 3.4 and Figure 3.5), while the calculated energy of 3056 keV is somewhat low. One can calculate the contributions of orbital M1 strength and M1 strength according to the spin part of the M1 transition operator separately for protons and neutrons just by choosing only one g-factor non-equal to zero. This was done and one finds that the transition matrix element contains a considerable portion from the orbital proton part. Nevertheless, the neutron spin part dominates the M1 transition matrix element. Note, that the spin g-factors are about a factor of 3 larger than the orbital proton g-factor. Therefore, comparably small admixtures of wave function components including $d_{5/2}$ and $d_{3/2}$ neutron configurations may play a big role for the matrix element. The main components of the wave function of the 1_1^+ state are given in Table 3.5. The largest component is $[\pi(g_{9/2}^2)_2\ \nu(d_{5/2}^2)_2]$, which resembles a two-phonon configuration as the one given by Eq. (2.102) or included in Figure 2.13 the most, just like the main configurations of the first two 2^+ states resemble one-phonon configurations. But there is a considerable contribution including $[\nu(d_{5/2}d_{3/2})_1]$ configurations of which the largest are to be

seen in the bottom part of Table 3.5. This portion of the wave function may be called spin-flip part as it corresponds to the spin-flip of a neutron from orbital $d_{5/2}$ in the ground state to the $d_{3/2}$ orbital in the excited state.

The 2_6^+ state

The 2_6^+ state at 3263 keV known from the experiment is compared to the 2_7^+ from the calculation at 3257 keV. This is because the 2_7^+ state from the calculation is the only 2^+ state asides from the 2_2^+ state that has considerable E2 strength to the ground state while being connected to the 2_1^+ state by a large M1 transition. This M1 transition is astonishing because it is usually the main signature for a mixed-symmetric one-phonon state. But the explanation of the enhanced M1 strength from an analysis of the wave function is simple. The main components shown in Table 3.5 obviously have spin-flip character. These configurations are responsible for the enhanced M1 strength to the 2_1^+ state, which has a large $\nu(d_{5/2}^2)_2$ component.

The $4_{1,2}^+$ states

The situation for the lowest two 4^+ states in ^{92}Zr is even more pronounced as in the similar findings for the 2^+ states. From the calculation one gets a seniority $\nu = 2$ neutron content of the 4_1^+ state of 91.2 %, while the 4_2^+ contains $\nu = 2$ proton configurations to an extent of 72.7 %. Also the most important configurations of the $4_{1,2}^+$ states are listed in Table 3.5. Due to the large neutron extent of the 4_1^+ state its g-factor is expected to be negative. The calculation gives $g(4_1^+) = -0.38$. This model prediction agrees very well the with the experimental value of $g(4_1^+) = -0.50(11)$. For the 4_2^+ state the model predicts a g-factor of $g(4_2^+) = 1.15$. From Table 3.5 one sees that the structures of both 4^+ states are very similar to those of the $2_{1,2}^+$ states. The broken pair of particles causing seniority $\nu = 2$ just couple to $j = 4$ instead of $j = 2$. A large M1 transition strength between the 4^+ states is predicted from the calculations (see Table 3.4) and was experimentally confirmed by the $(n, n'\gamma)$ data.

3.3 The N=52 isotones

The investigation of ^{92}Zr followed the discovery of mixed-symmetry states in the N=52 isotones ^{94}Mo and ^{96}Ru. In this section the findings for ^{92}Zr are compared to those in the N=52 neighboring nuclei.

3.3.1 Systematics of symmetric and mixed-symmetric states

The one-phonon symmetric 2_s^+ and mixed-symmetric 2_m^+ states have been observed in the N=52 isotones ^{94}Mo and ^{96}Ru [Pie01, Kle01] and absolute transition strengths were determined. This allows a comparison of ^{92}Zr to its N=52 neighbors. In Figure 3.7 some key observables are shown. Most striking is the behavior of the energies of the 0_2^+ states which are lowered drastically towards Z=40 or ^{92}Zr. This is due to the strong mixing with the ground state. Below Z=40 where the $p_{1/2}$ orbital is not occupied, the energies are shifted up again. Also the behavior of the 2_m^+ state is remarkable as it is also lowered towards Z=40, while the energy of the 2_s^+ peaks at the Zirconium. This behavior should be connected to the neutron content of the state that rises towards Z=40 due to the $p_{1/2}$ blocking of proton $j = 2$ configurations. This is also reflected in the E2 strengths of both 2^+ states. In the heavier isotones the E2 ground state transition strengths are separated by about an order of magnitude, while they come closer at Z=40 and are separated by a factor of only two, while the M1 strength between both 2^+ states drops by a factor of about two.

These signatures can be explained by the enhanced neutron content of the 2_m^+ state, due to the $p_{1/2}$ blocking effect. For the heavier N=52 nuclei, one should get comparably large proton and neutron contributions to the 2^+ states, which mix and form one p-n symmetric and one p-n mixed-symmetric state. In contrast, in ^{92}Zr $j = 2$ proton and neutron configurations are well separated in energy. This situation is illustrated in Figure 3.8, showing the low-lying states of ^{92}Zr and ^{94}Mo in comparison with those even-even neighbors that are lying on a closed proton or neutron shell with Z-38 or N=50. The proton 2_1^+ state in ^{90}Zr is lying very high compared to the 2_1^+ state in ^{90}Sr which is expected to have dominant neutron character. Identifying these two configurations with the proton and neutron $j = 2$ configurations contributing to the wave functions of ^{92}Zr, a mixing between both configurations is hindered by the large energy difference. The result is a low-lying 2^+ state with dominant neutron character in ^{92}Zr, while the second excited 2^+ state shows a pronounced proton character. The situation for the lowest 4^+ state is similar, while the probability for the mixing of proton and neutron configurations rises for higher-lying states.

In ^{94}Mo the situation is much different. The $g_{9/2}$ proton orbital is lowered to even below the energy of the $p_{1/2}$ orbital. This becomes evident from the ground state of ^{93}Nb which is a $9/2^+$ state, while the first excited state is a $1/2^-$ state at 31 keV, corresponding to the excitation of a single particle to the $p_{1/2}$ orbital. Note that the excitation energy of 31 keV is not simply due to the single particle energies, also the nucleon-nucleon interactions play a role. Figure 3.8 shows that the proton 2^+ state in ^{92}Mo is quite high, which hints at the proton $j = 2$ configuration still being blocked by the $p_{1/2}$ orbital. This contradicts the observed drastic lowering of the $g_{9/2}$ orbital only when neglecting the nucleon-

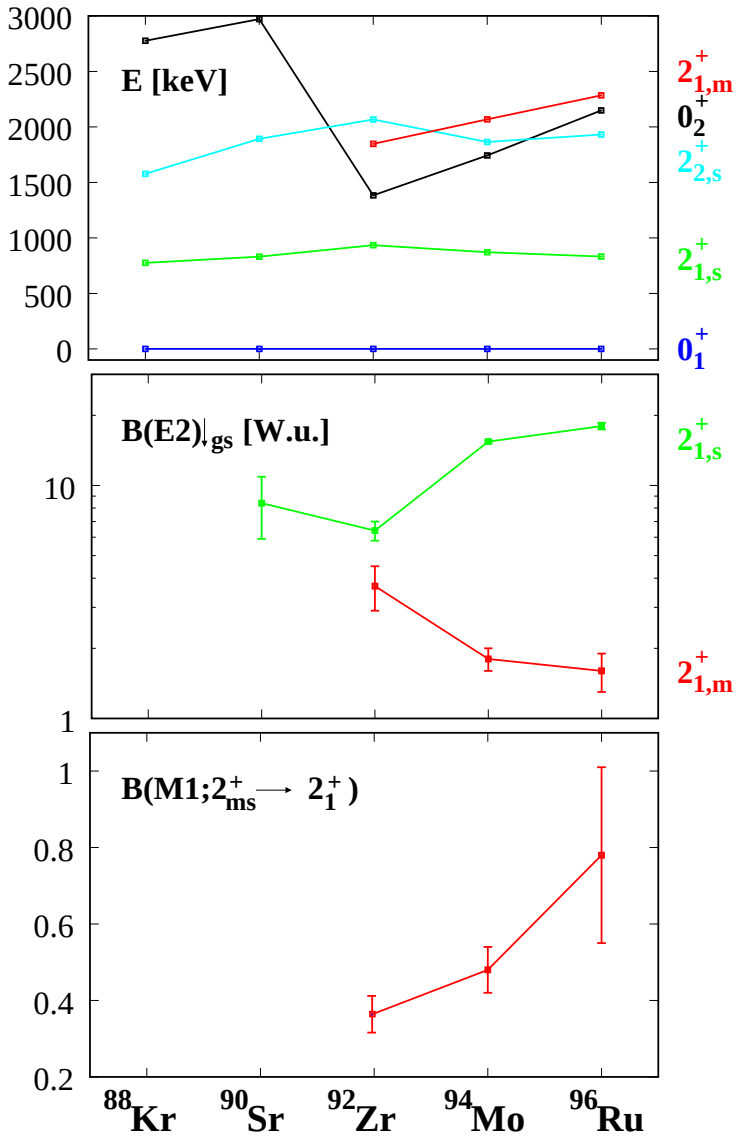

Figure 3.7: *The top panel shows the energies of low-lying states in N=52 nuclei around* ^{92}Zr. *In the middle panel the E2 transition strengths of the symmetric and mixed-symmetric* 2^+ *states to the ground state are plotted, whereas the* $2^+_{1,2}$ *states were chosen for the comparison in* ^{92}Zr. *The bottom panel shows the M1 strengths between both.*

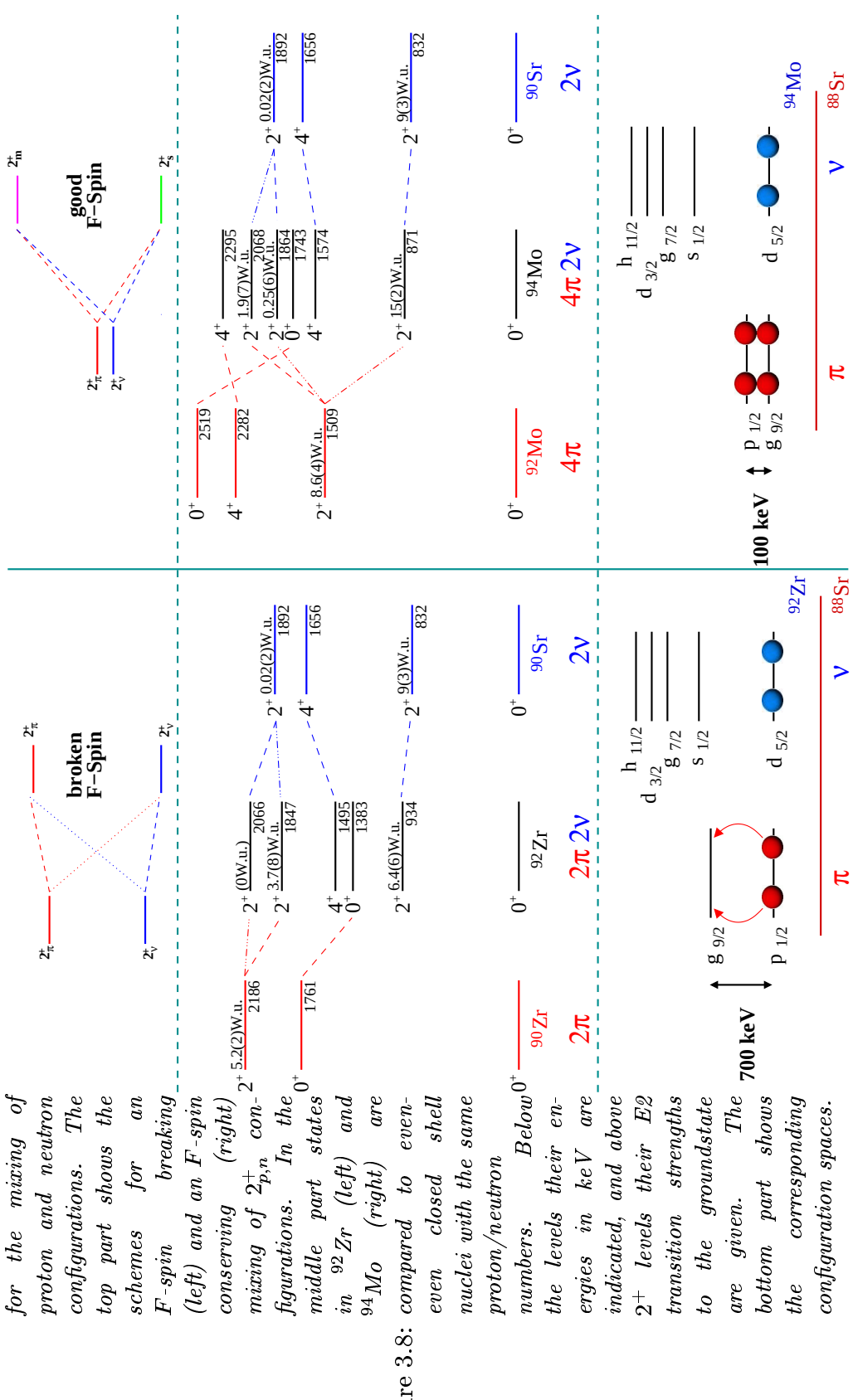

Figure 3.8: *Schematic picture for the mixing of proton and neutron configurations. The top part shows the schemes for an F-spin breaking (left) and an F-spin conserving (right) mixing of $2^+_{p,n}$ configurations. In the middle part states in ^{92}Zr (left) and ^{94}Mo (right) are compared to even-even closed shell nuclei with the same proton/neutron numbers. Below the levels their energies in keV are indicated, and above 2^+ levels their E2 transition strengths to the groundstate are given. The bottom part shows the corresponding configuration spaces.*

nucleon interactions. Nevertheless, in ^{92}Mo the 2_1^+ state is much closer to the neutron 2_1^+ state in ^{90}Sr. The proton configuration should even more be lowered in energy due to the interactions. Finally the mixing between proton and neutron $j = 2$ configurations in ^{94}Mo can be expected to be much larger than in ^{92}Zr.

3.3.2 Breaking F-spin

In the language of the IBM-2 the situation in and near ^{92}Zr can be discussed as F-spin breaking. The IBM should not be expected to be a good model for the description of a nucleus with only two bosons (one proton and one neutron boson), because the configuration space is very restricted, and important contributions to the wave functions will be missing. However, it gives an easy way to understand how F-spin can be broken around Z=40. The most important factor for the enhanced neutron character of the 2_1^+ state in ^{92}Zr in the shell model description was the $T = 0$ p-n interaction. This parameter was drastically reduced to 0.2 MeV compared to the 0.5 MeV in the calculations of Lisetskiy *et al.* done for ^{94}Mo [Lis00], while all the other interaction parameters were found to remain stable. This change is responsible for the negative g-factor of the 2_1^+ state and its dominant neutron structure. In the IBM, the most important p-n interaction is of the type $\boldsymbol{Q}_\pi.\boldsymbol{Q}_\nu$. Regarding the Hamiltonian (2.94) one can simulate the situation for ^{92}Zr in the IBM-2. Therefore, the energies of proton and neutron d-bosons have to be set to different values which complies to the higher energy of the proton $j = 2$ configuration. This leads to a severe breaking of F-spin in the resulting wave functions. Assuming a vibrational nucleus ($\kappa' = 0$), there is no quadrupole interaction. Setting, *e.g.*, $\varepsilon_\pi = 1.5$ MeV and $\varepsilon_\nu = 1$ MeV one gets one pure neutron 2^+ state at 1 MeV and a proton 2^+ state at 1.5 MeV as shown in the lower left part of Figure 3.9 for the example of $N_\pi = 4$ proton bosons and $N_\nu = 1$ neutron boson. On the other hand, choosing equal energies for proton and neutron d-bosons, proton and neutron wave functions are mixed also for $\kappa = 0$, and one gets a symmetric 2^+ state with $F = F_{max}$ and a mixed-symmetric 2^+ state with $F = F_{max} - 1$, which are degenerate. This is depicted in the upper left part of Figure 3.9 showing a calculation in the IBM-2 using Hamiltonian (2.94) without a Majorana term. Actually, F-spin is not completely conserved, even in the case of equal d-boson energies, because the p-p and n-n terms of the quadrupole interaction are missing in the Hamiltonian. The effect is small though, and the upper panels in Figure 3.9 are denoted with F "good". For $\varepsilon_\pi \neq \varepsilon_\nu$ without quadrupole interaction the breaking of F-spin is indeed maximal. As representatives of two-phonon states the symmetric two-phonon 2^+ state and the mixed-symmetric two-phonon 1^+ state are included in Figure 3.9. Increasing the value of κ the p-n interaction affects the wave functions and thus the key observables for both states.

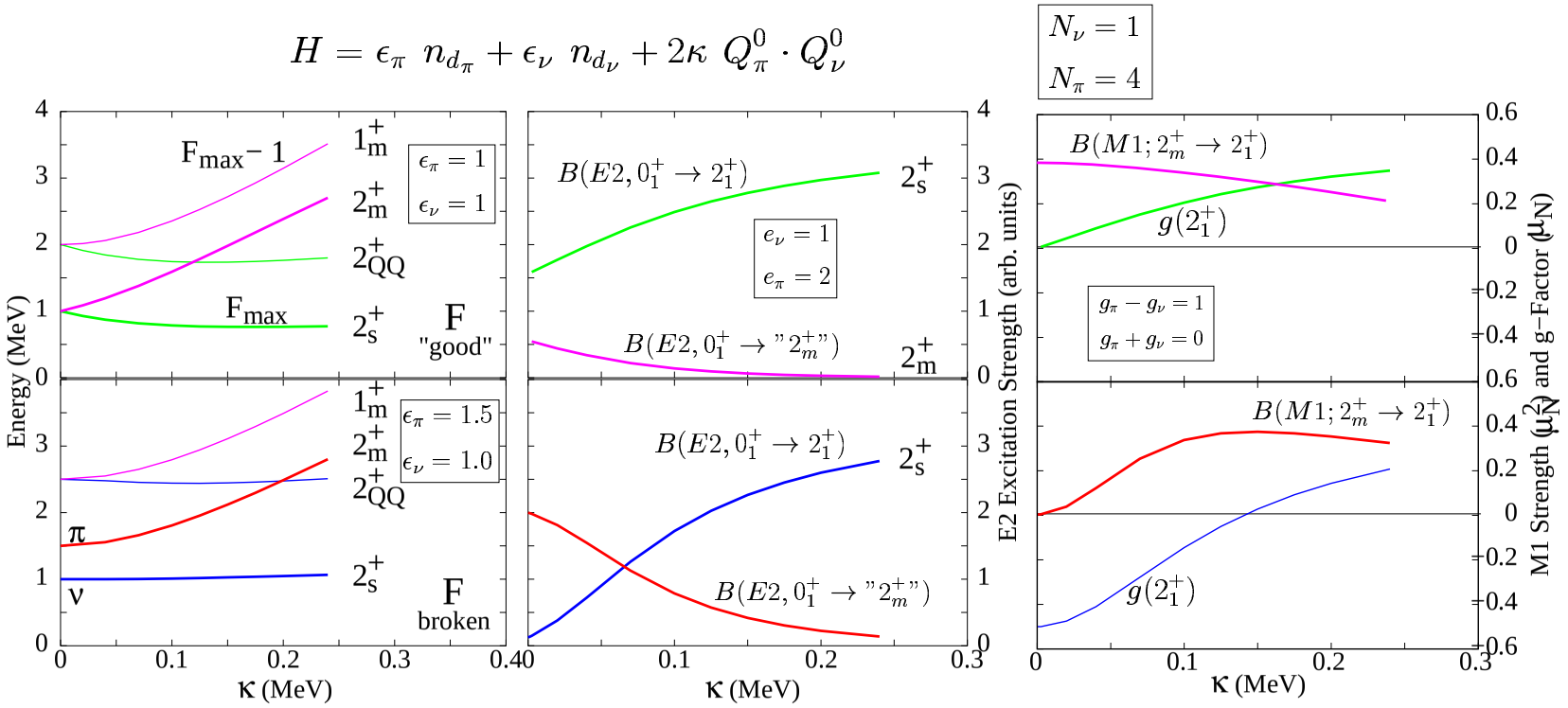

Figure 3.9: *IBM-2 calculations illustrating the F-spin breaking by the use of different d-boson energies. F-spin is restored by the p-n quadrupole interaction. Results of calculations shown in the upper row use equal d-boson energies for protons and neutrons, while different values are used in the bottom row. On the left the energies of the symmetric and mixed-symmetric, or the proton and the neutron 2^+ states are shown. The middle part illustrates the behavior of the E2 transition strengths to the ground state from both states, while the right part shows the M1 transition strength between both, and the g-factor of the 2^+_1 state. (Taken from a talk of N. Pietralla [Pie02b].)*

Energies

In the case of "good" F-spin, increasing the p-n interaction results in a separation of the F_{max} and $F_{max} - 1$ states, where the latter are strongly shifted upwards in energy, as shown in the upper left panel of Figure 3.9. For the case of broken F-spin, the p-n interaction causes a mixing of the thitherto pure proton and neutron states. The larger the interaction is, the more F-spin is restored, and states that gain mixed-symmetric character are shifted upwards, which is shown in the lower left panel. This complies to the N=52 systematics shown in Figure 3.7, where the energy of the 2^+_m state decreases in the vicinity of ^{92}Zr. Also the shell model calculations show that the p-n interaction is stronger in the heavier N=52 isotones, corresponding to the increase of κ in the IBM.

B(E2) strengths

For "good" F-spin the E2 strength of the 2^+_s state increases with κ while the E2 strength of the 2^+_m state drops almost to zero. This behavior agrees with data for near spherical nuclei where the transition of the 2^+_m to the ground state was found to be weakly collective. It is still unobserved for well-deformed nuclei. In the case of broken F-spin the situation is quite different. Due to the smaller effective boson charge for neutrons of $e_\nu = 1$ compared to $e_\pi = 2$ for the protons, the E2 strength of the pure neutron state is lower than that of the proton state. Increasing κ they come closer and finally the E2 strength of the state that evolves into the symmetric 2^+ state is dominant. This behavior is reflected in the data shown in Figure 3.7. The 2^+_s and the 2^+_m states come closer in E2 strength towards ^{92}Zr.

B(M1) strengths

For the M1 strength between both 2^+ states one gets a large value for $\kappa = 0$ in the "good" F case, while it decreases for increasing κ. For broken F-spin and small κ values the behavior is completely different. One starts with a zero M1 value ($\kappa = 0$). With increasing κ, the M1 strength increases strongly to a maximum value and then decreases weakly. Again, the drop towards small values of the p-n interaction is seen in the data shown in Figure 3.7, where the M1 strength towards ^{92}Zr decreases. The reproduction of the g-factor in the broken F case requires the use of a negative g-factor for neutron bosons. For small κ, corresponding to ^{92}Zr, the g-factor is negative and becomes positive for larger values of κ. This trend is also known from measurements of g-factors in Zirconium and Molybdenum isotopes [Jak99, Man01].

3.3.3 ^{96}Mo at N=54

The p-n quadrupole interaction is a deformation driving force. The decrease of the E2 strength of the 2^+_m state seems to agree well with the case of ^{96}Mo, where the E2 strength of the 2^+_m state as shown in the upper middle panel of Figure 3.9 could not be detected in a NRF experiment [Wer00a]. This decrease compared to the neighboring ^{94}Mo may be due to a gain in deformation by a stronger p-n quadrupole interaction. Meanwhile several measurements on ^{96}Mo followed [Wer00a]. One $\gamma\gamma$ correlation experiment was performed by the author in Cologne using the OSIRIS cube spectrometer, and another experiment using the (n,γ) reaction and the GRID technique [BoJ93] at the Institut Laue Langevin (ILL) in Grenoble. So far, both experiments are only partially analyzed and are therefore not included in this work. However, first results hint at a short lifetime of the 2^+_4 state in ^{96}Mo of about 100 fs and an almost pure M1 decay to the 2^+_1 state, identifying the 2^+_4 as the mixed-symmetric 2^+_m state. A recent experiment by the $(n,n'\gamma)$ group at the University of Kentucky [Les03] finally resolves ambiguities in the level scheme and also affirms the short lifetime. Furthermore, the ground state decay is observed for the first time in this experiment, and is an order of magnitude weaker than the ground state decay of the 2^+_m state in ^{94}Mo. Further analysis will provide substantial information for understanding the evolution of mixed-symmetric states on the path from near spherical towards deformed nuclei.

3.4 Q-phonon purity near closed shells

In 3.2.2 some parallels between shell model configurations of low-lying states in ^{92}Zr and bosons in the IBM or phonons were mentioned. Main contributions to the wave functions resemble phonon configurations in a vibrational nucleus. In this section the question is to which extent Q-phonon configurations describe the 2^+_1 and 2^+_2 states in ^{92}Zr, and also the 2^+_s and 2^+_m states in neighbor nuclei. Does the phonon picture break down for nuclei near closed shells due to shell effects?

3.4.1 Q-phonons in the shell model

In the IBM a Q-phonon excitation is equivalent to acting the E2 transition operator, in that case the quadrupole operator, on the ground state. This scheme is adopted for the shell model by identifying a Q-phonon with the shell model E2 operator, separately for protons and neutrons,

$$\boldsymbol{Q}_p = \boldsymbol{T(E2)}_p \quad \text{and} \quad \boldsymbol{Q}_n = \boldsymbol{T(E2)}_n \ . \tag{3.1}$$

Thus, a proton or neutron Q_ρ-phonon excitation can be written as

$$|2^+_{Q_\rho}\rangle = \mathcal{N}_\rho \ \boldsymbol{Q}_\rho \ |0^+_1\rangle = \sum_i \alpha_{\rho,i} \ |2^+_i\rangle \ , \tag{3.2}$$

being expanded into a sum over all 2_i^+ states with coefficients $\alpha_{\rho,i}$ and a normalization constant $\mathcal{N}_\rho$. With

$$t_{\rho,i} = \langle 0_1^+ || \boldsymbol{Q}_\rho || 2_i^+ \rangle \tag{3.3}$$

the normalization constant is

$$\mathcal{N}_\rho = \frac{1}{\sqrt{\sum_i t_{\rho,i}^2}} \ . \tag{3.4}$$

Note, that in general the configurations $|2_{Q_\rho}^+\rangle$ are not orthogonal due to the p-n interaction. Symmetric and mixed-symmetric Q-phonons are defined as

$$\boldsymbol{Q}_s = e_p \boldsymbol{Q}_p + e_n \boldsymbol{Q}_n \ , \tag{3.5}$$

$$\boldsymbol{Q}_m = e_p \boldsymbol{Q}_p - e_n \boldsymbol{Q}_n \ . \tag{3.6}$$

Again, a state created by acting $\boldsymbol{Q}_m$ on the ground state is generally not orthogonal to a state created by $\boldsymbol{Q}_s$. This is achieved by writing the symmetric $2_{Q_s}^+$ state as

$$|2_{Q_s}^+\rangle = \mathcal{N}_s \ \boldsymbol{Q}_s \ |0_1^+\rangle = \sum_i \alpha_{s,i} \ |2_i^+\rangle \ , \tag{3.7}$$

and the mixed-symmetric $2_{Q_m}^+$ state as

$$|2_{Q_m}^+\rangle = \mathcal{N}_m \ \left(\boldsymbol{Q}_m - \frac{\langle 0_1^+ | \boldsymbol{Q}_m \boldsymbol{Q}_s | 0_1^+ \rangle}{\langle 0_1^+ | \boldsymbol{Q}_s \boldsymbol{Q}_s | 0_1^+ \rangle} \ \boldsymbol{Q}_s \right) \ |0_1^+\rangle = \sum_i \alpha_{m,i} \ |2_i^+\rangle \ . \tag{3.8}$$

With

$$t_{f,i} = \langle 0_1^+ || \boldsymbol{Q}_f || 2_i^+ \rangle \ , \ f = s, m \tag{3.9}$$

the normalization constants are

$$\mathcal{N}_s = \frac{1}{\sqrt{\sum_i t_{f,i}^2}} \quad \text{and} \tag{3.10}$$

$$\mathcal{N}_m = \frac{1}{\sqrt{\sum_i t_{m,i}^2 - v \cdot t_{m,i} t_{s,i}}} \quad \text{with} \tag{3.11}$$

$$v = \frac{\langle 0_1^+ | \boldsymbol{Q}_m \boldsymbol{Q}_s | 0_1^+ \rangle}{\langle 0_1^+ | \boldsymbol{Q}_s \boldsymbol{Q}_s | 0_1^+ \rangle} = \frac{\sum_i t_{s,i} t_{m,i}}{\sum_i t_{s,i}^2} \ . \tag{3.12}$$

Thus, the amplitudes for the symmetric configuration are obtained by

$$\alpha_{s,i} = \langle 2_i^+ | 2_{Q_s}^+ \rangle = \mathcal{N}_s \cdot t_{s,i} \tag{3.13}$$

and for the mixed-symmetric configuration one gets

$$\alpha_{m,i} = \langle 2_i^+ | 2_{Q_m}^+ \rangle = \mathcal{N}_m \ (t_{m,i} - v \cdot t_{s,i}) \ . \tag{3.14}$$

Table 3.6: *SDI parameters for ^{94}Mo and ^{92,94}Zr. For an explanation of the parameters see Table 3.3.*

	$\epsilon^p_{g_{9/2}}$	$\epsilon^p_{p_{1/2}}$	$\epsilon^n_{d_{5/2}}$	$\epsilon^n_{s_{1/2}}$	$\epsilon^n_{g_{7/2}}$	$\epsilon^n_{d_{3/2}}$ [MeV]	$\epsilon^n_{h_{11/2}}$	$A^{T=1}_{pp}$	$A^{T=1}_{nn}$	$A^{T=1}_{pn}$
^{94}Mo	0.0	0.1	0.0	1.4	2.0	2.2	3.5	0.31	0.24	0.27
^{92}Zr	0.0	-0.7	0.0	1.5	1.9	2.0	3.5	0.31	0.24	0.27
^{94}Zr	0.0	-0.7	0.0	1.5	1.9	2.0	3.5	0.31	0.24	0.27
	$A^{T=0}_{pn}$ [MeV]	e_p	e_n	g^l_p		g^l_n		g^s_p		g^s_n
^{94}Mo	0.50	2.0	1.0	1		0		3.7983		-2.6019
^{92}Zr	0.20	2.1	1.1	1		0		3.7983		-2.6019
^{94}Zr	0.13	1.9	0.9	1		0		3.7983		-2.6019

These α coefficients comprise only E2 transition matrix elements that can directly be obtained from a shell model calculation. The squared overlap between the symmetric or mixed-symmetric configuration with a given 2^+ state from the calculation is a measure for the Q_s- or Q_m-phonon purity of the state. Note, that in principle one would express the wave function of the 2^+_n state as a sum over all multi-Q-configurations like

$$|2^+_n\rangle = \sum_{(Q\ldots Q)^{(2)}} a_{(Q\ldots Q)^{(2)}} \; (Q\ldots Q)^{(2)} \; |0^+_1\rangle \; , \tag{3.15}$$

in order to get the amplitude $a_{(Q\ldots Q)^{(2)}}$ of a configuration $(Q\ldots Q)^{(2)}$. However, for obtaining the Q_s- and Q_m-amplitudes this gives the same overlaps as given in Eqs. (3.13,3.14).

3.4.2 Q-phonon purity test for some nuclei

The Q-phonon purity of the two lowest 2^+ states in ^{92}Zr will be tested by using the shell model calculation. The results will be compared to the nucleus which so far is the prime example of mixed-symmetry structures, ^{94}Mo. Therefore, another shell model calculation was performed for ^{94}Mo, using the same methods as described in 3.2.1. Especially the lowering of the $g_{9/2}$ orbital was taken into account. Another calculation was done for ^{94}Zr in order to get predictions for the neighboring isotope of ^{92}Zr. Both Zirconium isotopes are expected to be very similar due to the proton substructure. The parameters for all calculations are given in Table 3.6. For the analysis of the Q-phonon purity in all the three nuclei, the 20 lowest 2^+ states were taken into account, each. Those states should carry almost the whole E2 strength from the ground state. First, the symmetric and

Table 3.7: *Q-phonon purities for ^{94}Mo, ^{92}Zr, and ^{94}Zr from the shell model calculations. i is the number of the 2^+ state that is identified with the symmetric 2^+ state, while k gives the number of the mixed-symmetric 2^+ state. $\alpha_{s,n}$ and $\alpha_{m,n}$ are the amplitudes of symmetric and mixed-symmetric one-phonon configurations in the n^{th} state, respectively. The numbers $\langle r|r\rangle$ in the two bottom lines give the impurities of one-phonon configurations in the wave functions of the states i and k.*

	^{94}Mo	^{92}Zr	^{94}Zr	
i	1	1	1	
k	3	2	2	3
$\alpha^2_{s,i}$	0.88	0.62	0.47	
$\alpha^2_{m,i}$	0.08	0.18	0.14	
$\alpha^2_{s,k}$	0.10	0.30	0.47	0.01
$\alpha^2_{m,k}$	0.68	0.53	0.27	0.48
$\langle r\|r\rangle_i$	0.04	0.20	0.39	
$\langle r\|r\rangle_k$	0.22	0.17	0.26	0.51

mixed-symmetric Q-phonon contents are analyzed. The results are given in Table 3.7. For ^{94}Mo the 2^+_1 state is a symmetric one-phonon state by 88 %, while the 2^+_3 state, identified as the 2^+_m one-phonon state in ^{94}Mo, has a Q_m-phonon purity of 68 %. This is the trend one would expect for symmetric and mixed-symmetric one-phonon states, while the impurities, especially to the 2^+_m state, are rather large. This becomes even more pronounced in ^{92}Zr, where the Q_s-purity of the 2^+_1 state drops to 62 % and the Q_m-purity of the 2^+_2 state to 53 %. This is an effect of the enhanced neutron and proton content of the 2^+_1 and 2^+_2 states, respectively, or, in the language of the IBM, an effect of F-spin breaking. Note that the $Q_{s,m}$-purities are enhanced using $\boldsymbol{Q}_s = \boldsymbol{Q}_p + \boldsymbol{Q}_n$ without effective charges, while a decrease in Zr remains. However, the amplitudes of the Q_m-configuration in the 2^+_1 state and the Q_s-configuration in the 2^+_2 state are quite large. Also for ^{94}Mo they are large enough to contain the missing one-phonon content. Therefore, it is interesting to get the one-Q-phonon content of both 2^+ states, regardless if it is symmetric or mixed-symmetric. The wave functions

$$|2^+_{Q,i}\rangle = \frac{1}{\sqrt{\alpha^2_{s,1} + \alpha^2_{m,1}}} \left(\alpha_{s,i}\ |2^+_{Q_s}\rangle + \alpha_{m,i}\ |2^+_{Q_m}\rangle\right) \tag{3.16}$$

are taken into account, which are one-Q-phonon wave functions. With the definition of a residual wave function $|r_i\rangle$ for the 2^+_i state by

$$|2^+_i\rangle = \beta\ |2^+_{Q,i}\rangle + |r_i\rangle \quad \text{, with} \tag{3.17}$$

$$\langle 2^+_{Q,i}|r_i\rangle = \langle 2^+_{Q_s}|r_i\rangle = \langle 2^+_{Q_m}|r_i\rangle = 0\ , \tag{3.18}$$

the norm $\langle r_i|r_i\rangle$ is a measure for the impurities to the one-phonon configuration of the state and should be small if the Q-phonon scheme holds for a given nucleus.

This quantity is given at the bottom of Table 3.7 for the 2_s^+ and 2_m^+ states of ^{94}Mo and ^{92,94}Zr. It is only 4 % for the 2_1^+ state in ^{94}Mo, which is remarkably small, and 22 % for the 2_3^+ state, which is quite small. Even for ^{92}Zr the one-Q-phonon content of the $2_{1,2}^+$ states is large with impurities of only 20 % and 17 %, respectively. This is a striking result, as this nucleus has only 4 valence particles and is usually expected to show only weak collectivity. But on the contrary, it shows typical collective features, although F-spin is severely broken in ^{92}Zr. This result is similar to the findings of the Tokyo shell model group that analyzed the Barium isotopic chain [Shi00]. The Q-phonon purity of the 2_1^+ state was found to be only about 90 % in ^{140}Ba, two neutrons above the N=82 shell closure. Despite the fact that in that work only the isoscalar quadrupole operator was considered, this purity is very high. This is probably because F-spin is not broken in the Ba region, as it is in the present case due to shell effects. Therefore, the one-phonon purity, considering also the isovector part of the quadrupole operator, should even rise for the Ba isotopes.

The Q-phonon purities of the first and second excited 2^+ states in ^{94}Zr are calculated to be much lower than in its neighbor. Nevertheless, it is obvious what happens when the 2_3^+ state is included. The first two 2^+ states are strongly mixed and share the symmetric one-phonon content. The third 2^+ state gets about 50 % of the mixed-symmetric one-phonon content, being mixed with the 2_2^+ state. Note, that so far no data is available for the 2_2^+ state in ^{94}Zr. A recent NRF experiment performed in Stuttgart may contribute data that allows a more sophisticated fit of the shell model parameters, that might separate the 2_2^+ and 2_3^+ states, changing the prediction of a strong mixing.

3.4.3 Are there low-lying g-bosons?

In section 3.2.2 the similarity between the 4^+ and the 2^+ states and their configurations was mentioned. Connecting this to the boson scheme of the IBM, the 2^+ configurations resemble very much what one would expect for d-bosons, while the 4^+ configurations are very g-boson like. Thus one may propose, that there are low-lying 4^+ states that contain large fractions of g-boson excitations. As there are two states of that kind, these excitations would comply with hexadecapole excitations of symmetric and mixed-symmetric character. If this holds, it might change the interpretation of the low-lying level scheme of near spherical nuclei very much, where usually only quadrupole, in some cases also octupole excitations are taken into account.

In this work signatures are identified which are in agreement with expectations for such low-lying g-bosons. But theoretical work in this direction should be resumed, in order to reveal expected influences on low-lying levels and unambiguous signatures that have to be searched for experimentally. Nevertheless, in view of the broken F-spin picture discussed for the one-phonon 2^+ states, one may adopt those findings to one-phonon 4^+ states, as the situation is very sim-

ilar in ^{92}Zr. Discussing 2^+ states, one starts from one proton and one neutron 2^+ state with a small p-n interaction, and ends with a symmetric 2^+ state at low energy and a mixed-symmetric 2^+ state shifted to higher energy in the case of a strong p-n interaction. The picture for 4^+ states may look the same. Proton and neutron 4^+ states should appear if the p-n interaction is small, as it seems to be the case in ^{92}Zr. With a larger p-n interaction one can assume, that both states get mixed into one symmetric and one mixed-symmetric configuration in this case as well, while the magnitudes of the energy shifts are unknown. Finally, a strong M1 transition between such symmetric and mixed-symmetric 4^+ configurations must be expected. Indeed, such a transition is evident from the data and the calculations. This is seen for ^{92}Zr in Table 3.4. The M1 strength amounts to 0.26(3) μ_N^2, while the model prediction is 0.47. Also in ^{94}Mo a strong M1 transition between the 4_1^+ and 4_2^+ states is known from the extensive data set collected for this nucleus [Fra03]. The measured M1 strength of the transition is remarkable with $B(M1)$=1.1(2) μ_N^2. In the shell model calculation for ^{94}Mo the 4_2^+ and 4_3^+ states seem to be interchanged, but they are close in energy and the M1 strength of the $4_3^+ \rightarrow 4_1^+$ transition is predicted to be 1.3 μ_N^2, agreeing very well with the measured value. This new data and the shell model predictions show that in the future, an analysis within a version of the IBM-2 including g-bosons is desirable, as the IBM was successful in the description of symmetric and mixed-symmetric quadrupole structures so far. The quadrupole phonon scheme, that is often extended by the inclusion of an octupole phonon, might be extended further to hexadecapole phonons. In near spherical nuclei, those might even be more important than octupole phonons, which are usually found at higher energies. More examples of M1 transitions between low-lying 4^+ states should be searched for. Note that low-lying 4^+ states should not be expected to have pure hexadecapole structure. This would rather mix with to two- or more quadrupole phonon excitations in the same energy region.

Chapter 4

The collective rotational limit

Mid-shell nuclei usually have many valence particles - especially in the A≈160 mass region, where stable mid-shell nuclei have up to 34 valence particles. Such nuclei are usually well-deformed and their level structure is of typical rotational character as protons and neutrons collectively rotate perpendicular to the symmetry axis. Another dominant but isovector collective excitation in rotational nuclei results from a counter wise oscillation of the deformed proton against the deformed neutron body, known as the scissors mode. The first observation of the decay of this excitation to the γ-band in a rotational nucleus is presented in this chapter.

4.1 The scissors mode

The scissors mode was predicted in the two-rotor model by Lo Iudice and Palumbo [LoP78, LoP79]. Their prediction of its excitation energy at about 10 MeV turned out to be far too high in their model when Richter *et al.* experimentally confirmed the scissors mode in an (e, e') experiment on ^{156}Gd [Ric83, BoR84] at an excitation energy of 3 MeV, as predicted in the IBM-2 [IaA87], identifying it as a valence space excitation. In near-spherical nuclei with vibrational character the analog of the scissors mode is the mixed-symmetry two-phonon 1^+_m state as discussed in sections 2.3.2 and 2.4.2. In the Q-phonon scheme a large M1 strength is expected between mixed-symmetric and symmetric states with the same number of Q-phonons. This implies, that the 1^+_m state should also be connected to the two-Q-phonon symmetric 2^+ state by a strong M1 transition. This has been observed for near spherical nuclei, *e.g.*, in the γ-soft ^{196}Pt [Bre96] and ^{134}Ba [Mas96], or in the vibrational ^{64}Zn [Gad02b], ^{92}Zr [Fra03b], ^{94}Mo [Fra03], and in ^{108}Cd [Gad02, Gad03]. Although the Q-phonon scheme applies to the rotational limit, where the excitation strength of the scissors mode is known to be largest, a decay to the 2^+ band head of the γ-band, which is identified with the symmetric two-Q-phonon state in well-deformed nuclei, has never been observed. The question

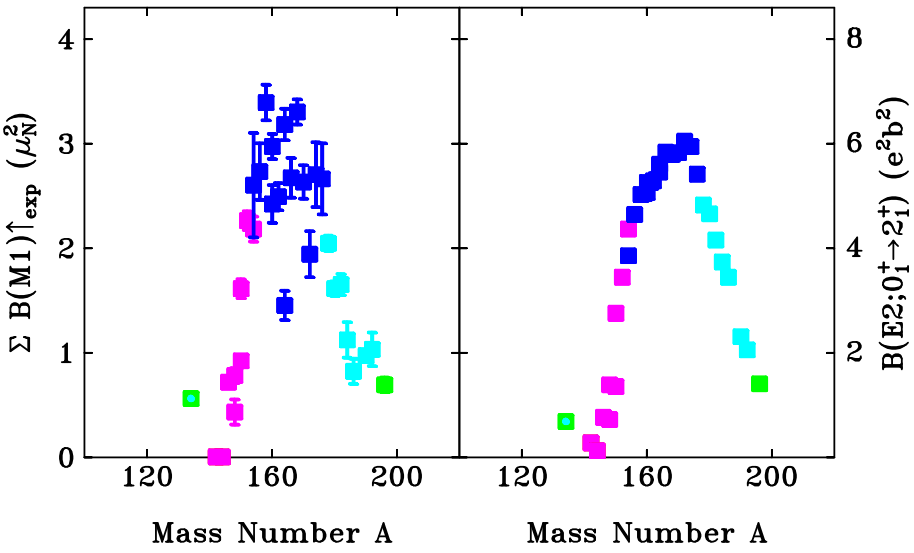

Figure 4.1: *Systematics of M1 excitation strength (left hand side) and E2 excitation strength (right hand side) across the N=82-126 neutron shell versus mass number. Both are at maximum for well-deformed rotors around mid-shell (taken from [Pie98b]).*

arises if this transition is allowed. Regarding the scissors mode as a scissors-like vibration of deformed proton and neutron bodies, which has to be annihilated, while a γ-vibration must be generated, the conclusion may be drawn, that such a two-phonon transition should be forbidden. On the other hand, from the Q-phonon picture and the IBM-2, this transition has to exist.

Searching for the decay of the scissors mode to the 2^+_γ state, one should consider nuclei where 1^+ states are known to be strongly excited from the ground state. From the extensive systematical studies of 1^+ states [Pie98b] the excitation strength of the scissors mode is known to be large in mid-shell rare earth nuclei. Figure 4.1 shows the M1 strengths in the rare earth region across a whole neutron shell, compared to the E2 excitation strength of the 2^+_1 state. As a consequence of their collective character, both show a very similar behavior with small values at shell closures and a maximum in the mid-shell region. The M1 excitation strengths are at maximum around A≈160. One of the nuclei in that region is ^{164}Dy, being especially interesting, as from NRF [Mar95] and $(n, n'\gamma)$ data [Joh95] a γ-transition at 2338 keV was observed that might represent a decay of a state at 3100 keV to the γ-band head.

4.2 Previous results for ^{164}Dy

From an early NRF experiment by Wesselborg *et al.* [Wes88] the total M1 excitation strength in ^{164}Dy was found to be considerably larger than in its neighbor ^{162}Dy. Two groups of positive parity dipole excitations have been observed, one

at low energies about 2.6 MeV, the other in the 3 MeV region where scissors mode states are expected. An earlier experiment using the ^{165}Ho(t,α) reaction [Fre89] showed a nearly pure two-quasiparticle M1 excitation in the lower energy region. A certain spin admixture in the wave functions of states in the 3 MeV region was found in an intermediate energy proton scattering experiment [Frk89], especially for a peak at 3.14 MeV, which actually at least contains the three states at 3112, 3159 and 3173 keV that were not resolved in that experiment. Taking into account the spin admixture, the orbital M1 excitation strength for the scissors mode was found to be in good agreement with the systematics [Mar95]. A serious discrepancy found in the $(n,n'\gamma)$ experiment by Johnson *et al.* for the strongest M1 excitations around 3.1 MeV was not confirmed in the remeasurement of Margraf *et al.* [Mar95] using the NRF technique. In the latter experiment many parities of $J = 1$ states were determined by Compton polarimetry, and others were proposed due to the assignment of K quantum numbers by comparison to predictions of the Alaga rules [Ala55].

The situation for some γ-transitions in ^{164}Dy is highly puzzling. For the following discussion please refer to Figure 4.2 showing various possibilities for the placement of those transitions. The most recent NRF data from [Mar95] leaves an observed γ-transition at 3027 keV unplaced. Having in mind that the 2_1^+ state is found at 73 keV, this γ-ray allows the assumption of a state at 3100 keV with spin $J = 1, 2$ decaying to the 2_1^+ state. In addition, Wesselborg *et al.* [Wes88, Wes88b] observed a γ-ray at 2337 keV in his NRF experiment with 4.1 MeV endpoint energy of the incident photons. From the known level scheme it was concluded that it should stem from a state above 2.9 MeV, because the transition was not observed in an experiment with an endpoint energy of 2.9 MeV. The ground state transition from a state at 3100 keV could impossibly have been observed, neither in this nor in the Margraf experiment, because at the same energy the peak of the strong decay of a 1^+ state at 3173 keV to the 2_1^+ state would have covered it completely. Nevertheless, in [Mar95] the 2337 keV γ-transition was placed as the decay of a 1^- state at 2412 keV to the 2_1^+ state. So the γ-ray at 3027 keV could also stem from the ground state decay of a level at that energy.

Another decay scheme can be proposed from the energies of the observed transitions. Assuming that a state at 3100 keV excitation energy exists, it might decay to the 2_1^+ and 2_γ^+ states via the 3027 keV and 2337 keV transitions, respectively. In that case one may assume that other states may show decays to the γ-band head, too. For example, the strong M1 excitation at 3173 keV might also decay to the 2_γ^+ state via a 2411 keV transition. From this, one would conclude that the pair of peaks at 2337 keV and 2412 keV observed by [Mar95] does not correspond to decays from a state at 2412 keV, but to decays from an unobserved state at 3100 keV and the 1^+ state at 3173 keV, respectively.

Since we find two contradictory possibilities for placing the observed γ-tran-

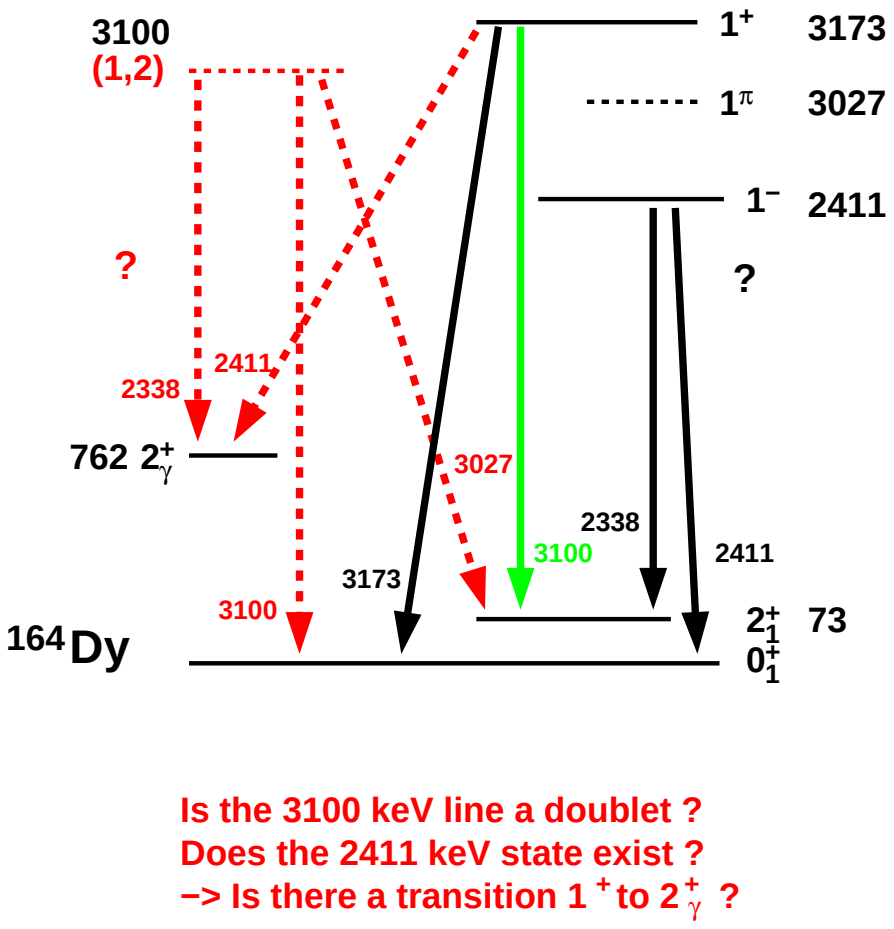

Figure 4.2: *The ^{164}Dy puzzle as discussed in the text. Solid lines and arrows denote placed states and transitions, while dashed lines and arrows represent unplaced γ-transitions or even assumed states and their γ-decays. Energies are given from the present experiment.*

sitions, the desired identification of decays to the γ-band makes a clear distinction between both unavoidable. Therefore new NRF experiments have been performed that are presented in the following, with the aim of the firm identification of decays from 1^+ states to the head of the $K = 2$ γ-band.

4.3 NRF experiment on ^{164}Dy at Stuttgart

4.3.1 Experimental details

^{164}Dy was measured at the NRF setup at the IfS Stuttgart as described in section 2.1.1. The target composition is given in appendix B. In a first experiment the target was irradiated for 6 days at an endpoint energy of 2.9 MeV. Beam was on target for about 134 hours with an electron current on the radiator target of 320 μA. In this experiment only states below 2.9 MeV were excited, without the possibility of observing decays of higher-lying states in the spectrum. A second experiment was done at an endpoint energy of 3.6 MeV during a 4 days beam time, resulting in 79 hours of beam on the target with a current of 200 μA. In this experiment, known scissors mode states above 3 MeV were expected to be excited, while eventual decays to the γ-band should still be observable (762 keV below the excitation energy). The endpoint energy was chosen in order to be sensitive in the 2.4 MeV energy region, while having enough photon flux around 3.1 MeV. The photon flux calibration of the low-energy measurement is shown in Figure 4.3. For a calibration at low energies natural LiF was added to the target, in order to observe γ-lines from ^{19}F with well-known cross sections.

4.3.2 Experimental results for ^{164}Dy

The results of both NRF measurements are summarized in Table 4.1. In total 33 states have been observed, 9 of them for the first time, and lifetimes were determined. The determination of such a number of new states clearly shows the increase in sensitivity compared to [Mar95]. Spins were assigned from angular distributions as explained in Figure 4.4. Data from the low- and the high-energy experiments are in very good agreement. Therefore, feeding of states below 2.7 MeV from higher-lying excited states can be excluded within the errors and weighted averages of both experiments are given. For transitions to lower-lying excited states with unknown multipolarities pure dipole radiation is assumed in all cases, except for quadrupole excitations, where E2 radiation is assumed. Parities have been assigned from K-quantum numbers following, or taken from [Mar95]. An overall error for all the energies of 0.5 keV has been considered. For the states at 3173 keV, 3317 keV, and 3415 keV, a detected branch to the 2^+_γ state at 762 keV has been taken into account in Table 4.1. The branching ratios Γ_γ/Γ_0 to the γ-band head are 0.05(1) for the state at 3173 keV, 1.2(3) for the

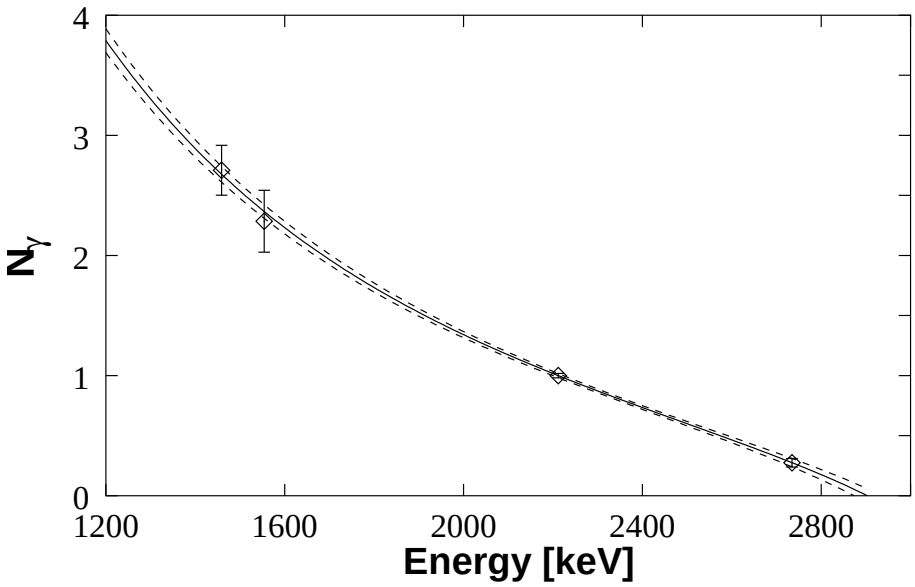

Figure 4.3: *Photon flux calibration for the experiment on ^{164}Dy at 2.9 MeV endpoint energy. The data points are from the calibration standards ^{27}Al and ^{19}F (two points at low energies), to which the Schiff formula [Sch51] is fitted. The dashed lines give the error of the function.*

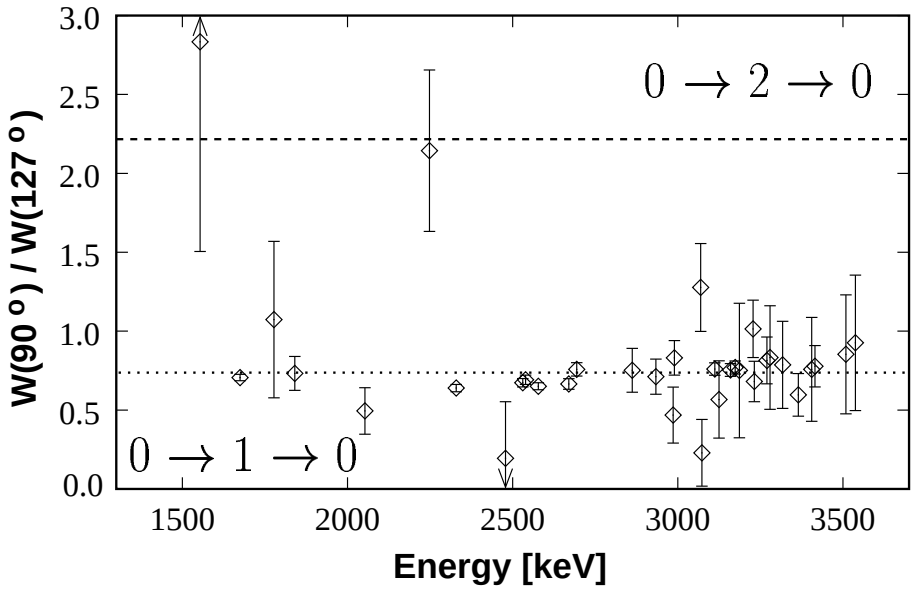

Figure 4.4: *Angular distribution ratio $W(90°)/W(127°)$ for the ground state transitions of states in ^{164}Dy. Dashed lines give the expectation values for dipole and quadrupole states. Data points below 2600 keV stem from the low-energy measurement, the others from the high-energy measurement.*

state at 3317 keV, and 1.5(2) for the state at 3415 keV. In all other cases at most a decay to the 2_1^+ state at 73 keV was detected.

Table 4.1: *Data obtained from the NRF experiment on ^{164}Dy. For each state the level energy E_x, spin and parity J^π, decay branching ratio R_{exp}, ground state transition width Γ_0, the integrated scattering cross section $I_{s,0}$, $B(\Pi\lambda)\uparrow$ excitation strength, and the lifetime τ are given. E1 strengths are given in units of $10^{-3}e^2fm^2$, M1 strengths in μ_N^2 and E2 strengths in e^2fm^4. In case of unknown parity possible M1 and E1 strengths are listed. For transitions to the 2_1^+ states pure dipole radiation is assumed from $J = 1$ states, and pure quadrupole radiation from $J = 2$ states.*

E_x [keV]	J	R_{exp}	Γ_0 [meV]	$I_{s,0}$ [eV·b]	$B(\Pi\lambda)\uparrow$ [μ_N^2],[10^{-3}e^{2}fm^2], [e^{2}fm^4]	τ [fs]
1554.1*	(2^+)	–	0.19(3)	1.5(2)	E2 127(22)	3550^{+720}_{-515}
1674.6	1^-	1.78(2)	24.6(6)	39.5(9)	E1 15.0(4)	10.5^{+3}_{-3}
1777.3*	(1)	–	0.18(5)	0.7(2)	M1 0.008(2) E1 0.09(3)	3660^{+1500}_{-825}
1840.4	1	0.93(11)	1.87(14)	3.5(2)	M1 0.077(6) E1 0.86(7)	194^{+16}_{-14}
2052.9	1^{-a}	2.00(20)	1.75(26)	1.7(2)	E1 0.58(8)	135^{+23}_{-17}
2248.1*	2^+	1.03(16)	0.80(9)	1.6(1)	E2 87(10)	440^{+53}_{-43}
2329.5	1^-	1.88(5)	31.6(10)	24.8(7)	E1 7.16(23)	7.7^{+3}_{-2}
2478.7*	(1)	–	0.42(13)	0.8(2)	M1 0.007(2) E1 0.08(2)	1570^{+720}_{-380}
2531.0	1^+	0.54(1)	23.2(6)	27.8(7)	M1 0.370(9)	19.0^{+5}_{-5}
2539.3	1^+	0.51(3)	19.4(6)	23.7(6)	M1 0.308(9)	23.1^{+7}_{-7}
2578.0	1^+	0.50(1)	34.1(10)	40.6(12)	M1 0.516(16)	13.2^{+4}_{-4}
2669.8	1^-	1.25(3)	29.0(11)	21.8(8)	E1 4.37(16)	10.5^{+4}_{-4}
2693.8	1^+	0.50(2)	41.8(16)	45.6(17)	M1 0.555(22)	10.8^{+4}_{-4}
2862.1	1^+	0.46(5)	9.9(9)	9.8(8)	M1 0.110(10)	46.7^{+47}_{-39}
2933.5*	1^{+b}	0.43(15)	5.5(7)	5.2(4)	M1 0.056(7)	86^{+12}_{-9}
2985.8	1^{-a}	1.86(33)	7.6(13)	3.6(5)	E1 0.82(14)	31.9^{+68}_{-48}
2989.7	1^{+b}	0.72(12)	11(1)	8.5(5)	M1 0.107(10)	35.6^{+36}_{-30}
3069.0	(1)	–	2.4(6)	2.9(7)	M1 0.021(5) E1 0.24(6)	277^{+86}_{-53}
3073.1*	1	–	1.5(4)	1.8(5)	M1 0.013(3) E1 0.15(4)	445^{+155}_{-90}
3111.7	1^+	0.52(2)	124.4(46)	99.8(35)	M1 1.070(39)	3.6^{+1}_{-1}

continued on next page

E_x [keV]	J	R_{exp}	Γ_0 [meV]	$I_{s,0}$ [eV·b]	$B(\Pi\lambda)\uparrow$ $[\mu_N^2]$,$[10^{-3}\mathrm{e}^2\mathrm{fm}^2]$, $[\mathrm{e}^2\mathrm{fm}^4]$	τ [fs]
3124.9*	1	1.3(3)	3.1(7)	1.6(3)	M1 0.026(6) E1 0.29(7)	99^{+30}_{-18}
3159.5	1^+	0.56(2)	115.6(44)	88.0(31)	M1 0.950(36)	3.7^{+1}_{-1}
3173.3	1^+	0.46(3)	100.9(40)	80.7(29)	M1 0.819(33)	4.4^{+2}_{-2}
3185.9	1*	–	0.93(20)	1.1(2)	M1 0.007(2) E1 0.08(2)	705^{+190}_{-120}
3227.8	1^-	2.0(4)	15.7(34)	6.1(11)	E1 1.34(29)	14.8^{+41}_{-26}
3231.6	1*	–	5.2(4)	5.7(4)	M1 0.040(3) E1 0.44(3)	127^{+10}_{-9}
3269.3	1	1.39(13)	8.0(7)	3.8(3)	M1 0.059(5) E1 0.66(6)	35.8^{+36}_{-30}
3278.7	1	–	1.36(20)	1.5(2)	M1 0.010(2) E1 0.11(2)	485^{+85}_{-60}
3316.8	$1^{(+)}$	0.64(15)	7.6(11)	2.9(4)	M1 0.059(5)	30.8^{+54}_{-40}
3364.5	1	1.20(13)	7.9(8)	3.8(3)	M1 0.053(5) E1 0.59(6)	39.4^{+45}_{-37}
3405.2*	1	–	1.56(25)	1.6(2)	M1 0.010(2) E1 0.11(2)	420^{+80}_{-55}
3414.7	1^{+b}	0.37(8)	16.1(13)	5.6(4)	M1 0.105(8)	14.3^{+12}_{-11}
3508.5*	1	1.23(24)	4.1(9)	1.8(3)	M1 0.025(5) E1 0.27(6)	75^{+21}_{-14}
3537.4*	1	–	1.9(3)	1.7(3)	M1 0.011(2) E1 0.12(2)	350^{+60}_{-45}

* New from present data.

[a] Tentative parity assignment based on K=0

[b] Tentative parity assignment based on K=1

Note, that the excitation strengths from the present data above 3.1 MeV show a systematical deviation to lower values, compared to [Mar95]. This may be because in the present experiment the highest point for the photon flux calibration is at 2980 keV. However, a strong deviation already 100-200 keV above this point seems unreasonable. Remarks to the identification of some states are given in the following.

1554 keV

The angular distribution ratio for this newly discovered state favors spin $J = 2$, while the error is still large and within two standard deviations (2σ) $J = 1$ cannot be excluded.

1777 keV

The γ-ray at 1777 keV was observed for the first time in the present experiment, showing an angular distribution ratio in agreement with a $J = 1$ assignment. Therefore, it is listed as the excitation energy of a state at that energy. Nevertheless, the energy is 762 keV below the rather strong M1 excitation at 2539 keV and may be a decay of that state to the γ-band. In that case a rather isotropic angular angular distribution would be expected, which is also in agreement with data. The only way to determine the placement of γ-transition unambiguously would afford a measurement with an endpoint energy below 2539 keV.

1980/1983 keV

A peak at 1981 keV has been identified as a doublet because of its peak width, that is considerably larger than that of other peaks in the region. Assuming that the whole peak area were from the decay of the 2053 keV state to the 2_1^+ state at 73 keV, the branching ratios deduced from the three independent spectra are inconsistent. Setting the peak width to a calibrated value and fitting a second peak results in two lines at energies of 1980 keV and 1983 keV. The 1980 keV fits well to the expected 2053 keV to 73 keV transition. The 1983 keV line is almost unverifiable under 127°. From this a spin $J = 2$ can be assumed. This data fits well to the known 2^+ state at that energy in ^{162}Dy, which it is hence identified with. Also the decay of that state to the 2_1^+ state in ^{162}Dy at 1902 keV has been observed in two of the detectors.

2479 keV

The γ-line at 2479 keV would usually be identified with the single escape of the 2990 keV γ-line. Nevertheless, it was also observed in the low-energy measurement, where the state at 2990 keV was not excited. Only the detectors at 127° and 150° provided satisfactory statistics. The tentative assignment $J = 1$ is given in parentheses.

2828 keV

In [Mar95] a γ-transition at 2828 keV was reported with an integrated cross section of $I_s = 2.52(44)$ eVb. This γ-line was not observed in the present experiment, where the sensitivity limit was definitely low enough. Thus, a γ-transition at 2828 keV cannot be confirmed.

3073 keV

This line was identified because of the asymmetry of the peak at 3069 keV. This results in a large error for the intensity of this transition, but the angular

distribution ratio is still in favor of $J = 1$.

3125 keV, 3269 keV, 3364 keV, and 3415 keV

The R_{exp} values of these states do not allow an unambiguous K-assignment and no assumption for the parities can be made. This may be an indication of K-mixing. For the 3364 keV state in [Mar95] a decay branching ratio of $R_{exp} = 0.56(50)$ was given and $K = 1$ assumed, which is not confirmed by the present data. Interestingly, in [Mar95] K-mixing was proposed only for the E1 excitations around 2.6 MeV, whereas it might also appear at these states around 3.3 MeV.

4.3.3 Decays to the γ-band

The key observation in the Stuttgart NRF experiments is depicted in Figure 4.5, showing parts of the spectra taken at 2.9 MeV and at 3.6 MeV endpoint energy, respectively. γ-transitions have been observed at 2338 keV, 2412 keV, 2554 keV, and 2653 keV, but *only* in the 3.6 MeV experiment. At 2.9 MeV endpoint energy they did not appear. Note that all other peaks visible in the spectra shown in Figure 4.5 are identified. The only transitions that are not placed are at the four given energies. The peak at 2412 keV is the smallest of all four, but can be identified in all the three detectors, some with large errors in the peak areas though. The other three peaks were clearly observed in all three spectra. The peak at 2653 keV is surrounded by single escape lines, whereas the largest peak of all is that at 2338 keV. From the measured intensities it is assured that all four peaks would have appeared in the 2.9 MeV spectrum if they corresponded to ground state decays of states at those energies, or to a decay to the 2_1^+ state in the case of the 2338 keV γ-ray (see Figure 4.2). But at the marked energies in the 2.9 MeV spectrum nothing but background is to be seen.

It is concluded that the four observed γ-rays stem from excited states above an excitation energy of 2.9 MeV, and hence are no ground state decays. From the known level scheme of ^{164}Dy the only possibility to place the γ-transitions at 2412 keV, 2554 keV, and 2653 keV is as decays from excited dipole states at 3173 keV, 3317 keV, and 3415 keV to the 2_γ^+ state at 762 keV. The state emitting the 2338 keV γ-ray should then be the so far only presumed state at 3100 keV. However, a direct measurement of the ground state decay of such a state is missing, that would finally consolidate a state at that energy. Using continuous bremsstrahlung, it is impossible to observe a state at 3100 keV, because at the same time the strong M1 excitation at 3173 keV would be excited, decaying to the 2_1^+ state via a 3100 keV γ-ray. From present data the decay branching ratio for the 3173 keV 1^+ state is $R_{exp} = 0.46(3)$, which is just about the value of 0.5 expected for a $K = 1$ state. If a considerable part of the peak area at 3100 keV originated from the ground state decay of a 3100 keV state, the R_{exp} value of the 1^+ state would decrease, leading to a contradiction with the Alaga rules that

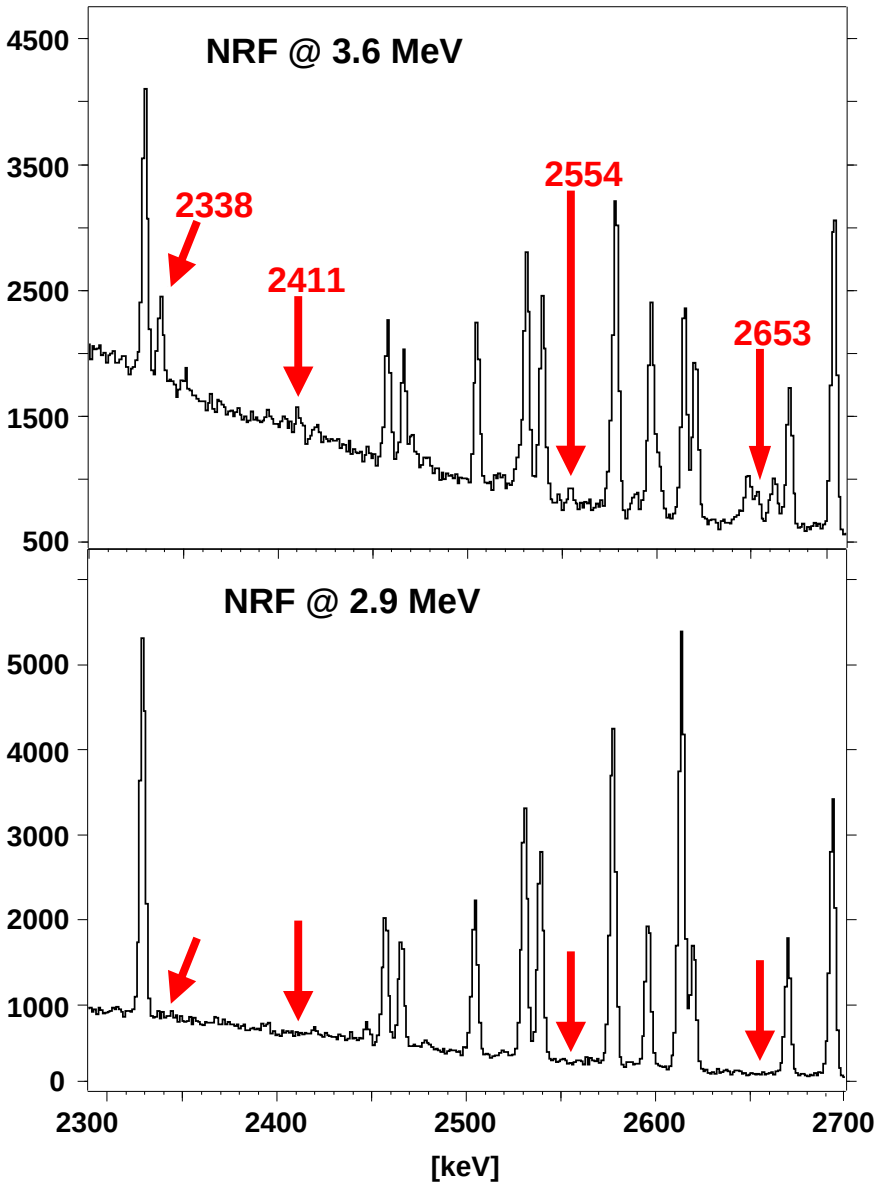

Figure 4.5: *Zoom into the spectra taken at 2.9 MeV and 3.6 MeV endpoint energy. At the energies marked by arrows, peaks have been observed in the high-energy experiment alone, whereas they are not observed in the low-energy experiment.*

are fulfilled for all the other 1^+ states observed. Therefore, one can assume that only a small portion of the 3100 keV peak area is due to an excited state at that energy. This means a weak excitation strength of that state, whereas the decays to the 2^+_γ and the 2^+_1 states are strong. These considerations led to a subsequent experiment at the HIγS, which is subject of the next section, before drawing final conclusions.

4.4 NRF experiment on ^{164}Dy at Duke

4.4.1 Experimental details

At the free electron laser laboratory at Duke University ^{164}Dy was investigated at two beam energies, 3100 keV and 3173 keV, respectively. During 4 days data was accumulated for about 29 hours at 3100 keV beam energy, and 11 hours at a beam energy of 3173 keV, respectively. In between there was time for energy and efficiency calibrations and direct measurements of the beam energy. Because the photon flux at HIγS is about 1-2 orders of magnitude lower than at Stuttgart, accordingly more target material is needed in order to gain enough statistics. The typical weight of a target is about 50-100 g, but no large amount of isotopically enriched ^{164}Dy target material was available. Therefore, about 79 g of natural Dy_2O_3 were used, together with the enriched material from the previous experiments. The exact target composition is given in appendix B. The natural Dy_2O_3 was contained in a plastic cylinder, the enriched material was placed on the front of that cylinder. In addition to the setup described in section 2.1.3 walls of lead bricks were installed in front of and behind the detectors, in order to suppress background radiation.

4.4.2 Results at 3100 keV

This was the first time that a NRF experiment at HIγS was performed with the aim of searching for decays of excited states to lower lying excited states. In the measurement with a beam energy of 3100 keV γ-rays at 3100 keV, 3027 keV, and 2338 keV have been observed. Figure 4.6 shows the regions of interest of the spectrum. From the appearance of the small peaks at 3100 keV and 3027 keV alone, one cannot conclude the existence of a state at 3100 keV in ^{164}Dy yet, because in ^{163}Dy a state at 3099 keV is known from [Mar95], also decaying via a 3027 keV transition to the first excited state. Nevertheless, the γ-ray at 2338 keV stems from ^{164}Dy and is evident in the spectra. Due to the small energy spread of the beam with a FWHM of about 65 keV, this decay must stem from a state around 3100 keV. The only possibility for placing this transition in the level scheme is as a transition from a state exactly at that energy to the 2^+_γ state. Therefore, the existence of a dipole or quadrupole excited state at 3100 keV is

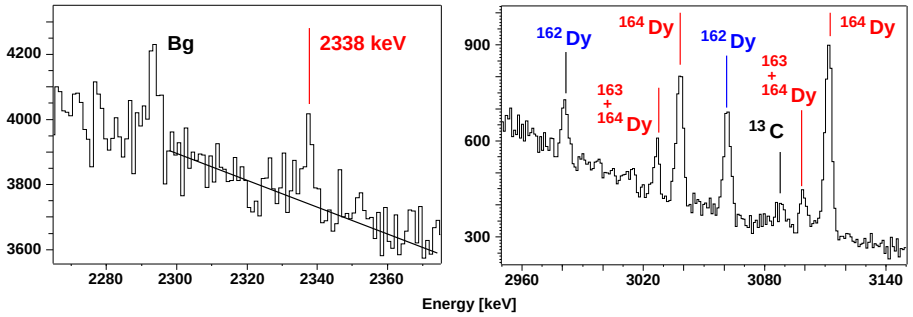

Figure 4.6: *The regions of interest of the spectrum taken at 3100 keV beam energy. The sum spectrum of all four detectors is shown. In the left picture the peak at 2338 keV from ^{164}Dy is marked, in the right picture peaks are marked according to the isotopes from which they originate.*

confirmed.

The prospect from the previous NRF experiment, that the ground state decay of this newly discovered state should be small, has been affirmed, too. A small decay branch to the ground state, but strong decays to lower-lying 2^+ states as observed in the experiment at the IfS Stuttgart are typical for a quadrupole excited state. Therefore, in the following, spin and parity 2^+ are tentatively assigned for that state. An obviously weak excitation strength of the 3100 keV state from the ground state, and the observed strong decays to the 2^+_1 and 2^+_γ states imply a short lifetime of the state. While the errors are quite large, the analyzing power (see Eq. (2.31) in section 2.1.4) for the small line at 2338 keV is given by $P_{ana}(2338) = 0.31(18)$. While this value does not allow a clear assignment of a multipole mixing ratio δ, it restricts to either almost pure M1 strength with possible small E2 admixtures, or dominant E2 strength with only small M1 admixtures (compare Figure 4.7). The decays to the lower-lying 2^+ states are assumed to have dominant M1 character, because extraordinary strong E2 decays are unlikely (due to the short lifetime).

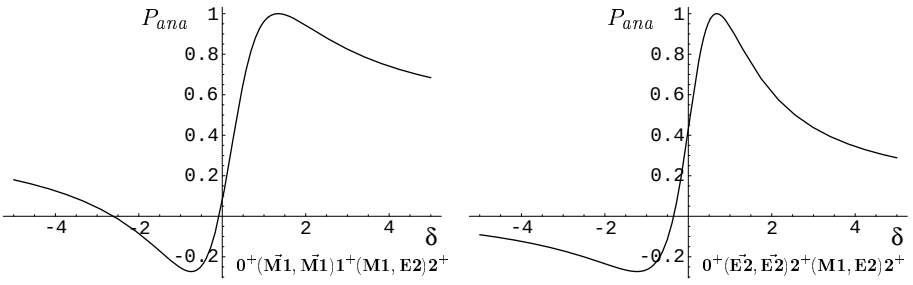

Figure 4.7: *Analyzing powers for magnetic dipole (left) and electric quadrupole (right) excitations from the ground state with a subsequent decay to a 2^+ state, as a function of the multipole mixing ratio delta of the latter transition.*

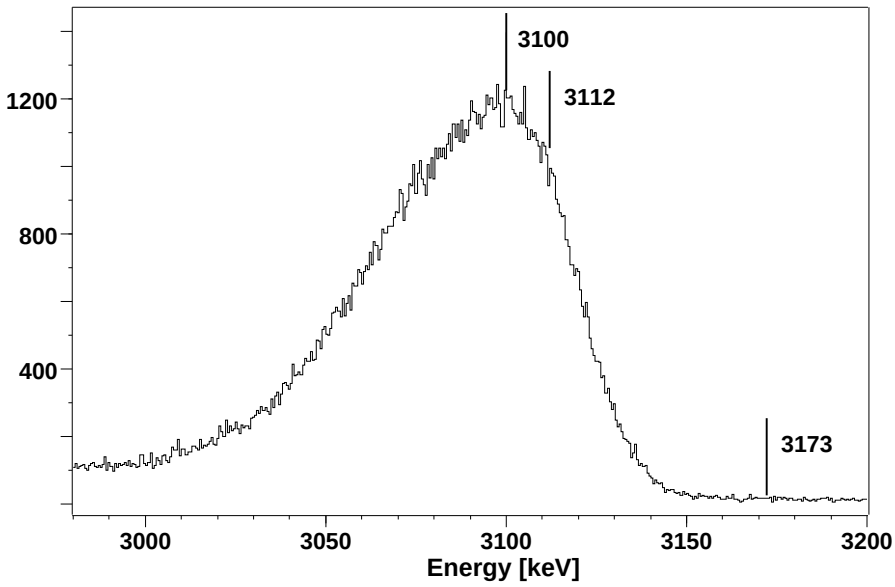

Figure 4.8: *Spectrum of the γ-ray beam, taken with a HPGe detector in beam direction at a beam energy of 3100 keV. 3112 keV is close to the beam maximum, while 3173 keV is not covered.*

Combining IfS and HIγS data for the 3100 keV state

From a combination of the NRF data taken at Stuttgart and Duke one can estimate the lifetime of the state at 3100 keV. The major problem is the contamination from ^{163}Dy in the 3100 keV line. Without any knowledge on the cross sections of both decays at 3100 keV it is not possible to separate the lines. Fortunately, the well known 3112 keV 1^+ state in ^{164}Dy is also excited due the finite energy spread of the beam, shown in Figure 4.8. Note, that this beam profile was taken with reduced beam and during the experiment the spread should be somewhat larger. Nevertheless, while the state at 3173 keV was obviously not excited, the state at 3112 keV lies close to the beam maximum. Due to the known integrated photon scattering cross sections for the γ-rays at 3112 keV from ^{164}Dy ($I_{s,0}$ = 99.8(35) eV barn, this work), and at 3100 keV from ^{163}Dy ($I_{s,0}$ = 8.8(12) eV barn, [Mar95]), it is possible to separate the two peaks at 3100 keV. Taking into account the relative amount of ^{163,164}Dy in the target, the known cross sections, and the angular correlation values for the specific spin cascades, the fraction of the area of the 3100 keV peak, that stems from ^{163}Dy, can be calculated for the sum spectra of the horizontal or all detectors. For this calculation the ratio between the photon fluxes at both energies plays a role and is estimated from the beam profile (see Figure 4.8) to be $N_\gamma(3100)/N_\gamma(3112) = 0.92$.

Therefrom, the contaminations from ^{163}Dy to the 3100 keV line can be corrected. This leads to a peak area of 40(60), *i.e.* consistent with zero, for the

ground state transition of the assumed 2^+ state in ^{164}Dy in the spectra of the vertical detectors. This is in agreement with the expectations for a 1^+ or 2^+ state (compare Figure 2.7). From the sum spectrum one gets a branching ratio for the decays of the 2^+ state to the 2^+_γ and the ground state of $\Gamma_\gamma/\Gamma_0 = 6.8(34)$.

The integrated cross section of the 2338 keV decay has been measured in Stuttgart to be $I_{s,\gamma} = 14.7(11)$ eV barn. The formulas

$$\frac{\Gamma_0\Gamma_\gamma}{\Gamma} = \left(\frac{2338\text{keV}}{\pi\hbar c}\right)^2 I_{s,\gamma} \tag{4.1}$$

(compare to Eq. (2.7)) and

$$\Gamma_0 = \frac{\Gamma_0\Gamma_\gamma}{\Gamma} \cdot \left(1 + \frac{\Gamma_0}{\Gamma_\gamma} + \frac{\Gamma_1}{\Gamma_\gamma}\right) \tag{4.2}$$

were used for the determination of the ground state transition width Γ_0 of the 3100 keV state. The ratios Γ_1/Γ_γ and $\Gamma_0\Gamma_\gamma/\Gamma$ are provided by Stuttgart data, and Γ_0/Γ_γ by HIγS data, resulting in $\Gamma_0 = 40.8(38)$ meV. The total decay width of the state is $\Gamma = 540(190)$ meV, equivalent to a lifetime of $\tau = 1.2^{+7}_{-3}$ fs.

Note, that the relative error is large due to low statistics and the weak ground state transition of the 3100 keV state. Assumptions on the spin of the state and the multipolarities of its decays were also made. Nevertheless, the lifetime resulting from the data is astonishing small. It would not change a lot if another spin for the state was assumed. The observed transitions to the lower-lying 2^+ state have strengths in the order of 1 μ_N^2. The possibility of E2 transitions cannot be excluded, and the strengths would be in the order of 20–100 W.u.

The 1^+ state at 3173 keV was measured to have a decay branching ratio of $R_{exp} = 0.46(3)$ at the IfS. The procedure described above leads to a correction of this value. This correction is small, because it is assured that the main part of the peak at 3100 keV in the Stuttgart spectra is due to the $1^+ \to 2^+_1$ decay. The corrected value is $R_{exp} = 0.43(3)$.

4.4.3 Results at 3173 keV

In the measurement with a beam energy of 3173 keV the branching ratio of the state at that energy to the 2^+_1 state has been determined directly. A contamination to the peak at 3100 keV from the decay to the 2^+_1 state can be neglected. The photon flux at this energy was about an order of magnitude lower than at 3173 keV, and the ground state decay branch of the state at 3100 keV is known to be small. The decay branching ratio is $R_{exp} = 0.41(5)$, in good agreement with the corrected IfS result given above. The weak decay to the 2^+_γ state was

Table 4.2: *Results from both HIγS measurements. For each state the excitation energy E_x, the γ energies of transitions to lower-lying levels E_γ, the level spin, and the parity, deduced from the analyzing power, are given. For each transition the analyzing power P_{ana}, the intensity relative to the ground state transition, and δ values determined from the analyzing power are listed.*

E_x [keV]	E_γ [keV]	J	π	P_{ana}	I_γ	δ
			^{164}Dy			
3099	3099.3(5)	(2)	(+)	–[a]	100	(E2)
	3026.7			–[a]	540(280)	
	2337.6(5)			0.31(18)	680(340)	-0.09^{+14}_{-14}
						5^{+15}_{-3}
3112	3111.6(5)	1	+	0.86(4)	100	M1
	3038.2(5)			0.01(5)	54(3)	-0.07^{+5}_{-5}
						-2.70^{+40}_{-45}
3160	3159.7(5)	1	+	0.88(6)	100	M1
	3086.3			–[a]		
3173	3173.4(5)	1	+	0.75(10)	100	M1
	3099.6(5)			0.06(11)	41(5)	-0.02^{+11}_{-11}
						-3.2^{+6}_{-16}
			^{162}Dy			
3062	3061.6(5)	1	+	0.83(5)	100	M1
	2981.2(5)			0.16(12)	36(5)	0.07^{+11}_{-10}
						-4.6^{+16}_{-40}

[a] doublet with a line from ^{163}Dy

not observed due to the high Compton background at 2411 keV.

In addition to the determination of branching ratios to lower-lying states, the measurements at both energies gave unambiguous confirmations of the parities of the dipole excited states in the energy region. To illustrate the analyzing power for the determination of parities, Figure 4.9 shows the peaks at 3160 keV and 3173 keV. There are strong lines in the spectrum measured with the horizontal detectors, whereas the peaks almost vanish in the spectrum from the vertical detectors. This is a clear indication for the positive parity of those states. There are still some counts in the vertical detectors due to the finite opening angle. Therefrom values of the analyzing power P_{ana} deviate somewhat from the ideal value, which is 1.

The information for all states observed in this experiment is summarized in Table 4.2. From the comparison of experimental and theoretical values of the analyzing power, shown in Figure 4.7, values of the multipole mixing ratio δ are

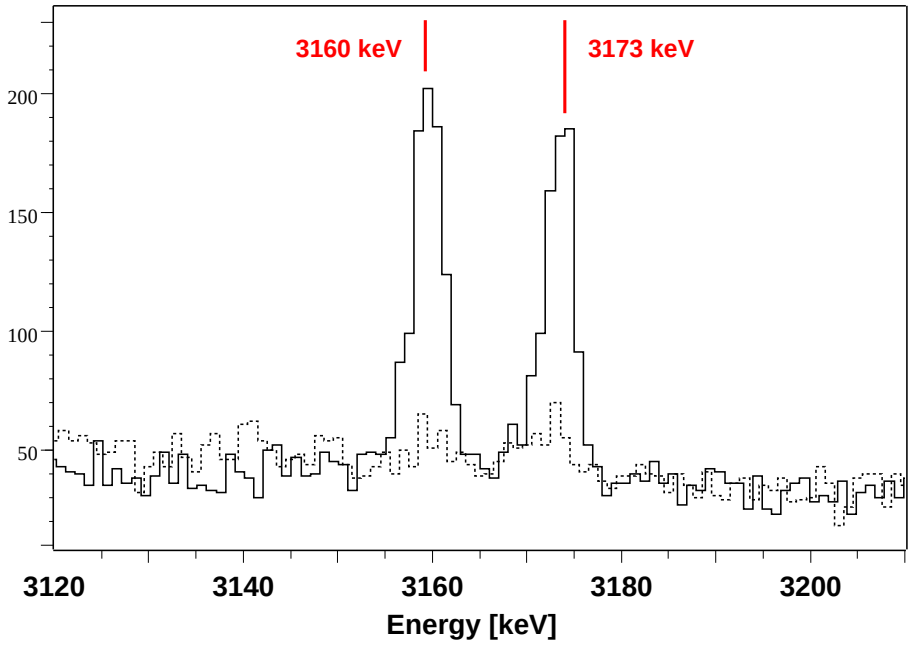

Figure 4.9: *The peaks at 3160 keV and 3173 keV are only observed in the spectrum from the horizontal detectors (solid line), while they are unobserved in the spectrum from the vertical detectors (dashed line). This allows a direct assignment of parity $\pi = +$ to the corresponding dipole excited states.*

given for transitions to 2^+ states. In all cases two solutions for δ are possible.

4.5 Summary of the results for ^{164}Dy

From the data gathered in the NRF experiments at Stuttgart and Duke the following conclusions are drawn for ^{164}Dy. There is a state at 3100 keV which shows a decay behavior typical for a 2^+ state. Strong transitions connect this state with the 2^+_1 and the 2^+_γ states, while it has a weak transition to the ground state. The observation of the decay of this state to the γ-band at HIγS backs the placement of the γ-transitions at 2338 keV, 2411 keV, 2554 keV, and 2653 keV from the IfS data to be transitions from states above 3 MeV to the 2^+_γ state. Therefore, the previously assigned 1^- state at 2412 keV does not exist. The puzzle described in section 4.2 is solved and the revised level scheme is shown in Figure 4.10.

The 1^+ state at 3173 keV is known as one main fragment of the scissors mode. The observation of its decay via a 2411 keV γ-ray is the first observation of a scissors mode fragment decaying to the γ-band in well-deformed, rotational nuclei. Table 4.3 gives the transition strengths of those 1^+ states, that show decays to the γ-band. For all transitions to 2^+ states pure M1 transitions are

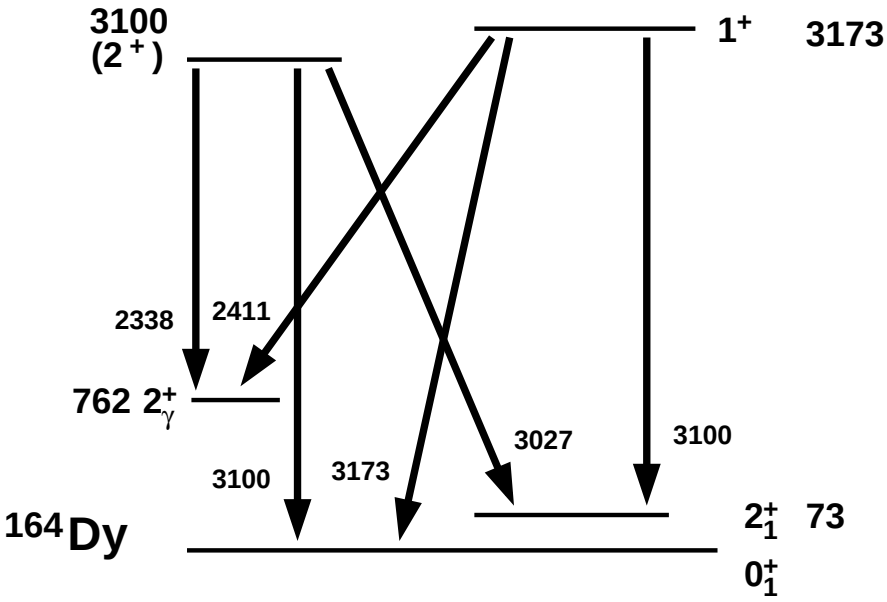

Figure 4.10: *Revised scheme of the discussed levels and transitions, presenting the solution of the ^{164}Dy puzzle.*

assumed. M1 strengths calculated within the SU(3) limit of the IBM-2 using the analytical expressions from [Isa86] are also given. The predicted absolute strength is not reproduced by any of the states. However, this cannot be expected, as each state may at most be a fragment of the calculated scissors mode state. Only the 1^+ state at 3173 keV shows relative transition strengths in the way they are expected for the scissors mode within the IBM-2. The transition to the 2^+_1 state amounts to about 50 % of the ground state transition strength, and the transition strength to the 2^+_γ state is about 10 % relative to the ground state transition strength. This supports the assignment of this state as a main fragment of the scissors mode. From their decay behavior, the structure of the other 1^+ states must be of different nature.

Table 4.3: *Transition strengths of the 1^+ states that show decays to the γ-band head. In the first column transition strengths of the scissors mode are given, calculated within the IBM-2 for boson numbers $N_\pi = N_\nu = 8$ and $g_\pi - g_\nu = 1$.*

$[\mu_N^2]$	IBM	3173 keV	3316 keV	3415 keV
$B(M1; 1^+ \to 0^+_1)$	1.3	0.28(1)	0.018(3)	0.035(3)
$B(M1; 1^+ \to 2^+_1)$	0.72	0.12(1)	0.012(4)	0.013(4)
$B(M1; 1^+ \to 2^+_\gamma)$	0.14	0.03(1)	0.05(1)	0.11(2)

Chapter 5

Summary and outlook

Two limiting cases of collectivity in nuclear structure have been highlighted in this work. ^{92}Zr, being close to the doubly magic sub-shell closure at ^{88}Sr, was investigated by a photon scattering experiment at the IfS Stuttgart. Due to the small number of valence particles and the underlying shell structure, ^{92}Zr is a representative of what has been called the limit of weak collectivity. From this experiment first lifetime information on the 2_2^+ state was obtained. The short lifetime leads to a strong M1 decay to the 2_1^+ state, which is the main signature for the one-phonon mixed-symmetry 2_m^+ state.

However, certain deviations from the picture of a symmetric one-phonon 2_1^+ state and its mixed-symmetric counterpart have been found and explained by a close look at the shell structure, that suppresses proton configurations in the 2_1^+ state. This leads to a small g-factor of this state as measured by Jakob *et al.* [Jak99]. A comparison of the NRF data and data from subsequent $(n, n'\gamma)$ and $(\vec{\gamma}, \gamma')$ experiments at the University of Kentucky and Duke University [Fra03b, FraPC], respectively, with shell model calculations performed within this work was made. The calculation for ^{92}Zr reproduces the low-lying levels and transitions between them very well. It clearly affirms the enhanced neutron content of the 2_1^+ state and other shell effects, *e.g.*, the strong mixing between the first excited 0^+ and the ground state. A signature of this mixing has also been found in the data on dipole excited states.

From the IBM-2 the enhanced neutron content of the 2_1^+ state is understood in terms of F-spin breaking. The significantly different energies of protons and neutrons needed to form a $j = 2$ configuration, and the weak proton-neutron interaction result in proton and neutron 2^+ states. In the IBM-2 this is modeled by choosing different energies for proton and neutron bosons. Systematic calculations in the IBM-2 for this case as a function of the p-n interaction nicely reproduce the systematics in the N=52 isotones. For a small p-n interaction, F-spin is severely broken, resulting in a situation, which is the same for ^{92}Zr. A larger p-n interaction restores F-spin, resulting in symmetric and mixed-symmetric one-phonon 2^+ states, as found in ^{94}Mo and ^{96}Ru. This is very similar to the shell

model results, where the proton-neutron structure of the lowest 2^+ states was found to be very sensitive to the $T = 0$ p-n interaction.

Despite these shell effects, ^{92}Zr shows collective characteristics. One is the possibility of a qualitative understanding in a collective model, the IBM-2, where a weakening of collectivity results in a breaking of F-spin. Another characteristic is that predictions of the Q-phonon scheme are fulfilled to a large extent in ^{92}Zr. Thus, the lowest two 2^+ states have been shown not to have symmetric or mixed-symmetric character, but they can still be described as one-quadrupole-phonon excitations from the ground state. 80 % of the wave functions of the 2^+_1 and 2^+_2 states have been found to be exhausted by one-phonon configurations. Already in ^{94}Mo with two more protons the one-phonon purity of the 2^+_1 and the 2^+_3 states is restored, and these states show pronounced symmetric and mixed-symmetric character, respectively. This is to be seen from theory and very well confirmed by the extensive data sets for this nucleus.

An interesting aspect for future works is the investigation of nuclei similar to ^{92}Zr, but without the blocking of a $j = 2$ proton configuration in the lowest 2^+ state due to the shell structure. Such an investigation may give insight into a system with one proton and one neutron boson in a case where F-spin is not broken. The question should be followed whether proton and neutron components mix into a symmetric and a mixed-symmetric 2^+ state in that case. Unfortunately, candidates for such studies are generally not easy to access experimentally, *e.g.*, as they are found at the edge of the valley of stability or even unstable. A first step to such investigations has recently been done in a Coulomb excitation experiment on ^{88}Kr in inverse kinematics at CERN using the MINIBALL spectrometer and a rare isotope beam (RIB). Other experiments on unstable neutron rich N=52 isotones are planned at the GSI using the RIB facility in combination with the newly installed RISING setup. Another, promising and much easier accessible nucleus is ^{84}Kr, which could be investigated in NRF using the newly accessible gas targets at Stuttgart, as well as by fusion evaporation reactions.

g-boson like excitations have been identified in ^{92}Zr and also seem to be evident in low-lying 4^+ states in ^{94}Mo. With the given experimental data base for such excitations, calculations within the *sdg*-IBM-2 would be important for a systematical investigation of g-boson admixtures to symmetric and mixed-symmetric states. Also more realistic microscopic calculations for ^{92}Zr are desirable, *e.g.* using Monte Carlo Shell Model (MCSM) methods as in [Shi00], or the quasiparticle-phonon model (QPM), which had very successfully been applied to ^{94}Mo by Lo Iudice and Stoyanov [LoS00, LoS02].

The other limit of collectivity addressed in this work is the rotational limit with a large number of valence nucleons. Corresponding nuclei with axially symmetric deformation are found at mid-shell. Proton neutron symmetric states at low energies form the rotational bands, *e.g.* the $K = 0$ ground state band or the $K = 2$ γ-band. The mixed-symmetric 1^+ scissors mode is found to be the band

head of a $K = 1$ band at excitation energies of about 3 MeV. From a geometrical point of view, a decay of the scissors mode to the 2^+_γ state should be forbidden, due to the two-phonon character of the transition. In contradiction, within the IBM-2, this transition is allowed with an M1 strength of about 10 % of the ground state transition strength.

A puzzle had been left for ^{164}Dy from previous experiments. Strong 1^+ excitations were identified around 3 MeV, the way they were expected for a rotational nucleus. γ-transitions were observed with energies, which made them candidates for transitions from one of the scissors mode's main fragments to the γ-band, but they were placed as decays from a lower lying state. This puzzle has been solved in the present work. From NRF data taken at Stuttgart it has been proven that γ-rays, including the previously observed, stem from dipole states above 3 MeV excitation energy. One of them is a decay of the mentioned scissors mode fragment to the 2^+_γ state.

Another NRF experiment using a polarized γ-beam at Duke University was performed in order to show the existence of a previously assumed state by direct observation. This aim was achieved, and, while spin $J = 1$ cannot be excluded, the newly identified state is probably a 2^+ state showing strong decays to the 2^+_1 and 2^+_γ state. From this observation the yet uncertain transition strength of the scissors mode fragment to the 2^+_1 state at the same energy has been fixed, too.

From both experiments it has been concluded that the scissors mode fragment at 3173 keV decays to the γ-band head, approving the predictions of the IBM-2. The relative transition strength from theory and experiment are in good agreement.

Nevertheless, spin-flip contributions to the wave functions of 1^+ states in the 3 MeV region were discussed by previous authors. While the agreement with the model prediction is striking, it cannot be excluded that the transition from the 1^+ state at 3173 keV in ^{164}Dy to the 2^+_γ state stems from a spin part in its wave function. Unfortunately, in the (p, p') experiment by Frekers *et al.* [Frk89] the energy resolution was about 90 keV and the fragments of the scissors mode around 3.1 MeV were not resolved. For the identification of the spin part in the wave functions of the single 1^+ states in that region it therefore would be interesting to repeat this experiment using particle detectors with enhanced resolution, as they are available today, *e.g.*, at the LMU München.

As future projects the decay of the scissors mode to the γ-band should be searched for in other well-deformed nuclei. One candidate is ^{162}Dy where the M1 excitation strength is large and no spin contaminations to the scissors mode are assumed. Most efficient would be the excitation of the strongest fragments of the scissors mode separately using a polarized γ-beam at HIγS. The present work showed that weak branches in the energy region 2-2.5 MeV are easily missed due to the high Compton background. In order to be sensitive to such decay branches, the experimental setup has to be enhanced. This can be done by a proper lead shielding of the detectors, comparable to the setup at the IfS Stuttgart. The lead

has to be very clean in order to suppress the γ-ray at 2614 keV from the β-decay of ^{208}Bi, which is responsible for a large part of the Compton background. In addition, Compton shields should be used for background suppression.

Also promising is the search for decays of the scissors mode using γ-spectroscopy following β-decay. This is possible for some nuclei in the rare earth region. Finally, it would be desirable to get more information on short lived 2^+ states in the 3 MeV energy region, as one candidate has been found in ^{164}Dy. Such states are candidates for fragments of the mixed-symmetric one-phonon 2^+ state expected in that energy region. Using exclusively isotopically enriched target material at HIγS would allow a firm assignment of a lifetime and, placing one detector at 45° in the horizontal plane, of a spin to the candidate in ^{164}Dy.

Appendix A

Parametrizations of the IBM-1 Hamiltonian

Different types of parametrizations of the ECQF Hamiltonian were used in the last years. Some confusion appeared when one tried to transform one parametrization into another in order to convert certain parameter sets. Especially in the context of the investigation of phase transitions in nuclei many parametrizations were used. Some parametrizations of the ECQF Hamiltonian are

$$\begin{aligned} H_{ECQF} &= \varepsilon\, \boldsymbol{n_d} - \kappa'\, \boldsymbol{Q}^{\chi}.\boldsymbol{Q}^{\chi} \\ &= \kappa' \left(\frac{\varepsilon}{\kappa'}\, \boldsymbol{n_d} - \boldsymbol{Q}^{\chi}.\boldsymbol{Q}^{\chi} \right) , \qquad \text{(A.1)} \\ H_{ECQF} &= \varepsilon\, \boldsymbol{n_d} + \kappa\, \boldsymbol{Q}^{\chi}.\boldsymbol{Q}^{\chi} \\ &= \kappa \left(\frac{\varepsilon}{\kappa}\, \boldsymbol{n_d} + \boldsymbol{Q}^{\chi}.\boldsymbol{Q}^{\chi} \right) , \qquad \text{(A.2)} \\ H_{ECQF} &= \tilde{\kappa} \left(\frac{1-\xi}{\xi}\, \boldsymbol{n_d} - \boldsymbol{Q}^{\chi}.\boldsymbol{Q}^{\chi} \right) , \qquad \text{(A.3)} \\ H_{ECQF} &= c \left(\eta\, \boldsymbol{n_d} - \frac{1-\eta}{N}\, \boldsymbol{Q}^{\chi}.\boldsymbol{Q}^{\chi} \right) , \qquad \text{(A.4)} \\ H_{ECQF} &= a \left((1-\zeta)\, \boldsymbol{n_d} - \frac{\zeta}{4N}\, \boldsymbol{Q}^{\chi}.\boldsymbol{Q}^{\chi} \right) . \qquad \text{(A.5)} \end{aligned}$$

The form (A.1) is the one originally used in [IaA87], using a positive parameter, κ', for the quadrupole interaction. Later on often a negative κ was used as in parametrization (A.2). In both parametrizations, κ' and κ, respectively, set an absolute energy scale, while ε/κ' and ε/κ, respectively, are the structural parameters distinguishing vibrational and rotational structures, just like ξ, η and ζ in the other parametrizations. The parameter χ is always the same in all parametrizations with common values of $\chi \in [-\sqrt{7}/2, \sqrt{7}/2]$. The parametrizations (A.3)–(A.5) were used recently in the discussion of shape phase transitions, having the advantage that infinite values for structural parameters are avoided, as

the range for ξ, η, and ζ is $[0,1]$ in all three cases, while only in (A.4) and (A.5) no infinite value appears in the Hamiltonian. The parametrization (A.3) was given by F. Iachello, *e.g.*, in [IaZ98]. Parametrization (A.4), used, *e.g.*, in [JoC99], takes into account the N-dependence of the quadrupole interaction. Thus, parameters derived for special structural regions of the model space are quite stable to changes of the boson number N. This is the same for parametrization (A.5) [Wer00b], while the main difference of both notations is the parameter where the rotational-vibrational shape phase transition occurs, which is at $\zeta_c = 0.5$ in (A.5) for $N \to \infty$. Table A.1 gives formulas for the conversions between parametrizations (A.1)–(A.5).

Table A.1: Conversions between the parameters of the ECQF Hamiltonian given in (A.1)–(A.5). The parameter ranges are $\varepsilon/\kappa' \in [0,\infty]$, $\varepsilon/\kappa \in [-\infty,0]$, and $\xi,\eta,\zeta \in [0,1]$.

	(A.1)	(A.2)	(A.3)	(A.4)	(A.5)
(A.1)		$\varepsilon/\kappa' = -\varepsilon/\kappa$ $\kappa' = -\kappa$	$\varepsilon/\kappa' = \dfrac{1-\xi}{\xi}$ $\kappa' = \tilde{\kappa}$	$\varepsilon/\kappa' = \dfrac{N\eta}{1-\eta}$ $\kappa' = \dfrac{c(1-\eta)}{N}$	$\varepsilon/\kappa' = 4N\dfrac{1-\zeta}{\zeta}$ $\kappa' = \dfrac{a\zeta}{4N}$
(A.2)	$\varepsilon/\kappa = -\varepsilon/\kappa'$ $\kappa = -\kappa'$		$\varepsilon/\kappa = \dfrac{\xi-1}{\xi}$ $\kappa = -\tilde{\kappa}$	$\varepsilon/\kappa = \dfrac{N\eta}{\eta-1}$ $\kappa = \dfrac{c(\eta-1)}{N}$	$\varepsilon/\kappa = 4N\dfrac{\zeta-1}{\zeta}$ $\kappa = -\dfrac{a\zeta}{4N}$
(A.3)	$\xi = \dfrac{1}{1+\varepsilon/\kappa'}$ $\tilde{\kappa} = \kappa'$	$\xi = \dfrac{1}{1-\varepsilon/\kappa}$ $\tilde{\kappa} = -\kappa$		$\xi = \dfrac{1-\eta}{1+(N-1)\eta}$ $\tilde{\kappa} = c\dfrac{1-\eta}{N}$	$\xi = \dfrac{\zeta}{4N+(1-4N)\zeta}$ $\tilde{\kappa} = \dfrac{a\zeta}{4N}$
(A.4)	$\eta = \dfrac{\varepsilon/\kappa'}{N+\varepsilon/\kappa'}$ $c = \kappa'(\varepsilon/\kappa'+N)$	$\eta = \dfrac{-\varepsilon/\kappa}{N-\varepsilon/\kappa}$ $c = \kappa(\varepsilon/\kappa-N)$	$\eta = \dfrac{1-\xi}{1+(N-1)\xi}$ $c = \tilde{\kappa}\dfrac{1+(N-1)\xi}{\xi}$		$\eta = \dfrac{4(\zeta-1)}{3\zeta-4}$ $c = \dfrac{1}{4}a(4-3\zeta)$
(A.5)	$\zeta = \dfrac{4N}{4N+\varepsilon/\kappa'}$ $a = \kappa'(4N+\varepsilon/\kappa')$	$\zeta = \dfrac{4N}{4N-\varepsilon/\kappa}$ $a = \kappa(\varepsilon/\kappa-4N)$	$\zeta = \dfrac{4N\xi}{1+(4N-1)\xi}$ $a = \tilde{\kappa}\dfrac{1+(4N-1)\xi}{\xi}$	$\zeta = \dfrac{4(\eta-1)}{3\eta-4}$ $a = c(4-3\eta)$	

Appendix B

Target compositions

The target composition for the ^{92}Zr experiment at the IfS Stuttgart is given in Table B.1. The same target was used for both, the high- and the low-energy measurement.

The compositions of the targets used in the measurements on ^{164}Dy at the IfS Stuttgart and HIγS are given in Tables B.2, B.3, and B.4. In the IfS low-energy experiment ^{27}Al and LiF$^{\text{nat.}}$ were added for the photon flux calibration. Adding LiF$^{\text{nat.}}$ was not necessary in the high-energy experiment, because the low-energy calibration points from ^{19}F were not needed. The enriched target material from the IfS experiments was also added to the HIγS target as it is equivalent to almost 10 g of natural Dy.

For the correct determination of the number of nuclei from a given isotope contained in the target, chemical contaminations and contaminations from other isotopes were taken into account in all cases. Target impurities were known from the producer's certificates.

Table B.1: *Target composition for the high- and low-energy NRF measurement on ^{92}Zr at the IfS Stuttgart.*

$^{92}ZrO_2$	1351 mg
enrichment in ^{92}Zr	91.4 %
^{27}Al	761.3 mg

Table B.2: *Target composition for the low-energy NRF measurement on ^{164}Dy at the IfS Stuttgart.*

$^{164}Dy_2O_3$	1486.4 mg
enrichment in ^{164}Dy	96.0 %
$^{164}Dy^{met.}$	1100 mg
enrichment	95.6 %
^{27}Al	780.5 mg
$LiF^{nat.}$	1217.9 mg

Table B.3: *Target composition for the high-energy NRF measurement on ^{164}Dy at the IfS Stuttgart.*

$^{164}Dy_2O_3$	1486.4 mg
enrichment in ^{164}Dy	96.0 %
$^{164}Dy^{met.}$	1100 mg
enrichment	95.6 %
^{27}Al	503.1 mg

Table B.4: *Target composition for the polarized NRF measurement on ^{164}Dy at HIγS.*

$^{nat.}Dy_2O_3$	78.71 g
$^{164}Dy_2O_3$	1486.4 mg
enrichment in ^{164}Dy	96.0 %
$^{164}Dy^{met.}$	1100 mg
enrichment	95.6 %

List of publications

Regular publications

First authorships – commented

These publications emanate from key topics of my work at the IKP Köln during the PhD project. They include topics different to those of this dissertation. Therefore, they are briefly commented.

- V. Werner, D. Belic, P. von Brentano, C. Fransen, A. Gade, H. von Garrel, J. Jolie, U. Kneissl, C. Kohstall, A. Linnemann, A.F. Lisetskiy, N. Pietralla, H.H. Pitz, M. Scheck, K.-H. Speidel, F. Stedile, and S.W. Yates,
  Proton-neutron structure of the N=52 nucleus ^{92}Zr,
  Phys. Lett. B **550** (2002) 140.

  This paper reports first lifetime data on the 2_2^+ state and the first observation of the strongest dipole excitations below 4 MeV in ^{92}Zr. Some of the aspects from in this thesis are given. Finding signatures of F-spin breaking as in ^{92}Zr may help in the discussion of so far unknown shell effects in the region of neutron rich nuclei in the future. This makes this nucleus an interesting object for studies how such effects manifest in data. The first NRF measurement already initiated two subsequent experiments [Fra03b, FraPC].

- V. Werner, P. von Brentano, R.F. Casten, and J. Jolie,
  Singular character of critical points in nuclei,
  Phys. Lett. B **527** (2002) 55.

  Basic observables like the ratio $B(E2;4_1^+ \rightarrow 2_1^+)/B(E2;2_1^+ \rightarrow 0_1^+)$, that is an approximation to the shape invariant K_4 commented below, or the energy ratio $R_{4/2} = E(4_1^+)/E(2_1^+)$, are shown to be indicators for quantum phase transitions in nuclei. Quadrupole shape invariants, characterizing nuclear deformation, are sensitive to drastic changes of nuclear structure as appearing at phase transitional points. Systematic calculations within the IBM show that these observables differ most between vibrational and rotational nuclei and show sharp rises in a certain parameter range of the

IBM, corresponding to the so-called critical point symmetries X(5) and E(5) suggested by F. Iachello [Iac00, Iac01]. The same behavior is shown in an analysis of wave function entropy. Considering the quadrupole moment $Q(2_1^+)$ led to the formal identification of the O(6) dynamical symmetry limit itself as a phase transitional point between prolate and oblate deformation in a later work [Jol01]. A further step led to the invention of a phase diagram for nuclei including first and second order phase transitions and a triple point, in analogy to the phase diagram of water, following Landau theory [Jol02].

- V. Werner, P. von Brentano, and R.V. Jolos,
  Simple relations among E2 matrix elements of low-lying states,
  Phys. Lett. B **521** (2001) 146.

  The quadrupole shape invariant $q_4^{(J)} = \langle 0_1^+|(QQ)^{(J)}(QQ)^{(J)}|0_1^+\rangle$ is defined using different intermediate coupling $J = 0, 2, 4$. From geometrical models these expressions are related by simple geometrical factors, with each involving sums over matrix elements of different nuclear eigenstates. This allows the formulation of relations between basic observables like
  $B(E2; 2_1^+ \to 2_1^+) + B(E2; 2_2^+ \to 2_1^+) = B(E2; 4_1^+ \to 2_1^+)$.
  The proportionality between the three expressions is generally not given, e.g., in the IBM where the quadrupole operators do not commute. However, from the selection rules of the Q-phonon scheme one gets approximations to the exact expressions for the shape invariants $q_4^{(J)}$ and obtains relations among them that are equivalent to the geometrical relations in the limit of large boson numbers N. It is shown within the IBM and comparing data for a variety of nuclei belonging to different structural regions, that the E2 relations hold with good accuracy.

- V. Werner, H. Meise, I. Wiedenhöver, A. Gade, and P. von Brentano,
  Collective bands in the triaxial nucleus ^{124}Xe,
  Nucl. Phys. A **693** (2001) 451.

  Non-yrast states of ^{124}Xe have been investigated with the ^{123}Te(^{3}He,2n) reaction using the Cologne OSIRIS *cube spectrometer [Mei99]. Data reveals pronounced Q-phonon structures and is compared to calculations within the IBM-1, showing a good agreement with a parameter set that is transitional between the O(6) and U(5) dynamical symmetry limits. The second excited 0^+ state is suggested as a state belonging to the O(6) class of states with quantum number $\sigma = N - 2$. Quadrupole shape invariants for the ground state and effective deformation parameters are calculated.*

- V. Werner, N. Pietralla, P. von Brentano, R.F. Casten, and R.V. Jolos,
  Quadrupole shape invariants in the interacting boson model,
  Phys. Rev. C **61** (2000) (R)021301.

This work was done within the diploma thesis and gives the systematical behavior of quadrupole shape invariants [Kum72, Cli86, Jol97] over the full parameter space of the ECQF Hamiltonian. The invariants are shown to be shape parameters like the deformation parameters β and γ in the geometrical model, to which they are directly related, whereas they represent a more general concept including fluctuations of the shape parameters due to vibrations. Analytical expressions of the shape invariants are given for the dynamical symmetry limits of the IBM-1. Rapid changes in the shape invariants are related to regions showing shape coexistence, that were to be associated with phase transitional regions. This paper was a foundation for some of the previously mentioned works.

Other publications

- M. Scheck, H. von Garrel, N. Tsoneva, D. Belic, P. von Brentano, C. Fransen, A. Gade, J. Jolie, U. Kneissl, C. Kohstall, A. Linnemann, A. Nord, N. Pietralla, H. H. Pitz, F. Stedile, C. Stoyanov, and V. Werner,
  Dipole strength distributions in the stable Ba isotopes $^{134--138}$Ba: A study in the mass region of a nuclear shape transition,
  accepted by Phys. Rev. C (2004).

- A. Gade, N. Pietralla, P. von Brentano, D. Belic, C. Fransen, U. Kneissl, C. Kohstall, A. Linnemann, H.H. Pitz, M. Scheck, N.A. Smirnova, F. Stedile, and V. Werner,
  Investigation of dipole excitations in ^{142}Ce using resonant photon scattering,
  Phys. Rev. C **69** (2004) 054321.

- C. Fransen, N. Pietralla, A. Linnemann, V. Werner, and R. Bijker,
  Low-spin γ-ray spectroscopy of the (critical-point?) nucleus ^{122}Ba,
  Phys. Rev. C **69** (2004) 014313.

- K. Jessen, A. Dewald, J. Eberth, G. Gersch, J. Jolie, N. Pietralla, T. Steinhardt, N. Warr, D. Weißhaar, V. Werner, P. von Brentano, and S.M. Lenzi,
  Investigation of low spin states in ^{48}Cr with the MINIBALL γ-ray spectrometer,
  Phys. Rev. C **68** (2003) 047302.

- N. Pietralla, C. Fransen, A. Gade, N.A. Smirnova, P. von Brentano, V. Werner, and S.W. Yates
  Proton-neutron structure of the effective quadrupole-octupole coupled E1 transition operator,
  Phys. Rev. C **68** (2003) 031305.

- M. Scheck, D. Belic, P. von Brentano, J.J. Carroll, C. Fransen, A. Gade, H. von Garrel, U. Kneissl, C. Kohstall, A. Linnemann, N. Pietralla, H.H. Pitz, F. Stedile, R. Toman, and V. Werner,
Photon scattering experiments off ^{176}Hf and the systematics of low-lying dipole modes in the stable even-even Hf isotopes ^{176,178,180}Hf,
Phys. Rev. C **67** (2003) 064313.

- A. Nord, J. Enders, A.E. de Almeida Pinto, D. Belic, P. von Brentano, C. Fransen, U. Kneissl, C. Kohstall, A. Linnemann, P. von Neumann-Cosel, N. Pietralla, H.H. Pitz, A. Richter, F. Stedile, and V. Werner,
Low-energy photon scattering experiments of ^{151,153}Eu, ^{163}Dy, and ^{165}Ho and the systematics of the M1 scissors mode in odd-mass rare-earth nuclei,
Phys. Rev. C **67** (2003) 034307.

- A. Gade, D. Belic, P. von Brentano, C. Fransen, H. von Garrel, J. Jolie, U. Kneissl, C. Kohstall, A. Linnemann, H.H. Pitz, M. Scheck, F. Stedile, and V. Werner,
Dipole excitations in ^{108}Cd,
Phys. Rev. C **67** (2003) 034304.

- C. Fransen, N. Pietralla, Z. Ammar, D. Bandyopadhyay, N. Boukharouba, P. von Brentano, A. Dewald, J. Gableske, A. Gade, J. Jolie, U. Kneissl, S.R. Lesher, A.F. Lisetskiy, M.T. McEllistrem, M. Merrick, H.H. Pitz, N. Warr, V. Werner, and S.W. Yates,
Comprehensive studies of low-spin collective excitations in ^{94}Mo,
Phys. Rev. C **67** (2003) 024307.

- J. Jolie, P. Cejnar, R.F. Casten, S. Heinze, A. Linnemann, and V. Werner,
Triple Point of Nuclear Deformations,
Phys. Rev. Lett. **89** (2002) 182502.

- A. Gade, A. Fitzler, C. Fransen, J. Jolie, S. Kasemann, H. Klein, A. Linnemann, V. Werner, and P. von Brentano,
Nonyrast states of ^{108}Cd: Investigation with complementary $\gamma\gamma$-spectroscopic methods,
Phys. Rev. C **66** (2002) 034311.

- L. Käubler, K.D. Schilling, R. Schwengner, F. Dönau, E. Grosse, D. Belic, P. von Brentano, M. Bubner, C. Fransen, M. Grinberg, U. Kneissl, C. Kohstall, A. Linnemann, P. Matschinsky, A. Nord, N. Pietralla, H.H. Pitz, M. Scheck, F. Stedile, and V. Werner,
Influence of the N=50 neutron core on dipole excitations in ^{87}Rb,
Phys. Rev. C **65** (2002) 054315.

- J. Bryssinck, L. Govor, F. Bauwens, D. Belic, P. von Brentano, D. De Frenne, C. Fransen, A. Gade, E. Jacobs, U. Kneissl, C. Kohstall, A. Linnemann, A. Nord, N. Pietralla, H.H. Pitz, M. Scheck, F. Stedile, and V. Werner,
  Low-Energy Electromagnetic Excitation Strengths in ^{121}Sb and ^{123}Sb,
  Phys. Rev. C **65** (2002) 024313.

- J. Jolie, R.F. Casten, P. von Brentano, and V. Werner,
  Quantum phase transition for gamma-soft nuclei,
  Phys. Rev. Lett. **87** (2001) 162501.

- C. Fransen, P. von Brentano, A. Gade, V. Werner, N. Pietralla, U. Kneissl, and H.H. Pitz,
  Identification of Mixed-Symmetry States in ^{94}Mo,
  Acta Phys. Pol. B **32** (2001) 777.

- C. Fransen, N. Pietralla, P. von Brentano, A. Dewald, J. Gableske, A. Gade, A. Lisetskiy, and V. Werner,
  First Observation of a Mixed-Symmetry Two-Q-Phonon $2^+_{2,ms}$ State in ^{94}Mo,
  Phys. Lett. **508B** (2001) 219.

- F. Stedile, E.E. Fill, D. Belic, P. von Brentano, C. Fransen, U. Kneissl, C. Kohstall, A. Linnemann, P. Matschinsky, A. Nord, N. Pietralla, H.H. Pitz, M. Scheck, and V. Werner,
  Generating inversion on a nuclear transition - photopumping of ^{103}Rh,
  Journal de Physique IV **11**(PR2) (2001) 271.

- F. Stedile, E. Fill, D. Belic, P. von Brentano, C. Fransen, A. Gade, U. Kneissl, C. Kohstall, A. Linnemann, P. Matschinsky, A. Nord, N. Pietralla, H.H. Pitz, M. Scheck, and V. Werner,
  Low-Lying Dipole Excitations in the Odd-Proton, Midshell Nucleus ^{103}Rh,
  Phys. Rev. C **63** (2001) 024320.

- C. Kohstall, D. Belic, P. von Brentano, C. Fransen, R.-D. Herzberg, J. Jolie, U. Kneissl, H. Lehmann, A. Linnemann, P. Matschinsky, A. Nord, N. Pietralla, H.H. Pitz, M. Scheck, F. Stedile, V. Werner, and S.W. Yates,
  Low-Lying Dipole Excitations in the Stable Cd Isotopes: A systematics,
  Yad. Fiz. **64**(6) (2001) 1217; Phys. Atomic Nuclei **64** (2001) 1143.

- C. Kohstall, D. Belic, P. von Brentano, C. Fransen, R.-D. Herzberg, J. Jolie, U. Kneissl, H. Lehmann, A. Linnemann, P. Matschinsky, A. Nord, N. Pietralla, H.H. Pitz, V. Werner, and S.W. Yates,
Systematics of Dipole Excitations in the Stable ^{110,111,112,113,114,116}Cd Isotopes,
Trans. Bulg. Nucl. Soc. **5** (2000) 179.

- T. Klug, A. Dewald, V. Werner, P. von Brentano, and R.F. Casten,
The $B(E2; 4_2^+ \rightarrow 2_2^+)$ Value in ^{152}Sm and β-Softness in Phase Coexisting Structures,
Phys. Lett. **495B** (2000) 55.

- A. Gade, I. Wiedenhöver, M. Luig, A. Gelberg, H. Meise, N. Pietralla, V. Werner, and P. von Brentano,
Non-Yrast States of 134Ce Populated in beta-Decay,
Nucl. Phys. A **673** (2000) 45.

- J. Bryssinck, L. Govor, V.Yu. Ponomarev, F. Bauwens, O. Beck, D. Belic, P. von Brentano, D. De Frenne, C. Fransen, R.-D. Herzberg, E. Jacobs, U. Kneissl, H. Maser, A. Nord, N. Pietralla, H.H. Pitz, and V. Werner,
Search for the Electric Dipole Excitations to the $3s_{1/2} \otimes [2_1^+ \otimes 3_1^-]$ Multiplet in ^{117}Sn,
Phys. Rev. C **62** (2000) 014309.

- J. Bryssinck, L. Govor, V.Yu. Ponomarev, F. Bauwens, O. Beck, D. Belic, P. von Brentano, D. De Frenne, T. Eckert, C. Fransen, K. Govaert, R.-D. Herzberg, E. Jacobs, U. Kneissl, H. Maser, A. Nord, N. Pietralla, H.H. Pitz, and V. Werner,
Systematic study of electric quadrupole excitations in the stable even mass Sn nuclei,
Phys. Rev. C **61** (2000) 024309.

- V.Yu. Ponomarev, J. Bryssinck, L. Govor, F. Bauwens, O. Beck, D. Belic, P. von Brentano, D. De Frenne, C. Fransen, R.-D. Herzberg, E. Jacobs, U. Kneissl, H. Maser, A. Nord, N. Pietralla, H.H. Pitz, and V. Werner,
Strong fragmentation of low-energy electromagnetic excitation strength in ^{117}Sn,
Phys. Rev. Lett. **83** (1999) 4029.

- N. Pietralla, C. Fransen, D. Belic, P. von Brentano, C. Frießner, U. Kneissl, A. Linnemann, A. Nord, H.H. Pitz, T. Otsuka, I. Schneider, V. Werner, and I. Wiedenhöver,
Transition Rates between Mixed Symmetry States: First Measurement in ^{94}Mo,
Phys. Rev. Lett. **83** (1999) 1303.

- J. Bryssinck, L. Govor, D. Belic, F. Bauwens, O. Beck, P. von Brentano, D. De Frenne, T. Eckert, C. Fransen, K. Govaert, R.-D. Herzberg, E. Jacobs, U. Kneissl, H. Maser, A. Nord, N. Pietralla, H.H. Pitz, V.Yu. Ponomarev, and V. Werner,
  Uniform Properties of $J^\pi = 1^-$ two-phonon states in the semi-magic even-even tin isotopes ^{116,118,120,122,124}Sn,
  Phys. Rev. C **59** (1999) 1930.

- N. Pietralla, D. Belic, P. von Brentano, C. Fransen, R.-D. Herzberg, U. Kneissl, H. Maser, P. Matschinsky, A. Nord, T. Otsuka, H.H. Pitz, V. Werner, and I. Wiedenhöver,
  Isovector Quadrupole Excitations in the Valence Shell of the Vibrator Nucleus ^{136}Ba: Evidence from photon scattering experiments,
  Phys. Rev. C **58** (1998) 796.

- A. Nord, S.W. Yates, O. Beck, D. Belic, P. von Brentano, T. Eckert, C. Fransen, R.-D. Herzberg, U. Kneissl, H. Maser, N. Pietralla, H.H. Pitz, and V. Werner,
  Low-Lying Dipole Strength in ^{207}Pb,
  Phys. Rev. C **57** (1998) 3459.

- N. Pietralla, T. Mizusaki, P. von Brentano, R.V. Jolos, T. Otsuka, and V. Werner,
  2_1^+ and 2_2^+ States in Collective Nuclei as Multiple Q-Phonon Excitations,
  Phys. Rev. C **57** (1998) 150.

Conference proceedings

- V. Werner, P. von Brentano, C. Fransen, J. Jolie, N. Pietralla, U. Kneissl, H.H. Pitz, S.W. Yates, H.G. Börner,
  Isovector excitations near the N=50 shell closure,
  Proceedings of the Eleventh International Symposium Capture Gamma-Ray Spectroscopy and Related Topics, (CGS11 2002), 2003, ISBN 981-238-391-3 (World Scientific), 150.

- V. Werner, P. von Brentano, C. Fransen, A. Gade, U. Kneissl, A. Linnemann, N. Pietralla, and H.H. Pitz,
  The mixed-symmetric one-phonon 2^+ state in ^{96}Mo,
  Exotic Nuclei and Atomic Masses (ENAM2001), Proceedings, Hämeenlinna Finland, 2001, ISBN 3-540-00101-8 (Springer Publishing), 341.

- V. Werner and R.V. Jolos,
Quadrupole shape invariants and simple E2-relations in the Q-phonon scheme,
International Symposium on Nuclear Structure Physics, Göttingen, 2001, ISBN 981-02-4654-4 (World Scientific, Singapore), 415.

- M. Scheck, D. Belic, H. von Garrel, U. Kneissl, C. Kohstall, H.H. Pitz, F. Stedile, J.J. Carroll, R. Toman, P. von Brentano, A. Gade, A. Linnemann, N. Pietralla, V. Werner,
The systematics of dipole modes in the even-even Hf nuclei,
Proceedings of the Eleventh International Symposium Capture Gamma-Ray Spectroscopy and Related Topics, (CGS11 2002), 2003, ISBN 981-238-391-3 (World Scientific), 809.

- C. Fransen, D. Bandyopadhyay, N. Boukharouba, P. von Brentano, S.R. Lesher, M.T. McEllistrem, N. Pietralla, V. Werner, S.W. Yates,
Investigating low-spin states in ^{92}Zr with inelastic neutron scattering,
Proceedings of the Eleventh International Symposium Capture Gamma-Ray Spectroscopy and Related Topics, (CGS11 2002), 2003, ISBN 981-238-391-3 (World Scientific), 660.

- N. Pietralla, C. Fransen, A.F. Lisetskiy, P. von Brentano, and V. Werner
Evolution of mixed-symmetry states near shell closures,
Proceedings of the Eleventh International Symposium Capture Gamma-Ray Spectroscopy and Related Topics, (CGS11 2002), 2003, ISBN 981-238-391-3 (World Scientific), 97.

- J. Jolie, S. Heinze, A. Linnemann, V. Werner, P. Cejnar, R.F. Casten,
Landau theory of phase transitions and nuclear groundstate deformation,
Proceedings of the Eleventh International Symposium Capture Gamma-Ray Spectroscopy and Related Topics, (CGS11 2002), 2003, ISBN 981-238-391-3 (World Scientific), 36.

- C. Fransen, D. Bandyopadhyay, N. Boukharouba, P. von Brentano, S.R. Lesher, M.T. McEllistrem, N. Pietralla, V. Werner, and S.W. Yates,
Investigating Low-spin States in ^{92}Zr With The (n,n'γ) Reaction,
MAPPING THE TRIANGLE: International Conference on Nuclear Structure, Grand Teton National Park, Wyoming (USA), 22-25 May 2002, AIP Conference Proceedings **638** (2002) 239-240.

- D. Bandyopadhyay, C. Fransen, N. Boukharouba, V. Werner, J.L. Weil, S.W. Yates, and M.T. McEllistrem,
Multiphonon Excitations in ^{124}Sn,

MAPPING THE TRIANGLE: International Conference on Nuclear Structure, Grand Teton National Park, Wyoming (USA), 22-25 May 2002, AIP Conference Proceedings **638** (2002) 231-232.

- J. Jolie, S. Heinze, P. von Brentano, V. Werner, and P. Cejnar,
  New Interpretation of the O(6) Limit of the Interacting Boson Model,
  MAPPING THE TRIANGLE: International Conference on Nuclear Structure, Grand Teton National Park, Wyoming (USA), 22-25 May 2002, AIP Conference Proceedings **638** (2002) 213-222.

- P. von Brentano, A. Gade, N. Pietralla, and V. Werner,
  Q-phonons, Q-invariants, and company,
  MAPPING THE TRIANGLE: International Conference on Nuclear Structure, Grand Teton National Park, Wyoming (USA), 22-25 May 2002, AIP Conference Proceedings **638** (2002) 69-76.

- N. Pietralla, C. Fransen, A. F. Lisetskiy, P. von Brentano, and V. Werner,
  Mixed Symmetry in the Symmetry Triangle,
  MAPPING THE TRIANGLE: International Conference on Nuclear Structure, Grand Teton National Park, Wyoming (USA), 22-25 May 2002, AIP Conference Proceedings **638** (2002) 11-16.

- C. Fransen, Z. Ammar, N. Boukharouba, A. Dewald, A. Gade, J. Jolie, U. Kneissl, M. Merrick, M.T. McEllistrem, N. Pietralla, N. Warr, V. Werner, and S.W. Yates,
  Investigating Mixed-Symmetry States in ^{94}Mo,
  International Symposium on Nuclear Structure Physics, Göttingen, 2001, ISBN 981-02-4654-4 (World Scientific, Singapore), 351.

- H.H. Pitz, F. Bauwens, D. Belic, J. Bryssinck, P. von Brentano, C. Fransen, D. De Frenne, L. Govor, R.-D. Herzberg, E. Jacobs, U. Kneissl, C. Kohstall, A. Linnemann, H. Maser, P. Matschinsky, A. Nord, N. Pietralla, V.Yu. Ponomarev, M. Scheck,F. Stedile, V. Werner,
  Systematics of Low-Lying E1 and M1 Excitations in Heavy Nuclei from Photon Scattering Experiments,
  Proceedings of the Tenth International Symposium on Capture Gamma-Ray Spectroscopy and Related Topics, Santa Fe, August 30 -Sept 3, 1999, AIP Conference Proceedings **529**, Editor Stephen Wender (2000) 621-623.

- A. Nord, F. Bauwens, O. Beck, D. Belic, P. von Brentano, J. Bryssinck, D. De Frenne, T. Eckert, C. Fransen, K. Govaert, L. Govor, R.-D. Herzberg, E. Jacobs, U. Kneissl, H. Maser, A. Nord, N. Pietralla, H.H. Pitz, V.Yu. Ponomarev, V. Werner,
  Systematics of Low-Lying Dipole Strength in Heavy Nuclei from

Resonance Fluorescence Experiments,
Proceedings of the International Conference The Nucleus: New Physics for the New Millenium, FAURE (South Africa), January 18 – 22, 1999. Editors: F.D Smit, R. Lindsay, and S.V. Förtsch, (Kluwer Academic / Plenum Publishers, New York) (2000) 315-319.

- P. von Brentano, N. Pietralla, C. Fransen, A. Gelberg, U. Kneissl, T. Otsuka, H.H. Pitz, and V. Werner,
Mixed-Symmetry Quadrupole States in Nuclei,
Contribution to the International Symposium on Nuclear Electro-Weak Spectroscopy (NEWS99) Osaka, 1999 (World Scientific).

- N. Pietralla, C. Fransen, P. von Brentano, C. Frießner, A. Gade, A. Linnemann, P. Matschinsky, I. Schneider, V. Werner, I. Wiedenhöver, D. Belic, U. Kneissl, A. Nord, and H.H. Pitz,
Investigation of Low-Spin Mixed-Symmetry States with Different Probes,
Contribution to the International Conference on Nuclear Models 1998 - Interacting Bosons and Fermions, Camerino, 1998, Universita degli Studi di Camerino, p. 25.

- P. von Brentano, H. Meise, N. Pietralla, V. Werner, and R. V. Jolos,
Q-Invariants and Multi-Phonon States,
Contribution to the International Conference on Nuclear Models 1998 - Interacting Bosons and Fermions, Camerino, 1998, Universita degli Studi di Camerino, p. 15.

- P. von Brentano, N. Pietralla, C. Fransen, C. Frießner, A. Gade, A. Gelberg, R.-D. Herzberg, U. Kneissl, T. Otsuka, H. H. Pitz, V. Werner, and I. Wiedenhöver,
Low-Energy Q-Phonon Excitations in Nuclei,
Contribution to the International Conference on Nuclear Structure, Gatlinburg, Tennessee, August 1998, American Institute of Physics Conference Proceedings **481** (1999) 449.

- P. von Brentano, N. Pietralla, H. Meise, A. Gade, A. Dewald, C. Fransen, C. Friessner, J. Gableske, A. Gelberg, A. Schmidt, I. Schneider, V. Werner, U. Kneissl, H.H. Pitz, I. Wiedenhöver,
Low Lying Isoscalar and Isovector Quadrupole Excitations,
Proc. of the First Balkan School on Nuclear Physics, Istanbul, Turkey, 1998, Balkan Physics Letters, special issue (1998) 11-32.

- U. Kneissl, O. Beck, D. Belic, T. Eckert, H. Maser, A. Nord, H.H. Pitz, P. von Brentano, C. Fransen, R.-D. Herzberg, N. Pietralla, V. Werner. F. Bauwens, J. Bryssinck, D. De Frenne, K. Govaert, E. Jacobs, L. Govor,

S.W. Yates,
Low-lying dipole excitations in heavy nuclei studied in photon scattering experiments,
Proceedings of the 6th International Spring Seminar on Nuclear Structure by Aldo Covello, ISBN 981-02-3708-1 (World Scientific, Singapore) (1998) p. 243-252.

- A.E. Almeido Pinto, J. Margraf, A. Nord, T. Eckert, U. Kneissl, H.H. Pitz, H. Maser, O. Beck, J. Besserer, B. Krischok, A. Wolpert, D. Belic, N. Pietralla, V. Werner,
Low Lying Excitations in Odd Deformed Nucleus Studied by Nuclear Resonance Fluorescence,
Proc. 20th Brazilian Workshop Nuclear Physics, Sao Paulo, Brazil, World Scientific, Singapore (1998) 93.

Bibliography

[Ala55] G. Alaga, K. Alder, A. Bohr, and B.R. Mottelson, Dan. Mat. Fys. Medd. **29**, no. 9 (1955).

[And01] W. Andrejtscheff, C. Kohstall, P. von Brentano, C. Fransen, U. Kneissl, N. Pietralla, and H.H. Pitz, Phys. Lett. B **506** (2001) 239.

[Ari77] A. Arima, T. Otsuka, F. Iachello, and I. Talmi, Phys. Lett. B **66** (1977) 205.

[Bag00] C.M. Baglin, Nucl. Data Sheets **91** (2000) 423.

[Ber85] U.E.P. Berg, *"Systematische Untersuchung elektrischer und magnetischer Übergänge im Atomkern mit Hilfe der Kernresonanzfluoreszenz"*, Habilitationsschrift, Justus-Liebig-Universität Gießen (1985).

[BiR53] L.C. Biedenharn and M.E. Rose, Rev. Mod. Phys. **25** (1953) 729.

[BoJ93] H.G. Börner and J. Jolie, J. Phys. G **19** (1993) 217.

[BoM75] A. Bohr and B. Mottelson, *"Nuclear Structure II"*, (Benjamin Reading, 1975).

[BoR84] D. Bohle, A. Richter, W. Steffen, A. E. L. Dieperink, N. Lo Iudice, F. Palumbo und O. Scholten, Phys. Lett. **B137** (1984) 27.

[Bre94] P. von Brentano, A. Zilges, R.-D. Herzberg, U. Kneissl, J. Margraf und H. H. Pitz, Nucl. Phys. A **577** (1994) 191c.

[Bre96] P. von Brentano, J. Eberth, J. Enders, L. Esser, R.-D. Herzberg, N. Huxel, H. Meise, P. von Neumann-Cosel, N. Nicolay, N. Pietralla, H. Prade, J. Reif, A. Richter, C. Schlegel, R. Schwengner, S. Skoda, H.G. Thomas, I. Wiedenhover, G. Winter, and A. Zilges, Phys. Rev. Lett. **76** (1996) 2029.

[Bre02] P. von Brentano, C. Fransen, A. Gade, A. Lisetskiy, and N. Pietrall, Eur. Phys. J. A **13** (2002) 99.

[BrG77] P.J. Brussaard and P.W.M. Glaudemans, *"Shell-model applications in nuclear spectroscopy* (North-Holland Publishing Co., Amsterdam, 1977).

[Bry99] J. Bryssinck, L. Govor, D. Belic, F. Bauwens, O. Beck, P. von Brentano, D. De Frenne, T. Eckert, C. Fransen, K. Govaert, R.-D. Herzberg, E. Jacobs, U. Kneissl, H. Maser, A. Nord, N. Pietralla, H. H. Pitz, V. Yu. Ponomarev und V. Werner, Phys. Rev. C **59** (1999) 1930.

[BrW36] G. Breit and E. Wigner, Phys. Rev. **49**, (1936) 519.

[Car96] T.S. Carman, V. Litvinenko, J. Madey, C. Neuman, B. Norum, P.G. O'Shea, N.R. Roberson, C.Y. Scarlett, E. Schreiber, and H.R. Weller, Nucl. Inst. Meth. A **378** (1996) 1.

[Cas00] R.F. Casten and N.V. Zamfir, Phys. Rev. Lett. **85** (2000) 3584.

[Cas01] R.F. Casten and N.V. Zamfir, Phys. Rev. Lett. **87** (2001) 052503.

[Cau99] E. Caurier, F. Nowacki, A.P. Zuker, G. Martinez-Pinedo, A. Poves, and J. Retamosa, Nucl. Phys. A **654** (1999) 747c.

[Cli86] D. Cline, Ann. Rev. Nucl. Part. Sci. **36** (1986) 683.

[DuZ96] M. Dufour and A.P. Zuker, Phys. Rev. C **54** (1996) 1641.

[EkL92] L.P. Ekstrom and J. Lyttkens-Linden, Nucl. Data Sheets **67** (1992) 1.

[FaH59] L.W. Fagg and S.S. Hanna, Rev. Mod. Phys. **31** (1959) 711.

[Fra98] C. Fransen, O. Beck, P. von Brentano, T. Eckert, R.-D. Herzberg, U. Kneissl, H. Maser, A. Nord, N. Pietralla, H. H. Pitz und A. Zilges, Phys. Rev. C **57** (1998) 129.

[Fra01] C. Fransen, N. Pietralla, P. von Brentano, A. Dewald, J. Gableske, A. Gade, A. Lisetskiy, and V. Werner, Phys. Lett. B **508** (2001) 219.

[Fra03] C. Fransen, N. Pietralla, Z. Ammar, D. Bandyopadhyay, N. Boukharouba, P. von Brentano, A. Dewald, J. Gableske, A. Gade, J. Jolie, U. Kneissl, S.R. Lesher, A.F. Lisetskiy, M.T. McEllistrem, M. Merrick, H.H. Pitz, N. Warr, V. Werner, and S.W. Yates, Phys. Rev. C **67** (2003) 024307.

[Fra03b] C. Fransen, D. Bandyopadhyay, N. Boukharouba, P. von Brentano, S.R. Lesher, M.T. McEllistrem, N. Pietralla, V. Werner, and S.W. Yates, *in preparation.*

[FraPC] C. Fransen, *priv. comm.*

[Fre89] J.S. Freeman, R. Chapman, J.L. Durell, M.A.C. Hotchkis, F. Khazaie, J.C. Lisle, J.N. Mo, A.M. Bruce, R.A. Cunningham, P.V. Drumm, D.D. Warner, and J.D. Garrett, Phys. Lett. B **222** (1989) 347.

[Frk89] D. Frekers, D. Bohle, A. Richter, R. Abegg, R.E. Azuma, A. Celler, C. Chan, T.E. Drake, K.P. Jackson, J.D. King, C.A. Miller, R. Schubank, J. Watson, and S. Yen, Phys. Lett. B **218** (1989) 439.

[FrS65] H. Frauenfelder and R.M. Steffen, *"Angular Correlations"* in *"Alpha-, Beta-, and Gamma-Ray Spectroscopy"*, *ed.* K. Siegbahn (North-Holland Publishing Co., Amsterdam, 1965).

[Gad02] A. Gade, A. Fitzler, C. Fransen, J. Jolie, S. Kasemann, H. Klein, A. Linnemann, V. Werner, and P. von Brentano, Phys. Rev. C **66** (2002) 034311.

[Gad02b] A. Gade, H. Klein, N. Pietralla, and P. von Brentano, Phys. Rev. C **65** (2002) 054311.

[Gad03] A. Gade, D. Belic, P. von Brentano, C. Fransen, H. von Garrel, J. Jolie, U. Kneissl, C. Kohstall, A. Linnemann, H.H. Pitz, M. Scheck, F. Stedile, and V. Werner, Phys.Rev. C 67 (2003) 034304.

[Har87] H.J. Harter, PhD thesis, Universität zu Köln, unpublished (1987).

[Hax49] O. Haxel, J.H.D. Jensen, and H.E. Suess, Phys. Rev. **75** (1949) 1766.

[Her95] R.-D. Herzberg, I. Bauske, P. von Brentano, T. Eckert, R. Fischer, W. Geiger, U. Kneissl, J. Margraf, H. Maser, N. Pietralla, H. H. Pitz, and A. Zilges, Nucl. Phys. A **592** (1995) 211.

[HeS86] K. Heyde and J. Sau, Phys. Rev. C **33** (1986) 1050.

[Hey88] K. Heyde, E.D. Kirchuk, and P. Federman, Phys. Rev. C **38** (1988) 984.

[Higs] HIGS web-pages, http://higs.tunl.duke.edu/~higs/whatishigs.

[Hon95] M. Honma, T. Mizusaki, and T. Otsuka, Phys. Rev. Lett. **75** (1995) 1284.

[IaA87] F. Iachello and A. Arima, *"The Interacting Boson Model"* (Cambridge University Press, Cambridge, 1987).

[Iac81] F. Iachello, Nucl. Phys. A **358** (1981) 89c.

[Iac84] F. Iachello, Phys. Rev. Lett. **53** (1984) 1427.

[Iac00] F. Iachello, Phys. Rev. Lett. **85** (2000) 3580.

[Iac01] F. Iachello, Phys. Rev. Lett. **87** (2001) 052502.

[IaZ98] F. Iachello, N.V. Zamfir, and R.F. Casten, Phys. Rev. Lett. **81** (1998) 1191.

[Isa86] P. Van Isacker, K. Heyde, J. Jolie, A. Sevrin, Ann. Phys. **171** (1986) 253.

[Jak99] G. Jakob, N. Benczer-Koller, J. Holden, G. Kumbartzki, T.J. Mertzimekis, K.-H. Speidel, C.W. Beausang, and R. Krücken, Phys. Lett. B **468** (1999) 13.

[JoC99] J. Jolie, P. Cejnar, and J. Dobeš, Phys. Rev. C **60** (1999) R061303.

[Jol97] R.V. Jolos, P. von Brentano, N. Pietralla, and I. Schneider, Nucl. Phys. **A618** (1997) 126.

[Jol01] J. Jolie, R.F. Casten, P. von Brentano, and V. Werner, Phys. Rev. Lett. **87** (2001) 162501.

[Jol02] J. Jolie, P. Cejnar, R.F. Casten, S. Heinze, A. Linnemann, and V. Werner, Phys. Rev. Lett. **89** (2002) 182502.

[Joh95] E.L. Johnson, E.M. Baum, D.P. DiPrete, R.A. Gatenby, T. Belgya, D. Wang, J.R. Vanhoy, M.T. McEllistrem, and S.W. Yates, Phys. Rev. C **52** (1995) 2382.

[Kelly] J. Kelly, "An introduction to FEL/HIGS", http://higs.tunl.duke.edu/ higs/documents.

[Kim98] K.-H. Kim, T. Otsuka, P. von Brentano, A. Gelberg, P. Van Isacker, and R. F. Casten, *Proceedings of the 9th International Symposium on Capture Gamma Ray Spectroscopy and Related Topics*, Budapest 1996, *ed.* G. Molnár, (Springer, Budapest, 1998).

[Kle01] H. Klein, A.F. Lisetskiy, N. Pietralla, C. Fransen, A. Gade, and P. von Brentano, Phys. Rev. C **65** (2002) 044315.

[Koh01] C. Kohstall, D. Belic, P. von Brentano, C. Fransen, R.-D. Herzberg, J. Jolie, U. Kneissl, H. Lehmann, A. Linnemann, P. Matschinsky, A. Nord, N. Pietralla, H.H. Pitz, M. Scheck, F. Stedile, V. Werner, and S.W. Yates, Yad. Fiz. **64** (2001) 1217; Phys. Atomic Nuclei **64** (2001) 1141.

[Kne96] U. Kneißl, H. H. Pitz, and A. Zilges, *Investigation of Nuclear Structure by Resonance Fluorescence Scattering*, Prog. Part. Nucl. Phys. **37** (1996) 349.

[KSW73] K.S. Krane, R.M. Steffen, and R.M. Wheeler, Nucl. Data Tab. **11** (1973) 351.

[Kum72] K. Kumar, Phys. Rev. Lett. **28** (1972) 249.

[Les03] S.R. Lesher, *priv. comm.*.

[Lip85] P.O. Lipas, P. Toivonen, and D.D. Warner, Phys. Lett. B **155** (1985) 295.

[Lis00] A. Lisetskiy, N. Pietralla, C. Fransen, R.V. Jolos, P. von Brentano, Nucl. Phys. A **677** (2000) 100.

[Lit97] V.N. Litvinenko, B. Burnham, M. Emamian, J.M.J. Madey, P. Morcombe, P.G. O'Shea, S.H. Park, R. Sachtschale, K.D.Straub, G. Swift, P. Wang, Y. Wu, R.S. Canon, C.R. Howell, N. R. Roberson, E.C. Schreiber, M. Spraker, W. Tornow, H.R. Weller, I.V. Pinayev, N.G. Gavrilov, M.G. Fedotov, G.N. Kulipanov, G.Y. Kurkin, S.F. Mikhailov, V.M. Popik, A.N. Skrinsky, N.A. Vinokurov, B.E. Norum, A. Lumpkin, and B. Yang, Phys. Rev. Lett. **78** (1997) 4569.

[LoP78] N. Lo Iudice and F. Palumbo, Phys. Rev. Lett. **41** (1978) 1532.

[LoP79] N. Lo Iudice and F. Palumbo, Nucl. Phys. **A326** (1979) 193.

[LoS00] N. Lo Iudice and Ch. Stoyanov, Phys. Rev. C **62** (2000) 047302.

[LoS02] N. Lo Iudice and Ch. Stoyanov, Phys. Rev. C **65** (2000) 064304.

[Man01] P.F. Mantica, A.E. Stuchbery, D.E. Groh, J.I. Prisciandaro, and M.P. Robinson, Phys. Rev. C **63** (2001) 034312.

[Mar95] J. Margraf, T. Eckert, M. Rittner, I. Bauske, O. Beck, U. Kneißl, H. Maser, H. H. Pitz, A. Schiller, P. von Brentano, R. Fischer, R.-D. Herzberg, N. Pietralla, A. Zilges and H. Friedrichs, Phys. Rev. C **52** (1995) 2429.

[Mas96] H. Maser, N. Pietralla, P. von Brentano, R.-D. Herzberg, U. Kneissl, J. Margraf, H.H. Pitz, and A. Zilges, Phys.Rev. C **54** (1996) R2129.

[MATH] MATHEMATICA, Version Number 4.2.1.0, Platform X, Copyright 1988-2002 Wolfram Research, Inc.

[May49] M. Göppert-Mayer, Phys. Rev. **75** (1949) 1969.

[May55] M. Göppert-Mayer and J.H.D. Jensen, *"Elementary Theory of Nuclear Shell Structure"*, (Wiley, New York, 1955).

[Mei99] H. Meise, PhD thesis, Universität zu Köln (1999).

[Met59] F.R. Metzger, Prog. Nucl. Phys. **7** (1959) 54.

[Met76] F.R. Metzger, Phys. Rev. C **14** (1976) 543.

[Ots78] T. Otsuka, A. Arima, F. Iachello, and I. Talmi, Phys. Lett. B **76** (1978) 139.

[Ots78b] T. Otsuka, PhD thesis, University of Tokyo, unpublished (1978).

[Ots94] T. Otsuka and K.-H. Kim, Phys. Rev. C **40**, (1994) R1768.

[Pie94] N. Pietralla, P. von Brentano, R. F. Casten, T. Otsuka, and N. V. Zamfir, Phys. Rev. Lett. **73** (1994) 2962.

[Pie95] N. Pietralla, I. Bauske, O. Beck, P. von Brentano, W. Geiger, R.-D. Herzberg, U. Kneißl, J. Margraf, H. Maser, H. H. Pitz, and A. Zilges, Phys. Rev. C **51**, 1021 (1995).

[Pie98] N. Pietralla, T. Mizusaki, P. von Brentano, R. V. Jolos, T. Otsuka, and V. Werner, Phys. Rev. C **57** (1998) 150.

[Pie98b] N. Pietralla, P. von Brentano, R.-D. Herzberg, U. Kneissl, N. Lo Iudice, H. Maser, H. H. Pitz, and A. Zilges, Phys. Rev. C **58** (1998) 184.

[Pie99] N. Pietralla, Phys. Rev. C **59** (1999) 2941.

[Pie99b] N. Pietralla, C. Fransen, D. Belic, P. von Brentano, C. Friessner, U. Kneissl, A. Linnemann, A. Nord, H.H. Pitz, T. Otsuka, I. Schneider, V. Werner, and I. Wiedenhöver, Phys. Rev. Lett. **83** (1999) 1303.

[Pie00] N. Pietralla, C. Fransen, P. von Brentano, A. Dewald, A. Fitzler, C. Friessner, and J. Gableske, Phys. Rev. Lett. **84** (2000) 3775.

[Pie01] N. Pietralla, C.J. Barton III, R. Krücken, C.W. Beausang, M.A. Caprio, R.F. Casten, J.R. Cooper, A.A. Hecht, H. Newman, J.R. Novak, and N.V. Zamfir, Phys. Rev. C **64** (2001) (R)031301.

[Pie02] N. Pietralla, Z. Berant, V.N. Litvinenko, S. Harman, F.F. Mikhailov, I.V. Pinayev, G. Swift, M.W. Ahmed, J.H. Kelley, S.O. Nelson, R. Prior, K. Sabourov, A.P. Tonchev, and H.R. Weller, Phys. Rev. Lett. **88** (2002) 012502.

[Pie02b] N. Pietralla, C. Fransen, A.F. Lisetskiy, P. von Brentano, and V. Werner, *Proceedings of the Eleventh International Symposium Capture Gamma-Ray Spectroscopy and Related Topics*, Prague 2002, ISBN 981-238-391-3 (World Scientific, 2003), 97.

[Pie03] N. Pietralla, M.W. Ahmed, C. Fransen, V.N. Litvinenko, A.P. Tonchev, and H.R. Weller, in *"Frontiers of Nuclear Structure"*, Berkeley, California, 29 July - 2 August, 2002, *ed.* P. Fallon and R. Clark, AIP Conf. Proc. **656** (Melville, New York, 2003) 365.

[Pla66] A. Plastino, R. Arvieu, and S.A. Moszkowski, Phys. Rev. **145** (1966) 837.

[Ric83] A. Richter, *Proc. of the Int. Conf. on Nuclear Physics*, Florenz 1983, *ed.* P. Blasi and R. A. Ricci, (Tipografica Compositori Bologna, Vol. 2) 189.

[Rob94] S. J. Robinson, J. Jolie, H. G. Börner, P. Schillebeeckx, S. Ulbig, and K. P. Lieb, Phys. Rev. Lett. **73** (1994) 412.

[Sat55] G.R. Satchler, Proc. Phys. Soc. (London) **A68** (1955) 1081.

[Sch51] L.I. Schiff, Phys. Rev. Lett. **83** (1951) 252.

[Shi00] N. Shimizu, T. Otsuka, T. Mizusaki, and M. Honma, Phys. Rev. Lett. **86** (2000) 1171.

[Sie94] G. Siems, U. Neuneyer, I. Wiedenhöver, S. Albers, M. Eschenauer, R. Wirowski, A. Gelberg, P. von Brentano, and T. Otsuka, Phys. Lett. B **320** (1994) 1.

[Tul92] J.K. Tuli, Nucl. Data Sheets **66** (1992) 1.

[WaC82] D.D. Warner and R.F. Casten, Phys. Rev. Lett. **48** (1982) 1385.

[Wer00a] V. Werner, diploma thesis, Institut für Kernphysik, Universität zu Köln, unpublished (2000).

[Wer00b] V. Werner, N. Pietralla, P. von Brentano, R.F. Casten, and R.V. Jolos, Phys. Rev. C **61** (2000) (R)021301.

[Wer02] V. Werner, D. Belic, P. von Brentano, C. Fransen, A. Gade, H. von Garrel, J. Jolie, U. Kneissl, C. Kohstall, A. Linnemann, A.F. Lisetskiy, N. Pietralla, H.H. Pitz, M. Scheck, K.-H. Speidel, F. Stedile, and S.W. Yates, Phys. Lett. B **550** (2002) 140.

[Wer02b] V. Werner, P. von Brentano, R.F. Casten, and J. Jolie, Phys. Lett. B **527** (2002) 55.

[Wes88] C. Wesselborg, P. von Brentano, K.O. Zell, R.D. Heil, H.H. Pitz, U.E.P. Berg, U. Kneissl, S. Lindenstruth, U. Seemann, and R. Stock, Phys. Lett. B **207** (1988) 22.

[Wes88b] C. Wesselborg, PhD thesis, Universität zu Köln (1988).

[Zil90] A. Zilges, P. von Brentano, C. Wesselborg, R. D. Heil, U. Kneissl, S. Lindenstruth, H. H. Pitz, U. Seemann, and R. Stock, Nucl. Phys. **A507** (1990) 399.

[Zwa85] D. Zwarts, Comp. Phys. Commun. **38** (1985) 365.

Acknowledgments

Such work cannot be done alone, therefore I want to thank all the people who helped me on my way to this point in many various ways. I cannot mention all, but want to especially thank the following persons:

Prof. Dr. P. von Brentano, for his great support, his intense interest in the progress, for always being open for inspiring discussions, and for his great ability to discover interesting physics in between a mess of letters and numbers.

Prof. Dr. N. Pietralla, for years of very productive collaboration, for always actively discussing new findings and giving important theoretical hints.

Prof. Dr. J. Jolie, who was a spring of new ideas joining the IKP in Cologne, giving me several new impulses, for ensuring the possibility of good γ-spectroscopy.

Prof. Dr. A. Gelberg, for valuable explanations and remarks to questions in the IBM.

Prof. Dr. R.F. Casten for many enlightening discussions, his simple perspectives that helped me a lot in this work, and his enthusiasm that always made work with him a pleasure.

I am much obliged to Prof. Dr. U. Kneissl and his associate Dr. H.H. Pitz for many years of a close collaboration in photon scattering experiments at Stuttgart. I am also grateful to the members of the Stuttgart photon scattering group C. Kohstall, F. Stedile, M. Scheck, H. von Garrel, and S. Walter for the support in the experiments, the good working atmosphere, and hospitality during the beam-times. Thank you to DYNAMITRON crew for the wonderful electron beam and sorry for what we did with it.

Prof. Dr. H.R. Weller and his associate Dr. A. Tonchev, as well as N. Pietralla, for giving me the opportunity to use 100 % polarized high-energy γ-rays, something that photon scatterers dreamt of for a long time. Many thanks also to Dr. M.W. Ahmed, and Dr. Y. Wu from the free electron laser laboratory, and, in

addition to already mentioned persons, to D. Savran and S. Müller from Darmstadt for their great help during the Duke experiment and my fight with light at much lower energies.

Prof. Dr. H.G. Börner, Dr. M. Jentschel, and Dr. P. Mutti for their help in the experiment on ^{96}Mo in Grenoble and the kind hospitality in Grenoble, as well as Dr. S. Baechler and Dr. T. Materna for help in my first encountering with good neutrons at the PSI, and of course J. Jolie for giving me these opportunities.

Prof. Dr. T. Otsuka, Prof. Dr. E. Caurier, Dr. F. Nowacki, and Dr. A. Lisetskiy for discussions about ^{92}Zr and many insights on the shell model.

Dr. K.O. Zell and Dr. S. Kasemann for providing perfect targets for experiments at Cologne, A. Fitzler for keeping the analyzer running, the Cologne TANDEM crew for always well-focussed beams and Dr. G. Pascovici for much electronic help.

Special thanks to A. Linnemann for many years of fun and discussions in- and outside the office, as well as to the so far not mentioned other Cologne photon scatterers Dr. C. Fransen, D. Mücher, Prof. Dr. A. Gade, and our new accretion C. Scholl (who helped me a lot during finishing this thesis) for the good atmosphere and many discussions.

Thank you to the bookworms for digging carefully through this work, namely K. Jessen(!), C. Fransen, A. Linnemann, and S. Heinze.

All the helping hands at the IKP responsible for the unique familiar atmosphere in Cologne!

Those who took part in training eye-hand coordination in various explosive meetings.

A special thank you to A. Imig for being present for various more or less serious discussions and providing hot flavored water. Lycka till, Asterix - och mycket framgång med din kittel!

It would not be enough just to say thank you to K. Gellrich, C. Mzyk, W. Schmitz, and S. Schiweck for always standing by me, helping me out of the worst, having fun and showing me from time to time that there are various points of view.

At last the most important persons that contributed to the completion of this work by their great support shall be mentioned. A big “Danke” to my parents and of course to my sister for the great moral support.

Erklärung

Ich versichere, daß ich die von mir vorgelegte Dissertation selbständig angefertigt, die benutzten Quellen und Hilfsmittel vollständig angegeben und die Stellen der Arbeit - einschließlich Tabellen, Karten und Abbildungen -, die anderen Werken im Wortlaut oder dem Sinn nach entnommen sind, in jedem Einzelfall als Entlehnung kenntlich gemacht habe; daß diese Dissertation noch keiner anderen Fakultät oder Universität zur Prüfung vorgelegen hat; daß sie - abgesehen von unten angegebenen Teilpublikationen - noch nicht veröffentlicht worden ist, sowie, daß ich eine solche Veröffentlichung vor Abschluß des Promotionsverfahrens nicht vornehmen werde. Die Bestimmungen dieser Promotionsordnung sind mir bekannt. Die von mir vorgelegte Dissertation ist von Professor Dr. P. von Brentano betreut worden.

Teilveröffentlichungen:

- Teile der Ergebnisse aus Kapitel 3 wurden bereits in [Wer02] veröffentlicht.
- Teile der Ergebnisse aus Kapitel 4 werden zur Veröffentlichung vorbereitet.

Lebenslauf

Name:	Volker Werner
Geburtsdatum:	4. September 1973
Geburtsort:	Köln
Eltern:	Peter Werner
	Waltraud Werner, geb. Rekittke
Staatsangehörigkeit:	deutsch
Familienstand:	ledig

Schulausbildung:

1979 – 1983	Katholische Grundschule Köln Deutz
1983 – 1992	Städtisches Gymnasium Thusneldastraße Köln Deutz
06/1992	Abitur

Hochschulstudium:

10/1992	Immatrikulation an der Universität zu Köln für das Studienfach Physik/Diplom
10/1994	Diplom-Vorprüfung
03/1996	Miniforschung am Institut für Kernphysik
02/1999	letzte mündliche Diplomprüfung
04/2000	Diplom im Fach Physik mit dem Thema: "Suche nach gemischtsymmetrischen Zuständen in den Kernen ^{96}Mo und ^{82}Se und Untersuchung der Deformation schwerer Kerne"
04/2000 –	Promotionsstudium

Arbeitsverhältnisse am Institut für Kernphysik der Universität zu Köln:

05/1996 – 04/2000	Studentische Hilfskraft
05/2000 – 08/2000	Wissenschaftliche Hilfskraft
09/2000 –	Wissenschaftlicher Mitarbeiter